Charles University in Prague
Faculty of Mathematics and Physics

MASTER THESIS

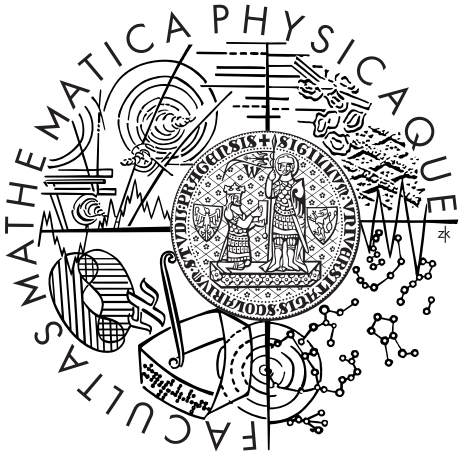

Bc. Martin Řehoř

Behaviour of new types of material models in a squeeze flow geometry

Mathematical Institute of Charles University

Supervisor of the master thesis: Mgr. Vít Průša, Ph.D.

Study programme: Mathematics

Specialization: Mathematical Modelling in Physics and Technology

Prague

2012

First and foremost, I would like to thank my supervisor, Mgr. Vít Průša, Ph.D., for all his friendly guidance coupled with incessant encouragement at all phases of this work. I really appreciate all the advice he provided me during many valuable consultations.

My special thanks also belong to the group of Mathematical modelling in the Mathematical Institute of Charles University, in particular to my consultant, prof. RNDr. Josef Málek, CSc., DSc., for the great background which made it enjoyable to work on this thesis.

My deepest gratitude goes to my family and to my dearest Pavla – thank you for your understanding, support and endless patience.

I declare that I carried out this master thesis independently, and only with the cited sources, literature and other professional sources.

I understand that my work relates to the rights and obligations under the Act No. 121/2000 Coll., the Copyright Act, as amended, in particular the fact that the Charles University in Prague has the right to conclude a license agreement on the use of this work as a school work pursuant to Section 60 paragraph 1 of the Copyright Act.

In ..... date ..... signature

Název práce: Chování nových typů materiálových modelů ve *squeeze flow* geometrii

Autor: Bc. Martin Řehoř

Katedra / Ústav: Matematický ústav Univerzity Karlovy

Vedoucí práce: Mgr. Vít Průša, Ph.D., Matematický ústav Univerzity Karlovy

Abstrakt: Studium chování nejrůznějších materiálů při lisování (*squeeze flow*) představuje důležitou techniku využívanou v reologii a je relevantní rovněž z hlediska technologického (zjednodušený popis některých typů tlumičů, lisování plastických hmot). Problém *squeeze flow* nebyl doposud vyřešen pro materiály tekutinového typu, jejichž materiálové koeficienty závisí na tlaku. Předkládaná práce se zaměřuje na studium tohoto problému pro nestlačitelnou tekutinu s tlakově závislou viskozitou při volbě okrajových podmínek typu *perfect-slip* a *no-slip*. Již na úrovni analytických řešení, které lze obdržet uvážením jistých fyzikálně ospravedlnitelných zjednodušení, je ukázáno, že zvolený model vykazuje zajímavé odchylky ve srovnání s klasickým modelem pro vazkou tekutinou (Navier-Stokes). V rámci diplomové práce je pak vyvíjena numerická simulace pro *no-slip squeeze flow*, což je problém s volnou hranicí, a to za použití metody *body-fitted curvilinear coordinates* a spektrální metody. Zajímavé chování je očekáváno v rozích výpočetní oblasti, kde jsou obvykle lokalizovány tlakové singularity. Numerické výsledky však odhalují základní nedostatky použitého fyzikálního modelu, přičemž jeho možné vylepšení je diskutováno v závěru práce.

Klíčová slova: Lisování; nestlačitelná tekutina; tlakově závislá viskozita; volná hranice; *no-slip*.

Title: Behaviour of new types of material models in a squeeze flow geometry

Author: Bc. Martin Řehoř

Department / Institute: Mathematical Institute of Charles University

Supervisor: Mgr. Vít Průša, Ph.D., Mathematical Institute of Charles University

Abstract: Investigation of material behaviour in a squeeze flow geometry provides an important technique in rheology and it is relevant also from the technological point of view (some types of dampers, compression moulding). To our best knowledge, the squeeze flow has not been solved for fluids-like materials with pressure-dependent material moduli. In the main scope of the present thesis, an incompressible fluid whose viscosity strongly depends on the pressure is studied in both the perfect-slip and the no-slip squeeze flow. It is shown that such a material model can provide interesting departures compared to the classical model for viscous (Navier-Stokes) fluid even on the level of analytical solutions, which are obtained using some physically relevant simplifications. Numerical simulation of a free boundary problem for the no-slip squeeze flow is then developed in the thesis using body-fitted curvilinear coordinates and spectral collocation method. An interesting behaviour is expected especially in the corners of the computational domain where the stress singularities are normally located. Unfortunately, numerical results reveal some fundamental drawbacks related to the physical model and its possible improvement is discussed at the end of the thesis.

Keywords: Squeeze flow; incompressible fluid; pressure-dependent viscosity; free boundary; no-slip.

Contents

Nomenclature

Symbol	*Meaning*
α	pressure-viscosity coefficient
γ	surface tension
$\dot{\epsilon}$	compression rate ($\dot{\epsilon} = \dot{H}/H = \dot{h}/h$)
μ_0	reference viscosity
ξ	sample radius
π_0	ambient pressure
ϱ	sample density
Σ	free surface
$\boldsymbol{\tau}$	tangent vector on free surface
Ω	physical domain occupied by fluid
A_0	initial contact area ($A_0 = \pi R_0^2$)
Ca	Capillary number
$\mathbb{D}$	symmetric part of velocity gradient
$\boldsymbol{f}$	external forces
F	normal force exerted on plates
$\mathbb{F}$	deformation gradient
H	plate separation ($H = 2h$)
H_0	initial plate separation ($H_0 = 2h_0$)
$\mathbb{I}$	unit tensor
L	characteristic length scale
$\mathbb{L}$	velocity gradient
$\boldsymbol{n}$	normal vector on free surface
$\mathbb{N}$	set of natural numbers
p	pressure (mean normal stress)
R_0	initial sample radius
R_p	radius of plates
$\mathbb{R}$	set of real numbers
Re	Reynolds number
t	time
$\mathbb{T}$	Cauchy stress tensor
$\boldsymbol{v}$	velocity field
V	characteristic velocity
V_{cl}	constant closure speed (positive)
$\boldsymbol{x}$	position vector in current frame
$\boldsymbol{X}$	position vector in reference frame

1. Introduction

The problem studied in the present thesis is that of the isothermal axisymmetric squeeze flow of homogeneous, incompressible fluids-like materials whose material moduli depend on the pressure. In order to describe those fluids, advanced material models have to be considered. We shall deal with a model which is used to describe an incompressible fluid with pressure-dependent viscosity primarily. We shall examine whether behaviour of such a model in the squeeze flow geometry can provide some interesting departures from solutions obtained for the classical Navier-Stokes fluid.

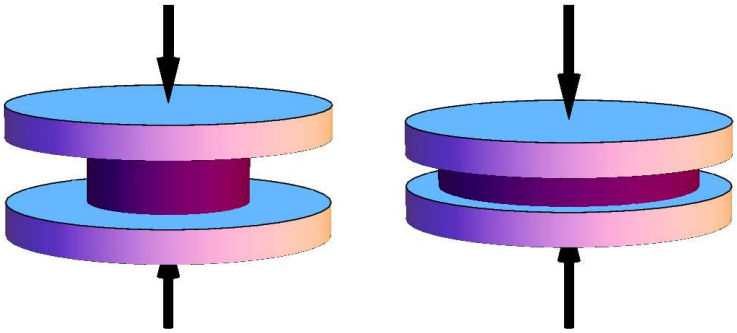

Figure 1: Illustration of an axisymmetric squeeze flow with constant mass of sample between plates.

By the term *squeeze flow* we shall understand the flow in which a constant mass of a material is compressed (squeezed) between two parallel plates approaching each other. Exactly this situation is sketched in Figure 1. To be more precise, we should call it an axisymmetric squeeze flow. During this compression process the sample of a material expands biaxially and shrinks along preferred axis. From this point of view one can meet frequently used synonyms for squeeze flows such as *uniaxial compression* or *biaxial extension*.

The squeeze flow phenomenon is found in many engineering, biology and also rheometry domains. In fact, it is one of the few deformations which has applications for a wide class of materials. Concerning the engineering domain, squeeze flows are involved in various technological issues such as *compression moulding* processes of metals and polymers, some types of *dampers* or *bearings*. On the other hand, compression with irregular and not exactly parallel plates poses similar but undoubtedly more complex problem, and so *chewing* between teeth or *diathrodial joints* – for example knee – are found to be relevant examples involving squeeze flows in biology and bioengineering respectively.

The situation described and depicted above provides an important technique in rheology, where it is used for examining rheological properties of materials that create difficulties in standard rheometers. Particularly, materials with extremely high viscosity and fluids with apparent yield stress belong into the mentioned category. The methodology is closely related to food processing, since various foodstuffs (cheese, wheat flour dough, mustard, tomato paste, mayonnaise, etc.) has been examined using several types of squeeze flow tests. Basically it is possible to carry out experiments with constant plate speed, constant load or constant strain rate. Recent research in this

field covers those and similar tests for personal care products and biomaterials.

Characterization of various materials is often associated with the development of solutions for specific models. Plenty of material models, including many non-Newtonian fluids, has been examined using the squeeze flow geometry. At this point the reader is referred to the nice review article by Engmann et al. (2005). However, the problem has not been solved, to our best knowledge, for fluids-like materials with pressure-dependent material moduli.

The influence of pressure on material properties was systematically investigated by Bridgman. In his pioneering work Bridgman (1926) showed that the viscosity (of many organic fluids) can dramatically increase with the applied pressure while the density is almost constant. It implies that it is reasonable to consider models for incompressible fluids with pressure-dependent viscosity. Later, pressure dependent material moduli were identified even for viscoelastic models, see the discussion by Ferry (1980) for instance, and they have their special place concerning material properties of polymers. For example Sedláček et al. (2004) fitted experimental data for several polymers using the modified White-Metzner model.

Although the fact that the material moduli can depend on the pressure is relatively well known, and the exact form of the functional dependence has been identified for various fluids, it is almost ignored in many applications[1]. For instance in polymer engineering materials are subjected to an extensive range of pressures and the mentioned property could play an important role.

Similar situation arises in the case of squeeze flows. Nature of the squeeze flow problem is substantially influenced by the choice of boundary condition at the sample-plate interfaces. It becomes the most interesting when the *no-slip* boundary condition is assumed there. As we shall see later, in such a case, pressure variation in the squeezed specimen is significant. Particularly, for an incompressible fluid with constant viscosity – classical Navier-Stokes fluid – we expect complex solution behaviour in the corners of the computational domain, with a possibility that the stress singularities will be located there. Hence, behaviour of fluids with pressure-dependent viscosity can be expected to be markedly different in such a case.

To close this introductory section let us remark that one can also meet a situation in which the space between plates is completely filled with a material. It is subsequently squeezed out from that region, while the contact area between the sample and plates remains constant. Some authors has also analysed conceptually simpler planar squeeze flow alongside the axisymmetric case. We shall not consider these variations here.

[1] Some exceptions can be found in elastohydrodynamics and hydrodynamic lubrication, see for example Gwynllyw et al. (1996), Rajagopal and Szeri (2003), Lanzendörfer (2011).

2. Specification of the problem

In this chapter we shall specify the problem we want to solve. In the first part we shall formulate governing equations for the creeping flow of an incompressible fluid-like material with pressure-dependent material moduli, in the second part we shall provide a detailed description of the problem geometry and we shall point out all the simplifications involved in the physical model.

2.1 Governing equations

In the present thesis we are interested in squeeze flows of fluids-like materials that are idealized as incompressible and homogeneous with constant density ϱ_0. Influence of the temperature on material properties is neglected in the sense we consider an isothermal process.

2.1.1 Kinematic considerations and balance equations

Let us mention a brief discussion about kinematics at this point. More information can be found for example in Ogden (1984), Gurtin (1981). From the viewpoint of continuum physics, a sample of a material forms a body $\mathcal{B}$ consisting of continuously distributed matter. Formally, body $\mathcal{B}$ is a set of material points which occupy some region in a three dimensional Euclidian space $\mathcal{E}$.

We define a configuration of $\mathcal{B}$ to be one-to-one mapping $\kappa : \mathcal{B} \to \mathcal{E}$ which takes the material points of $\mathcal{B}$ to the places they occupy in $\mathcal{E}$. By a motion of $\mathcal{B}$ we mean a one parameter family of configurations $\kappa_t : \mathcal{B} \to \mathcal{E}$, where the subscript identifies the time t as parameter. We shall refer to $\kappa_0(\mathcal{B})$ as to the reference configuration of $\mathcal{B}$ at time $t = 0$, whereas $\kappa_t(\mathcal{B})$ denotes the current configuration of $\mathcal{B}$ at any particular instant $t \in \mathbb{R}$. It follows that all the material points $P \in \mathcal{B}$ can be uniquely identified with the points in the reference configuration throughout

$$\boldsymbol{X} = \kappa_0(P), \qquad P = \kappa_0^{-1}(\boldsymbol{X}),$$

and consequently a motion of $\mathcal{B}$ can be identified with a one-to-one mapping

$$\boldsymbol{\chi} : \kappa_0(\mathcal{B}) \times \mathbb{R} \longrightarrow \kappa_t(\mathcal{B}).$$

We write

$$\boldsymbol{x} = \boldsymbol{\chi}(\boldsymbol{X}, t), \qquad \boldsymbol{X} = \boldsymbol{\chi}^{-1}(\boldsymbol{x}, t). \tag{2.1}$$

We shall suppose that $\boldsymbol{\chi}$ together with its inverse are sufficiently smooth[1] to render the operations defined on it meaningful. As it is usual in continuum mechanics, we admit standard Lagrangian and Eulerian description of quantities – scalars, vectors and tensors – associated with body $\mathcal{B}$.

For an arbitrary point $\boldsymbol{X} \in \kappa_0(\mathcal{B})$, the set of points

$$\{\boldsymbol{\chi}(\boldsymbol{X}, t) |\ t \in \mathbb{R}\} \tag{2.2}$$

[1] It should be enough for our purposes to assume that $\boldsymbol{\chi}$ is a $\mathcal{C}^2$-diffeomorphism.

is called the trajectory (pathline) of $\boldsymbol{X}$. The velocity field $\boldsymbol{v}$ is then defined through

$$\boldsymbol{v}(\boldsymbol{X},t) = \frac{\partial \boldsymbol{\chi}}{\partial t}(\boldsymbol{X},t). \tag{2.3}$$

In Eulerian description we have

$$\boldsymbol{v}(\boldsymbol{x},t) = \frac{\partial \boldsymbol{\chi}}{\partial t}(\boldsymbol{X},t)\Big|_{\boldsymbol{X}=\boldsymbol{\chi}^{-1}(\boldsymbol{x},t)}. \tag{2.4}$$

As we have mentioned earlier, we are interested in modelling of fluids-like materials primarily, and thus the determination of the velocity field, as a part of the solution that is sought-after, will be the crucial issue for us. Another important quantity is the velocity gradient

$$\mathbb{L} = \operatorname{grad} \boldsymbol{v} \equiv \frac{\partial \boldsymbol{v}}{\partial \boldsymbol{x}}, \qquad \mathrm{L}_{ij} = \frac{\partial v_i}{\partial x_j}, \tag{2.5}$$

and especially its symmetric part

$$\mathbb{D} = \frac{1}{2}\left(\mathbb{L} + \mathbb{L}^{\mathsf{T}}\right), \qquad \mathrm{D}_{ij} = \frac{1}{2}\left(\frac{\partial v_i}{\partial x_j} + \frac{\partial v_j}{\partial x_i}\right). \tag{2.6}$$

The deformation gradient $\mathbb{F}$ is defined through

$$\mathbb{F} = \operatorname{Grad} \boldsymbol{\chi} \equiv \frac{\partial \boldsymbol{\chi}}{\partial \boldsymbol{X}}, \qquad \mathrm{F}_{ij} = \frac{\partial \chi_i}{\partial X_j}. \tag{2.7}$$

An incompressible body naturally undergoes an isochoric flow. It means we have

$$\det \mathbb{F} = 1 \tag{2.8}$$

and consequently[2]

$$\operatorname{div} \boldsymbol{v} = 0. \tag{2.9}$$

Let us remark that the latter constraint is sometimes called the *incompressibility condition* and it can be equivalently expressed in terms of the tensorial quantity $\mathbb{D}$, through

$$\operatorname{tr} \mathbb{D} = 0, \tag{2.10}$$

where tr denotes the trace of a tensor.

The concept of balance of mass in its local form (from the "Eulerian perspective") leads to the partial differential equation, also known as continuity equation,

$$\frac{\partial \varrho}{\partial t} + \boldsymbol{v} \cdot \operatorname{grad} \varrho + \varrho \operatorname{div} \boldsymbol{v} = 0. \tag{2.11a}$$

For an incompressible flow it immediately follows, with the use of (2.9), that

$$\frac{\mathbf{d}\varrho}{\mathbf{d}t} = 0, \tag{2.11b}$$

where $\frac{\mathbf{d}}{\mathbf{d}t}$ denotes the material time derivative. Since the material is supposed to be homogeneous with constant density ϱ_0 in the reference configuration, previous relation

[2]For details see the references stated at the beginning of this paragraph or any other textbook on continuum mechanics.

implies that $\varrho \equiv \varrho_0$ remains constant. Similarly, balance of linear momentum in its local form leads to the equation

$$\frac{\partial(\varrho \boldsymbol{v})}{\partial t} + \operatorname{div}(\varrho \boldsymbol{v} \otimes \boldsymbol{v}) = \varrho \boldsymbol{f} + \operatorname{div} \mathbb{T}, \tag{2.12a}$$

where $\mathbb{T}$ denotes the Cauchy stress tensor (see the next paragraph) and $\boldsymbol{f}$ represents external forces (e.g. the gravitation force). Using the continuity equation one can write previous relation in the form

$$\varrho \frac{\mathrm{d}\boldsymbol{v}}{\mathrm{d}t} = \varrho \boldsymbol{f} + \operatorname{div} \mathbb{T}. \tag{2.12b}$$

In what follows we put $\boldsymbol{f}$ equal to zero[3]. One can suppose the absence of internal couples for our purposes, so that balance of angular momentum implies the symmetry of the Cauchy stress tensor.

Under above considerations, the system of governing equations for the flow of an incompressible, homogeneous fluid reads

$$\operatorname{div} \boldsymbol{v} = 0, \tag{2.13a}$$

$$\varrho \frac{\mathrm{d}\boldsymbol{v}}{\mathrm{d}t} = \operatorname{div} \mathbb{T}, \tag{2.13b}$$

$$\mathbb{T} = \mathbb{T}^{\mathsf{T}}. \tag{2.13c}$$

In order to close this system, we need to provide a constitutive equation for the Cauchy stress $\mathbb{T}$.

2.1.2 Constitutive equation for the Cauchy stress

In the main scope of the thesis we study behaviour of an incompressible fluid that can be described using the simple model

$$\mathbb{T} = -p\mathbb{I} + 2\mu(p)\mathbb{D}. \tag{2.14}$$

It is obvious that $\mathbb{T}$ satisfying the latter relation immediately satisfies (2.13c). Moreover, taking (2.10) into account it follows that the Lagrange multiplier p in (2.14) fulfills

$$p = -\frac{1}{3} \operatorname{tr} \mathbb{T}, \tag{2.15}$$

thus it represents the mean normal stress which is simply called the pressure. Now it should be clear that the viscosity is, in fact, a function of the mean normal stress and so (2.14) provides an implicit relationship between $\mathbb{T}$ and $\mathbb{D}$. From the theoretical point of view, the material model just presented belongs to the category of implicit constitutive relations satisfying

$$\mathfrak{g}(\mathbb{T}, \mathbb{D}) = 0, \tag{2.16}$$

where $\mathfrak{g}$ denotes an appropriate tensor function, and it fits into the thermodynamical framework developed by Rajagopal and Srinivasa (2008).

[3]We will generally assume that proportions of the sample in question are small enough (perhaps a few centimeters) to safely neglect the gravitation force.

It remains to determine a specific form of the function $\mu(p)$. Some simple flows of fluids satisfying above relations were studied by Hron et al. (2001), when they assumed different formulas relating the viscosity and the pressure. Here we shall use the exponential dependence

$$\mu(p) = \mu_0 e^{\alpha p}, \tag{2.17}$$

where μ_0 should be understood as the reference viscosity at $p = 0$ (the reference pressure), while α is a material constant usually interpreted as the *pressure-viscosity coefficient*. Such kind of functional dependence is often called the Barus law. As one would expect, and it is confirmed by experimental studies, the viscosity μ increases with increasing pressure, and thus we assume that α is positive.

Some particular values of μ_0 and α for specific materials can be found in Table 1 which was taken from Průša et al. (2012) with permission. Another fluids obeying the above relation are some food products, see for example Schaschke et al. (2006), or various polymeric liquids and polymer solutions, see for example Liang (2001), Harris and Bair (2007).

Note that for $\alpha = 0$ one obtains, from (2.14), the classical constitutive equation for an incompressible Navier-Stokes fluid

$$\mathbb{T} = -p\mathbb{I} + 2\mu_0\mathbb{D}. \tag{2.18}$$

Fluid	μ_0 [Pa · s]	α [1/GPa]
Octamethyltrisiloxane[a]	0.12×10^{-3}	13
Vegetable biodiesel[b]	7.5×10^{-3}	12
Diisodecyl phthalate[c]	123×10^{-3}	26
Paraffinic oils[d]	810×10^{-3}	34
PαMSAN[e]	1.08×10^{3}	35

[a] Data taken from King et al. (1992). (Our fit of original tabulated data.)
[b] Data taken from Paton and Schaschke (2009). Controlled temperature of 20 °C.
[c] Data taken from Harris and Bair (2007), sample B at 20 °C.
The authors have fitted the data fit for the formula $\mu = e^{a_0 + a_1 p + a_2 p^2 + a_3 p^3}$. Here we have calculated μ_0 and α from a_0 and a_1.
[d] Data taken from Neale (1973). (Generic cylinder paraffinic oil, temperature 30 °C.)
[e] Data taken from Cardinaels et al. (2007). (Our fit of original data in Figure 8, temperature 210 °C, shear stress level 270 kPa.)

Table 1: Parameter values for some fluids with pressure dependent viscosity, fit of formula (2.17). Reprinted from Průša et al. (2012) with permision.

2.1.3 Governing equations in dimensionless variables

Now we derive a dimensionless version of governing equations (2.13) and (2.14). Let L be a characteristic length, V a characteristic velocity and μ_0 the reference viscosity as stated above. Using these characteristic quantities we define dimensionless counterparts (denoted by asterisk) of $t, \boldsymbol{x}, \boldsymbol{v}, \mathbb{D}$ and $\mathbb{T}$ as follows,

$$t^* = \frac{V}{L}t, \qquad \boldsymbol{x}^* = \frac{\boldsymbol{x}}{L}, \qquad \boldsymbol{v}^* = \frac{\boldsymbol{v}}{V}, \qquad \mathbb{D}^* = \frac{L}{V}\mathbb{D}, \qquad \mathbb{T}^* = \frac{L}{\mu_0 V}\mathbb{T}.$$

Let us remark that dimensionless pressure p^* is naturally defined in the same way as the dimensionless Cauchy stress, i.e. $p^* = \frac{L}{\mu_0 V} p$, see (2.15). Dimensionless version of governing equations then reads

$$\operatorname{div}^* \boldsymbol{v}^* = 0, \tag{2.19a}$$

$$\mathrm{Re} \frac{\mathbf{d}\boldsymbol{v}^*}{\mathbf{d}t^*} = \operatorname{div}^* \mathbb{T}^*, \tag{2.19b}$$

$$\mathbb{T}^* = -p^* \mathbb{I} + 2e^{\hat{\alpha} p^*} \mathbb{D}^*, \tag{2.19c}$$

where the dimensionless Reynolds number is given as $\mathrm{Re} = \frac{\varrho L V}{\mu_0}$ (the ratio of inertial and viscous forces). Another dimensionless parameter corresponding to the pressure-viscosity coefficient appears in (2.19c) and is given through

$$\hat{\alpha} = \frac{\mu_0 V}{L} \alpha. \tag{2.20}$$

Further, we shall follow the situation stated in the article by Engmann et al. (2005): *"In many practical applications one is dealing with very viscous fluids and/or slow plate movements so that the Reynolds number is small enough to safely neglect the left hand side of the equations."* In fact, we are neglecting inertia in this way and equation (2.19b) is reduced to

$$\operatorname{div}^* \mathbb{T}^* = 0. \tag{2.21}$$

Substituting (2.19c) to (2.21) we get the system of dimensionless equations[4]

$$\operatorname{div}^* \boldsymbol{v}^* = 0, \tag{2.22a}$$

$$-\operatorname{grad}^* p^* + e^{\hat{\alpha} p^*} \left(\Delta^* \boldsymbol{v}^* + 2\hat{\alpha} \mathbb{D}^* \operatorname{grad}^* p^* \right) = 0. \tag{2.22b}$$

We would like to solve these equations for the axisymmetric squeeze flow setting described further.

2.1.4 Discussion on suitable material parameters

It is worth emphasizing that in order to stay consistent with all the assumptions made so far, one has to ensure the dimensionless parameter $\hat{\alpha}$ to be greater in magnitude than the Reynolds number (at least about one order). Otherwise, we should probably neglect also the terms appearing with $\hat{\alpha}$. If we did it, equations (2.22) would reduce to become the well-known Stokes system[5]. Nevertheless, it is possible to meet the requirement as stated above, when parameters of the experiment are chosen carefully.

Let us have a look at the ratio of $\hat{\alpha}$ and the Reynolds number, which is

$$\frac{\hat{\alpha}}{\mathrm{Re}} = \frac{\alpha \mu_0^2}{\varrho L^2}.$$

Although materials mentioned in Table 1 do not represent ideal exemplars to fit our assumptions (they were selected in the context of measurements with falling cylinder

[4] $\mathbb{D}^* \operatorname{grad} p^*$ is a vector obtained simply by application of the tensor $\mathbb{D}^*$ on the vector $\operatorname{grad} p^*$, thus its i-th component in Cartesian coordinates is given by $\sum_{j=1}^{3} \mathrm{D}^*_{ij} \frac{\partial p^*}{\partial x^*_j}$.

[5] In fact, it is open to debate whether to neglect those terms or not. In comparison with the inertial effects, the pressure and pressure gradients themselves could be quite large (especially in a corner). The pressure-dependent viscosity, although with $\hat{\alpha}$ being small, still can play an important role in such cases.

viscometer), the reader can get the idea that the pressure-viscosity coefficient α takes the values of order about $10^{-7} - 10^{-8}\,{}^{1}/_{\mathrm{Pa}}$ for a wide class of materials. It should be clear that the requirement $\frac{\hat{\alpha}}{\mathrm{Re}} \gg 1$ can be satisfied for those materials with relatively high reference viscosity and/or small density, when the characteristic length scale is small enough. For instance, taking into account materials with the reference viscosity of order $10^5\,\mathrm{Pa}\cdot\mathrm{s}$ and the density about $10^3\,{}^{\mathrm{kg}}/_{\mathrm{m}^3}$ (e.g. some polymer melts), it is suitable to squeeze specimens with an initial height of several centimeters.

2.2 Axisymmetric squeeze flow

Once we have governing equations we need to specify a domain in which they have to be solved. At the same time we need to know boundary conditions that are expected to be satisfied on boundaries of the domain in question.

2.2.1 Geometry

A sketch of an axisymmetric squeeze flow problem is shown in Figure 1. According to geometry of the problem it is convenient to work within a cylindrical coordinate system $\{r, \theta, z\}$[6]. Indeed, given axial symmetry causes that all quantities describing the problem are independent of the angular coordinate θ. In other words, the description of the problem does not depend upon the chosen angle and it suffices to restrict our observations to the plane $\{r, z\}$[7].

We claimed above that the effect of external forces, including the gravitation force, is not considered here (the specimen between plates is quite small). Hence, one can also use the symmetry along the central plane parallel to both plates.

An appropriate coordinate system for this case is introduced in Figure 2. We shall describe the deformation process – the flow – during the time interval $[0, t_{\mathrm{end}}]$. Then $H(t)$ denotes the distance between plates at some particular time instant, while $h(t) = \frac{1}{2}H(t)$ is the distance between the upper plate and the central plane[8]. For initial values we use the notation H_0, h_0 respectively. Let us suppose that both plates are identical, their radius R_p is constant and much larger than the initial radius of the sample, R_0.

Since we consider the sample of an incompressible material to be compressed, it has to expand in radial direction during the compression itself. Therefore the sample radius ξ evolves in time and simultaneously it is a function of z (except the case when the perfect-slip boundary condition is prescribed, as we shall see later). Further it is assumed that the sample forms an ideal cylinder at the beginning of our observation, thus we have

$$\xi(z, 0) = R_0, \qquad \forall z \in [-h_0, h_0]. \tag{2.23}$$

Now it should be clear that it is not necessary to consider whole inherently transient domain occupied by the fluid, but it suffices to restrict our attention to the upper-right

[6] See Appendix A for detailed information about cylindrical coordinates.

[7] More precisely we should probably say the plane $\{r, 0, z\} \cup \{r, \pi, z\},\ \forall r \in [0, \infty), \forall z \in \mathbb{R}$. For simplicity, let us introduce the notation

$$\{-r, z\} \equiv \{r, \pi, z\}, \qquad \forall r \in (0, \infty), \forall z \in \mathbb{R}.$$

[8] Of course we suppose $H(t) > 0$ for all $t \in [0, t_{\mathrm{end}}]$.

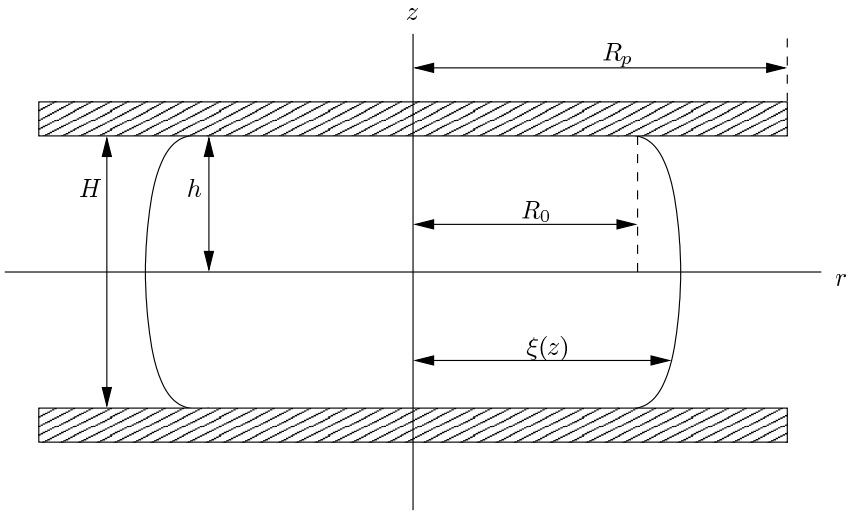

Figure 2: Coordinate system for an axisymmetric squeeze flow with basic labels.

quadrant in the coordinate system just given. We denote

$$\Omega_t = \{(r,z) : z \in [0, h(t)],\ r \in [0, \xi(z,t)]\} \tag{2.24}$$

the mentioned part of the physical domain at time t. With the knowledge of a solution which pertains to Ω_t, the complete solution can be simply reconstructed due to symmetries.

Velocity of the upper plate is given as the time derivative $\dot{h}$ of the function h, and quantity called compression rate,

$$\dot{\epsilon} = \frac{\dot{h}}{h}, \tag{2.25}$$

is introduced quite commonly. Various settings are available in order to examine material properties in the squeeze flow rheometry. One possibility is to use a constant load and observe, for instance, how much the sample shrinks its height. Another commonly used test requires a constant closure speed (it means that the velocity of plates is constant) and measures, besides other things, the force exerted by the sample on the plate against the direction of plate motion. Last but not least, it is possible to consider experiments with a constant compression rate $\dot{\epsilon}$.

In the present paper we are limiting ourselves to the case with constant closure speed $\dot{H} = -V_{\mathrm{cl}}$, $V_{\mathrm{cl}} > 0$, and we put $V = \frac{1}{2}V_{\mathrm{cl}}$ to be the characteristic velocity discussed in Section 2.1.3. Motion of the upper plate is then given through

$$h(t) = h_0 - Vt, \qquad \dot{h}(t) = -V. \tag{2.26}$$

In order to avoid an abrupt (discontinuous) activation of the motion, which implies an inconsistency of initial conditions, it is more convenient to allow a smooth start-up, let us say during the time interval $[0, t_0]$ with $0 < t_0 < t_{\mathrm{end}}$. One possible choice is

$$h(t) = \begin{cases} h_0 + V\left(\dfrac{t}{t_0}\right)^3\left(\dfrac{1}{2}t - t_0\right), & t \in [0, t_0], \\ h_0 + V\left(\dfrac{1}{2}t_0 - t\right), & t \in (t_0, t_{\mathrm{end}}], \end{cases} \tag{2.27a}$$

$$\dot{h}(t) = \begin{cases} V\left(\frac{t}{t_0}\right)^2\left(\frac{2t}{t_0}-3\right), & t \in [0,t_0], \\ -V, & t \in (t_0,t_{\mathrm{end}}]. \end{cases} \tag{2.27b}$$

It is important that for all $t \in [0,t_{\mathrm{end}}]$ we know the exact value of h and $\dot{h}$ respectively.

2.2.2 Boundary conditions

Let Ω_t is the domain given in (2.24). Its boundary $\partial\Omega_t$ consists of three different parts, see Figure 3. It is the sample-plate interface, the artificial boundaries along both axes of symmetry and the free surface Σ_t. Quantities $v_r,\ v_\theta,\ v_z$ are used to denote physical components of vector $\boldsymbol{v}$ in cylindrical coordinates and similarly $\mathrm{T}_{rr}, \mathrm{T}_{r\theta}, \mathrm{T}_{rz}$, etc., represent physical components of the second order symmetric tensor $\mathbb{T}$ (see Appendix A for detailed information). Let us consider squeeze flow without superimposed rotation. It means that there is no velocity component in θ-direction ($v_\theta = 0$ everywhere in the physical domain occupied by the fluid, and consequently the shear stresses $\mathrm{T}_{r\theta},\ \mathrm{T}_{z\theta}$ are also zero).

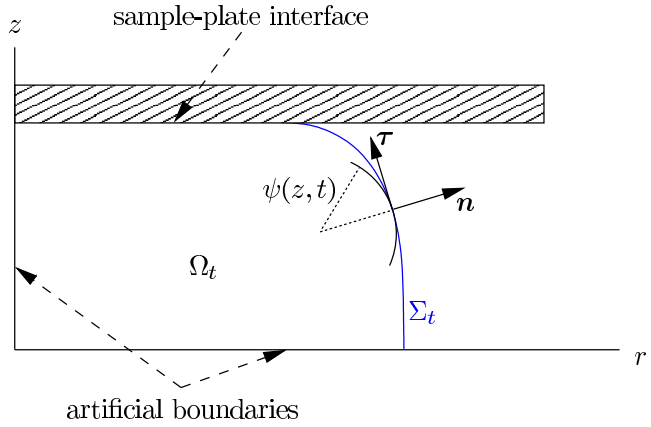

Figure 3: Specification of the boundary $\partial\Omega_t$.

Conditions enforcing symmetry of the solution have to be prescribed along each of both axes. We put

$$v_z\big|_{z=0} = 0, \qquad \mathrm{T}_{rz}\big|_{z=0} = 0, \qquad v_r\big|_{r=0} = 0, \qquad \mathrm{T}_{rz}\big|_{r=0} = 0. \tag{2.28}$$

On the free surface one has to prescribe two different kinds of boundary conditions. The dynamic boundary condition is usually given in the form

$$\mathbb{T}\boldsymbol{n} = -\pi_0\boldsymbol{n} + \gamma\left(\frac{1}{\xi}+\frac{1}{\psi}\right)\boldsymbol{n}, \tag{2.29}$$

where $\boldsymbol{n}$ is the outward unit vector normal to the free surface, π_0 is the ambient pressure, γ is the surface tension and ξ, ψ are the principal radii of curvature of the free surface. The ambient pressure is usually set to zero and it is used as the reference value for the pressure scale[9].The dynamic condition rewritten in dimensionless variables then reads

$$\mathbb{T}^*\boldsymbol{n} = \frac{1}{\mathrm{Ca}}\left(\frac{1}{\xi^*}+\frac{1}{\psi^*}\right)\boldsymbol{n},$$

[9]It can be understood that we redefine the Cauchy stress to be $\tilde{\mathbb{T}} = \mathbb{T} + \pi_0\mathbb{I}$.

with $\xi^* = \frac{1}{L}\xi$, $\psi^* = \frac{1}{L}\psi$ and Capillary number $\mathrm{Ca} = \mu_0 V \gamma^{-1}$ (the ratio of viscous and surface tension forces). Since we are dealing with very viscous fluid, Ca is typically very large[10] and the latter condition is reduced to *no traction* condition

$$\mathbb{T}^* \boldsymbol{n} = \mathbf{0}. \tag{2.30}$$

Before we formulate another condition (this time a kinematic one), which has to be satisfied on the moving free surface, we define $f(r,z,t) =_{\mathrm{def}} r - \xi(z,t)$ to be a function that enables to describe the free surface at time t implicitly as a set of points

$$\Sigma_t = \{(r,z) : f(r,z,t) = 0\}. \tag{2.31}$$

The free surface naturally creates a material surface at any time instant, thus it has to satisfy the condition

$$\left(\frac{\partial f}{\partial t} + \boldsymbol{v} \cdot \operatorname{grad} f\right)\Big|_{\Sigma_t} = 0. \tag{2.32}$$

It means that the material derivative of f has to be zero on the free surface. This statement is also known as *Lagrange criterion* and it is proved for example in the book of Maršík (1999), pages 83-85. In our case the kinematic condition reads

$$\left(-\frac{\partial \xi}{\partial t} + v_r - v_z \frac{\partial \xi}{\partial z}\right)\Big|_{r=\xi} = 0. \tag{2.33}$$

At the sample-plate interfaces boundary conditions play an important role concerning the nature of the flow. At first, we assume that no fluid can penetrate into the plate, thus in the vertical direction we set

$$v_z\big|_{z=h} = \dot{h}. \tag{2.34}$$

If the sample is able to move freely without friction at the interface in question, we use *perfect-slip* in the form

$$\mathrm{T}_{rz}\big|_{z=h} = 0. \tag{2.35a}$$

As we shall see later, there is no curvature of the free boundary during the compression and solution of the problem can be obtained in a quite straightforward manner. However, it is very complicated (even almost impossible) to ensure such type of condition in practice. Chatraei et al. (1981) introduced a "lubricated squeeze flow" technique to obtain a nearly pure biaxial extension.

On the other hand, one can consider *no-slip* boundary condition with the sample being fixed at the sample-plate interfaces. It means that no motion along radial axis is allowed there and

$$v_r\big|_{z=h} = 0. \tag{2.35b}$$

Curvature of the free surface of the specimen between plates is observed in this case and one needs to solve a *free boundary problem*. The fact that the outward unit normal $\boldsymbol{n}$ is unknown makes it cumbersome to use the condition (2.30) in search for an exact solution of the problem. As we shall see later, there is a way how to use the dynamic condition in a numerical treatment of the problem, however, for analytical computations an assumption about the pressure or normal stress at the edge of the plates is usually made (see the following section).

[10] It means that surface tension effects are negligible.

Presence of the well-known phenomenon of moving contact line further complicates the situation, see for example Huh and Scriven (1971), Bonn et al. (2009). Apparent motion of the contact line[11] is observed due to "barrelling" of the sample along plates and it has been nicely illustrated experimentally and numerically for example by Mavridis et al. (1992). This phenomenon is discussed again in Section 5.2.1.

Finally, there are several possibilities how to employ *partial-slip* at the interfaces (see the discussion by Engmann et al. (2005) together with references therein). One possible option, known as *Navier slip boundary condition,* is obtained as a combination of the two extreme cases mentioned above and it reads

$$-\lambda \mathrm{T}_{rz}\big|_{z=h} + (1-\lambda)\, v_r\big|_{z=h} = 0, \qquad \lambda \in (0,1). \tag{2.35c}$$

The same condition is sometime used in the form

$$v_r\big|_{z=h} = \beta\, \mathrm{T}_{rz}\big|_{z=h},$$

where $\beta = \frac{\lambda}{1-\lambda}$ is the "slip coefficient" with values from $(0,\infty)$. It is worth noting that limiting behaviour for $\lambda \to 0_+$ and $\lambda \to 1_-$ (alternatively $\beta \to 0_+,\ \beta \to \infty$) recovers the no-slip and the perfect-slip respectively.

2.2.3 Dimensionless variables

At this point we need to specify characteristic quantities introduced in Section 2.1.3. Scaling lengths with $L = h_0$, velocities with $V = \frac{1}{2}V_{\mathrm{cl}}$ and time with $\frac{L}{V}$, we put

$$\Omega_t^* = \{(r^*, z^*) : z^* \in [0, h^*(t^*)],\ r^* \in [0, \xi^*(z^*, t^*)]\} \tag{2.36}$$

to be the corresponding dimensionless version of the domain Ω_t where governing equations (2.22) have to be solved. For initial radius we have $\xi^*(z^*, 0) = \hat{R}_0$ with

$$\hat{R}_0 = \frac{R_0}{L} = \frac{R_0}{h_0}. \tag{2.37}$$

Relations (2.26) and (2.27) in their dimensionless form read[12]

$$h^*(t^*) = 1 - t^*, \qquad \dot{h^*}(t^*) = -1, \tag{2.38}$$

and

$$h^*(t^*) = \begin{cases} 1 + \left(\dfrac{t^*}{t_0^*}\right)^3 \left(\dfrac{1}{2}t^* - t_0^*\right), & t^* \in [0, t_0^*], \\ 1 + \dfrac{1}{2}t_0^* - t^*, & t^* \in (t_0^*, t_{\mathrm{end}}^*], \end{cases} \tag{2.39a}$$

$$\dot{h^*}(t^*) = \begin{cases} \left(\dfrac{t^*}{t_0^*}\right)^2 \left(\dfrac{2t^*}{t_0^*} - 3\right), & t^* \in [0, t_0^*], \\ -1, & t^* \in (t_0^*, t_{\mathrm{end}}^*]. \end{cases} \tag{2.39b}$$

The above functions are depicted in Figure 4 together with the dimensionless compression rate

$$\dot{\epsilon}^* = \frac{\dot{h^*}}{h^*}. \tag{2.40}$$

[11] By contact line we mean the intersection of fluid, plate and surrounding medium.

[12] The superimposed dot this time denotes the time derivative with respect to t^*.

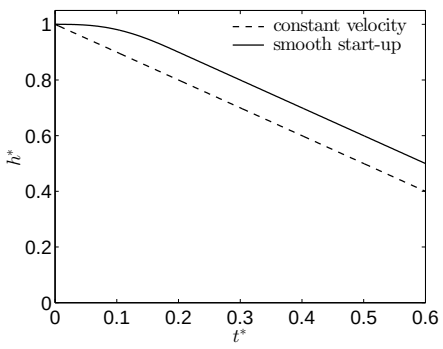

(a) Position h^* of the plate.

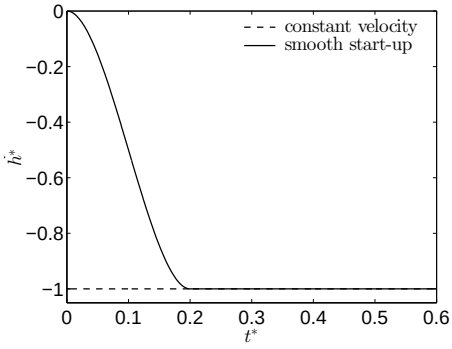

(b) Velocity $\dot{h}^*$ of the plate.

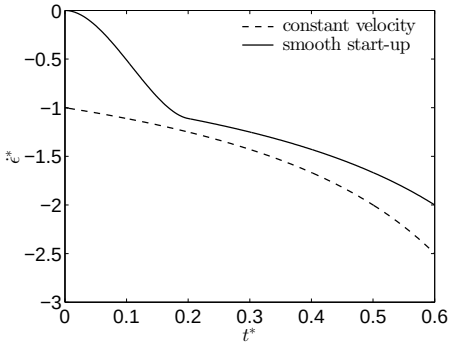

(c) Compression rate $\dot{\epsilon}^*$.

Figure 4: Motion of the upper plate in agreement with (2.38) and (2.39) for $t_0^* = 0.2$, $t_{\text{end}}^* = 0.6$.

2.2.4 Summary of simplifying assumptions

For clarity, before we formulate the dimensionless problem in cylindrical coordinates, let us summarize all the simplifying assumptions introduced throughout this section.

■ KINEMATICS:

- Problem is axisymmetric, therefore all quantities are independent of coordinate θ.
- There is no superimposed rotation of the sample between plates, hence $v_\theta = 0$.

■ DYNAMICS:

- External forces are neglected (hence symmetry along the central plane is considered).
- Inertial effects are neglected (we deal with the creeping flow).
- Surface tension on the free surface is not considered.

2.2.5 Dimensionless problem in cylindrical coordinates

From now on we will use only dimensionless variables and hence we will omit asterisk denoting dimensionless variables in the equations above. Governing equations (2.22) in cylindrical coordinates read

$$0 = \frac{\partial v_r}{\partial r} + \frac{v_r}{r} + \frac{\partial v_z}{\partial z}, \tag{2.41a}$$

$$\frac{\partial p}{\partial r} = e^{\hat{\alpha}p}\left[\frac{\partial^2 v_r}{\partial r^2} + \frac{1}{r}\frac{\partial v_r}{\partial r} + \frac{\partial^2 v_r}{\partial z^2} - \frac{v_r}{r^2} + 2\hat{\alpha}\frac{\partial p}{\partial r}\frac{\partial v_r}{\partial r} + \hat{\alpha}\frac{\partial p}{\partial z}\left(\frac{\partial v_r}{\partial z} + \frac{\partial v_z}{\partial r}\right)\right], \tag{2.41b}$$

$$\frac{\partial p}{\partial z} = e^{\hat{\alpha}p}\left[\frac{\partial^2 v_z}{\partial r^2} + \frac{1}{r}\frac{\partial v_z}{\partial r} + \frac{\partial^2 v_z}{\partial z^2} + \hat{\alpha}\frac{\partial p}{\partial r}\left(\frac{\partial v_r}{\partial z} + \frac{\partial v_z}{\partial r}\right) + 2\hat{\alpha}\frac{\partial p}{\partial z}\frac{\partial v_z}{\partial z}\right]. \tag{2.41c}$$

The remaining equation in (2.22b), corresponding to θ-direction, is identically satisfied. System (2.41) is supplemented with boundary conditions discussed in Section 2.2.2. These conditions, when they are rewritten using dimensionless variables, are of the same form as above. At this point, the set of boundary conditions is presented in a well arranged way and in the rest of the thesis we shall often reference ourselves to the following list.

- At the sample-plate interface ($z = h$) we consider either a couple of boundary conditions for the perfect-slip, it means

$$v_z\big|_{z=h} = \dot{h}, \qquad \mathrm{T}_{rz}\big|_{z=h} = 0, \tag{2.42a}$$

  or for the no-slip, which is

$$v_z\big|_{z=h} = \dot{h}, \qquad v_r\big|_{z=h} = 0. \tag{2.42b}$$

- On the axes of symmetry ($r = 0,\ z = 0$) we have symmetry conditions

$$v_r\big|_{r=0} = 0, \qquad \mathrm{T}_{rz}\big|_{r=0} = 0, \tag{2.43}$$

$$v_z\big|_{z=0} = 0, \qquad \mathrm{T}_{rz}\big|_{z=0} = 0. \tag{2.44}$$

- No traction condition (2.30) on the free surface ($r = \xi$) provides two equations

$$\left(\mathrm{T}_{rr} - \frac{\partial \xi}{\partial z}\mathrm{T}_{rz}\right)\Big|_{r=\xi} = 0, \qquad \left(\mathrm{T}_{rz} - \frac{\partial \xi}{\partial z}\mathrm{T}_{zz}\right)\Big|_{r=\xi} = 0, \tag{2.45}$$

  since the outward unit normal $\boldsymbol{n}$ satisfies

$$\boldsymbol{n}(\xi(z), z) = \left(1 + \left(\frac{\partial \xi}{\partial z}\right)^2\right)^{-\frac{1}{2}} \begin{bmatrix} 1 \\ 0 \\ -\frac{\partial \xi}{\partial z} \end{bmatrix}, \qquad z \in [0, h].$$

- The kinematic condition reads

$$\left(-\frac{\partial \xi}{\partial t} + v_r - v_z\frac{\partial \xi}{\partial z}\right)\Big|_{r=\xi} = 0. \tag{2.46}$$

3. Analytical solutions

At the beginning of this section let us emphasize that we do not seek an exact solution of the problem discussed above. Even worse, in the case with no-slip boundary condition we solve a slightly different problem obtained from the original one considering another simplifying assumptions. However, main purpose of this section is to provide some analytical results that can reveal in what way the pressure-dependent viscosity influences solution behaviour[1], and moreover, later we will use the results obtained here to propose a benchmark problem for the numerical simulation (see Section 4.3).

Solutions will be obtained using the *perturbation method* with respect to parameter $\hat{\alpha}$, see for example Bush (1992). The method is based on the fact that we seek velocity $\boldsymbol{v}$ and pressure p of the form

$$\left.\begin{aligned} v_r &= v_{r,0} + v_{r,1}\hat{\alpha} + v_{r,2}\hat{\alpha}^2 + \dots\,, \\ v_z &= v_{z,0} + v_{z,1}\hat{\alpha} + v_{z,2}\hat{\alpha}^2 + \dots\,, \\ p &= p_0 + p_1\hat{\alpha} + p_2\hat{\alpha}^2 + \dots\,, \end{aligned}\right\} \tag{3.1}$$

which is usually called the *perturbation expansion*. Substitution of (3.1) into (2.41) and subsequent expansion of the exponential term,

$$e^{\hat{\alpha}p} = 1 + p\hat{\alpha} + \frac{1}{2}p^2\hat{\alpha}^2 + O\big(\hat{\alpha}^3\big) = 1 + p_0\hat{\alpha} + \left(p_1 + \frac{1}{2}p_0^2\right)\hat{\alpha}^2 + O\big(\hat{\alpha}^3\big)\,, \tag{3.2}$$

provide straightforward decomposition of the system of equations. Indeed, subsystem of order k (for $k = 0, 1, 2, \dots$) is obtained comparing the terms that appear together with $\hat{\alpha}^k$.

Of course, to each subsystem we add corresponding terms from the perturbation expansion of boundary conditions (then we talk about subproblems instead of subsystems). For example, the first condition in (2.42a) satisfies

$$\big(v_{z,0} + v_{z,1}\hat{\alpha} + \dots\big)\big|_{z=h} = \dot{h} + 0\hat{\alpha} + \dots\,,$$

and similarly the first condition in (2.45) reads

$$\left(\mathrm{T}_{rr,0} - \frac{\partial\xi_0}{\partial z}\mathrm{T}_{rz,0} + \left(\mathrm{T}_{rr,1} - \frac{\partial\xi_0}{\partial z}\mathrm{T}_{rz,1} - \frac{\partial\xi_1}{\partial z}\mathrm{T}_{rz,0}\right)\hat{\alpha} + \dots\right)\Bigg|_{r=\xi} = 0 + 0\hat{\alpha} + \dots\,.$$

To be more precise, let us do some remarks on notation used in the latter expression. According to (2.19c), for the rz-component of the stress tensor we have

$$\begin{aligned} \mathrm{T}_{rz} &= e^{\hat{\alpha}p}\left(\frac{\partial v_r}{\partial z} + \frac{\partial v_z}{\partial r}\right) = \\ &= \frac{\partial v_{r,0}}{\partial z} + \frac{\partial v_{z,0}}{\partial r} + \left(p_0\left(\frac{\partial v_{r,0}}{\partial z} + \frac{\partial v_{z,0}}{\partial r}\right) + \frac{\partial v_{r,1}}{\partial z} + \frac{\partial v_{z,1}}{\partial r}\right)\hat{\alpha} + O\big(\hat{\alpha}^2\big)\,, \end{aligned}$$

thus

$$\mathrm{T}_{rz,0} = \frac{\partial v_{r,0}}{\partial z} + \frac{\partial v_{z,0}}{\partial r}, \tag{3.3a}$$

$$\mathrm{T}_{rz,1} = \frac{\partial v_{r,1}}{\partial z} + \frac{\partial v_{z,1}}{\partial r} + p_0\left(\frac{\partial v_{r,0}}{\partial z} + \frac{\partial v_{z,0}}{\partial r}\right). \tag{3.3b}$$

[1] In comparison to the case with an incompressible Navier-Stokes fluid.

In the same way we deduce

$$\mathrm{T}_{rr,0} = -p_0 + 2\frac{\partial v_{r,0}}{\partial r}, \tag{3.4a}$$

$$\mathrm{T}_{rr,1} = -p_1 + 2\frac{\partial v_{r,1}}{\partial r} + 2p_0\frac{\partial v_{r,0}}{\partial r}. \tag{3.4b}$$

In what follows we deal only with subproblems of orders zero and one. We shall solve these subproblems step-by-step for the perfect-slip setting and then for the no-slip setting. Particular equations are listed below.

- **Subsystem of order zero** (or "zeroth-order subsystem"):

$$0 = \frac{\partial v_{r,0}}{\partial r} + \frac{v_{r,0}}{r} + \frac{\partial v_{z,0}}{\partial z}, \tag{3.5a}$$

$$\frac{\partial p_0}{\partial r} = \frac{\partial^2 v_{r,0}}{\partial r^2} + \frac{1}{r}\frac{\partial v_{r,0}}{\partial r} + \frac{\partial^2 v_{r,0}}{\partial z^2} - \frac{v_{r,0}}{r^2}, \tag{3.5b}$$

$$\frac{\partial p_0}{\partial z} = \frac{\partial^2 v_{z,0}}{\partial r^2} + \frac{1}{r}\frac{\partial v_{z,0}}{\partial r} + \frac{\partial^2 v_{z,0}}{\partial z^2}. \tag{3.5c}$$

- **Subsystem of order one** (or "first-order subsystem")[2]:

$$0 = \frac{\partial v_{r,1}}{\partial r} + \frac{v_{r,1}}{r} + \frac{\partial v_{z,1}}{\partial z}, \tag{3.6a}$$

$$\begin{aligned}\frac{\partial p_1}{\partial r} = {} & \Delta v_{r,1} - \frac{v_{r,1}}{r^2} + 2\frac{\partial p_0}{\partial r}\frac{\partial v_{r,0}}{\partial r} + \\ & + \frac{\partial p_0}{\partial z}\left(\frac{\partial v_{r,0}}{\partial z} + \frac{\partial v_{z,0}}{\partial r}\right) + p_0\left(\Delta v_{r,0} - \frac{v_{r,0}}{r^2}\right),\end{aligned} \tag{3.6b}$$

$$\frac{\partial p_1}{\partial z} = \Delta v_{z,1} + \frac{\partial p_0}{\partial r}\left(\frac{\partial v_{r,0}}{\partial z} + \frac{\partial v_{z,0}}{\partial r}\right) + 2\frac{\partial p_0}{\partial z}\frac{\partial v_{z,0}}{\partial z} + p_0\,\Delta v_{z,0}. \tag{3.6c}$$

It is worth emphasizing that the zeroth-order subproblem corresponds to axisymmetric squeeze flow of an incompressible fluid with constant viscosity. Hence, its solution is nothing but solution for the Navier-Stokes fluid. Higher order subproblems then represent some perturbation which has to be added to this solution, and the most significant contribution is naturally provided by the first-order subproblem.

3.1 Perfect-slip at the sample-plate interface

Let us remind that in this paragraph we would like to solve governing equations in (2.41) together with the set of boundary conditions (2.42a), (2.43) – (2.46). Perfect-slip ensures that the sample moves freely without friction along sample-plate interfaces, therefore its deformation in this case corresponds to homogeneous biaxial extension with the velocity field given by

$$\boldsymbol{v} = \begin{bmatrix} v_r \\ v_\theta \\ v_z \end{bmatrix} = \begin{bmatrix} v_{r,0} \\ 0 \\ v_{z,0} \end{bmatrix} = \begin{bmatrix} -\frac{1}{2}\dot{\epsilon}r \\ 0 \\ \dot{\epsilon}z \end{bmatrix}. \tag{3.7}$$

[2]For the definition of Laplace operator in cylindrical coordinates see Appendix A.

Compression rate $\dot{\epsilon}$ is defined in (2.40) (see also Figure 4c).

It is obvious that the velocity field of the form (3.7) automatically satisfies the incompressibility condition (2.41a). Moreover, since v_r does not depend on z, free surface remains vertical and $\frac{\partial \xi}{\partial z} \equiv 0$. Kinematic condition (2.46) then reads

$$v_r\big|_{r=\xi} = \frac{\partial \xi}{\partial t}, \tag{3.8}$$

which really means that radial velocity of material points lying on the free surface coincides with the velocity of the free surface. Relation (3.8) provides the ordinary differential equation

$$-\dot{\epsilon}\xi = 2\dot{\xi},$$

which is easily solved using the initial condition $\xi(0) = \hat{R}_0$, and results in radius

$$\xi(t) = \hat{R}_0 \sqrt{\frac{1}{h(t)}}\,. \tag{3.9}$$

Once we know the velocity field, we can write

$$\mathbb{D} = \begin{bmatrix} -\frac{1}{2}\dot{\epsilon} & 0 & 0 \\ 0 & -\frac{1}{2}\dot{\epsilon} & 0 \\ 0 & 0 & \dot{\epsilon} \end{bmatrix} \tag{3.10}$$

and according to (2.19c) we have

$$\mathbb{T} = -p\mathbb{I} + 2e^{\hat{\alpha}p} \begin{bmatrix} -\frac{1}{2}\dot{\epsilon} & 0 & 0 \\ 0 & -\frac{1}{2}\dot{\epsilon} & 0 \\ 0 & 0 & \dot{\epsilon} \end{bmatrix}. \tag{3.11}$$

The latter relation reveals that the shear stress T_{rz} vanishes throughout the sample.

Now it is clear that our choice of the velocity field (3.7) under above considerations naturally satisfies all the conditions (2.42a), (2.43), (2.44), and also the relation on the right hand side in (2.45). On top of that, we can express governing equations (2.41b) and (2.41c) in the form

$$\frac{\partial p}{\partial r} = -\dot{\epsilon}\hat{\alpha}\frac{\partial p}{\partial r}e^{\hat{\alpha}p}, \tag{3.12}$$

$$\frac{\partial p}{\partial z} = 2\dot{\epsilon}\hat{\alpha}\frac{\partial p}{\partial z}e^{\hat{\alpha}p}. \tag{3.13}$$

It is obvious that p has to be homogeneously distributed throughout the sample (it cannot depend on spatial variables r and z), nevertheless, it changes with time. Boundary condition in (2.45) on the left is usually used to determine pressure values. Unfortunately, in our case we have

$$\mathrm{T}_{rr} = -p - \dot{\epsilon}e^{\hat{\alpha}p} = 0. \tag{3.14}$$

It means that p is defined implicitly by the relation $g(t,p) = 0$, where

$$g(t,p) =_{\text{def}} -p - \dot{\epsilon}(t)e^{\hat{\alpha}p} \tag{3.15}$$

is continuously differentiable on an open set $\mathbf{S_1} \times \mathbf{S_2} \subset \mathbb{R}^2$, with $[0, t_{\text{end}}] \subset \mathbf{S_1}$[3]. Let $p_\star \in \mathbf{S_2}$ satisfies

$$g(0,p_\star) = 0, \quad \text{and} \quad \frac{\partial g}{\partial p}(0,p_\star) \neq 0. \tag{3.16}$$

[3]To avoid discontinuity of $\dot{\epsilon}$ we suppose that $\sup \mathbf{S_1} < t_{\text{cl}}$, where t_{cl} is the time needed to close the gap between plates.

Then, according to well-known *implicit function theorem*[4], there is a neighborhood $\mathbf{U}$ of $t = 0$ in $\mathbb{R}$ on which is defined a unique continuously differentiable function $p : \mathbf{U} \longrightarrow \mathbb{R}$ such that $p(0) = p_\star,$ and $g(t, p(t)) = 0,\ t \in \mathbf{U}$. Moreover,

$$\dot{p}(t) = -\frac{\ddot{\epsilon}(t)}{1 + \hat{\alpha}\dot{\epsilon}(t)e^{\hat{\alpha}p(t)}} e^{\hat{\alpha}p(t)}, \quad t \in \mathbf{U}. \tag{3.17}$$

In what follows we shall verify conditions in (3.16) for two different settings depending on the choice of h, see (2.38) and (2.39).

- Considering the case with constant closure speed, and so with h defined by (2.38), we have $\dot{\epsilon}(0) = -1$ and we seek p satisfying

  $$-p + e^{\hat{\alpha}p} = 0.$$

  Since $\hat{\alpha} > 0$, the latter equation can be satisfied only for some $p > 1$.

  Let us suppose that $\hat{\alpha} \in (0, e^{-1})$. We consider a function $w : (0, \infty) \longrightarrow (0, \infty)$ given by $w(x) = x^{-1} \ln x$, which is monotonically increasing on the interval $(1, e)$ and maps this interval onto $(0, e^{-1})$. It means that for each $\hat{\alpha} \in (0, e^{-1})$ there exists $p_\star \in (1, e)$ such that

  $$\hat{\alpha} = w(p_\star) = \frac{\ln p_\star}{p_\star}.$$

  The latter relationship between $\hat{\alpha}$ and $p_\star$ at the same time implies $e^{\hat{\alpha}p_\star} = e^{\ln p_\star} = p_\star$, thus

  $$g(0, p_\star) = 0$$

  and

  $$\frac{\partial g}{\partial p}(0, p_\star) = -1 + \hat{\alpha}e^{\hat{\alpha}p_\star} = -1 + \ln p_\star \neq 0.$$

  Using (3.17) we see that

  $$\dot{p}(0) = \frac{p_\star}{1 - \ln p_\star} > 1.$$

  It is worth noting that for an incompressible Navier-Stokes fluid one gets $p(t) = -\dot{\epsilon}(t)$, which gives $p(0) = \dot{p}(0) = 1$. It follows that for the fluid with pressure-dependent viscosity the initial pressure value together with the corresponding rate of change are larger.

- Now let $\dot{\epsilon}$ is defined using h given by (2.39). Then we have $\dot{\epsilon}(0) = 0$ and conditions in (3.16) hold for $p_\star = 0$. Unfortunately, in this case with smooth start-up we have $p(0) = \dot{p}(0) = 0$, which coincides with values of the solution for the Navier-Stokes fluid. Therefore, the observation similar to that in the previous case is not explicitly available this time.

In order to express p as a function of t at least approximately, we shall use the perturbation method as described above.

[4] See for example Rudin (1976) or any other book on mathematical analysis.

As we have already mentioned, normal force exerted on plates by the sample is usually measured in experiments with prescribed compression. The force exerted on the upper plate is defined as

$$F(t) = -2\pi \int_0^{\xi(h,t)} r\mathrm{T}_{zz}(r,h,t)\,\mathrm{d}r. \tag{3.18}$$

Actual radius ξ was computed in (3.9). Supposing that p is an exact solution satisfying (3.14), we have

$$F = -2\pi \int_0^{\xi} \left(-p + 2\dot{\epsilon}e^{\hat{\alpha}p}\right) r\,\mathrm{d}r = \frac{3p}{h}\hat{A}_0, \tag{3.19}$$

with $\hat{A}_0 = \pi\hat{R}_0^2$ denoting the dimensionless form of initial contact area.

3.1.1 Zeroth-order subproblem

We solve the system of equations (3.5) with boundary conditions

$$\begin{aligned} v_{z,0}\big|_{z=h} &= \dot{h}, & v_{r,0}\big|_{r=0} &= 0, & v_{z,0}\big|_{z=0} &= 0, \\ \mathrm{T}_{rz,0}\big|_{z=h} &= 0, & \mathrm{T}_{rz,0}\big|_{r=0} &= 0, & \mathrm{T}_{rz,0}\big|_{z=0} &= 0. \end{aligned}$$

Supposing that the free surface remains vertical during the compression, we seek a solution which further satisfies

$$\mathrm{T}_{rr,0}\big|_{r=\xi} = 0, \qquad \mathrm{T}_{rz,0}\big|_{r=\xi} = 0.$$

Using velocity components

$$v_{r,0} = -\frac{1}{2}\dot{\epsilon}r, \qquad v_{z,0} = \dot{\epsilon}z \tag{3.20}$$

in equations (3.5b) and (3.5c) we can see that

$$\frac{\partial p_0}{\partial r} = \frac{\partial p_0}{\partial z} = 0.$$

According to (3.4a) we have $\mathrm{T}_{rr,0} = -p_0 - \dot{\epsilon}$. Thus, the corresponding boundary condition on the free surface provides

$$p_0 = -\dot{\epsilon}. \tag{3.21}$$

Finally, relation (3.19) yields

$$F_0 = -\frac{3\dot{\epsilon}}{h}\hat{A}_0. \tag{3.22}$$

3.1.2 First-order subproblem

In the sense of previous discussion we shall seek a solution of the system (3.6) satisfying boundary conditions

$$\begin{aligned} v_{z,1}\big|_{z=h} &= 0, & v_{r,1}\big|_{r=0} &= 0, & v_{z,1}\big|_{z=0} &= 0, \\ \mathrm{T}_{rz,1}\big|_{z=h} &= 0, & \mathrm{T}_{rz,1}\big|_{r=0} &= 0, & \mathrm{T}_{rz,1}\big|_{z=0} &= 0, \end{aligned}$$

and

$$\mathrm{T}_{rr,1}\big|_{r=\xi} = 0, \qquad \mathrm{T}_{rz,1}\big|_{r=\xi} = 0.$$

Our choice of the velocity field (3.7) implies

$$v_{r,1} = 0, \qquad v_{z,1} = 0. \tag{3.23}$$

Substituting these velocity components, together with (3.20) and (3.21), into equations (3.6b) and (3.6c) one obtains

$$\frac{\partial p_1}{\partial r} = \frac{\partial p_1}{\partial z} = 0.$$

An analogy of previous relations is obviously true also for higher order subproblems, hence our statement that pressure is homogeneously distributed throughout the sample seems to be confirmed also in this way. Pressure p_1 is simply determined using the boundary condition

$$\mathrm{T}_{rr,1}\big|_{r=\xi} = -p_1 - p_0\dot{\epsilon} = 0,$$

which yields

$$p_1 = \dot{\epsilon}^{\,2}. \tag{3.24}$$

3.1.3 Results and discussion

In the sense of (3.1) we see that

$$p \approx p_0 + p_1\hat{\alpha} = \frac{\dot{h}}{h}\left(\hat{\alpha}\frac{\dot{h}}{h} - 1\right) \tag{3.25}$$

is a rough estimate of pressure values. Substituting the latter result into (3.19), we obtain an estimate for the normal force

$$F \approx \frac{3\dot{h}}{h^2}\left(\hat{\alpha}\frac{\dot{h}}{h} - 1\right)\hat{A}_0. \tag{3.26}$$

Our calculations were based on the assumption that the velocity field (3.7), corresponding to homogeneous biaxial extension, is the same as for the Navier-Stokes fluid (see Figure 5). This seems to be reasonable as we have perfect-slip at the interface, materials in question are incompressible and the compression is prescribed. It follows that

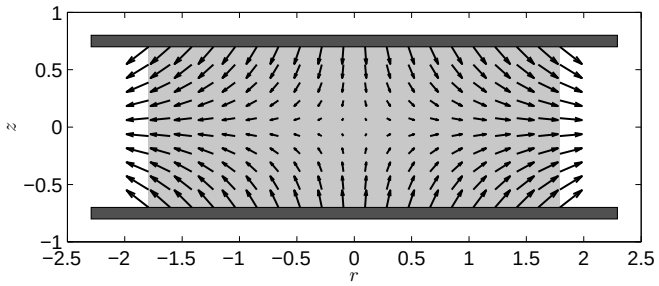

Figure 5: Dimensionless velocity field (3.7) for squeeze flow with perfect-slip at $t = 0.3$. Computed for $h(t) = 1 - t$, $\hat{R}_0 = 1.5$. Vectors are scaled by a factor of 0.15.

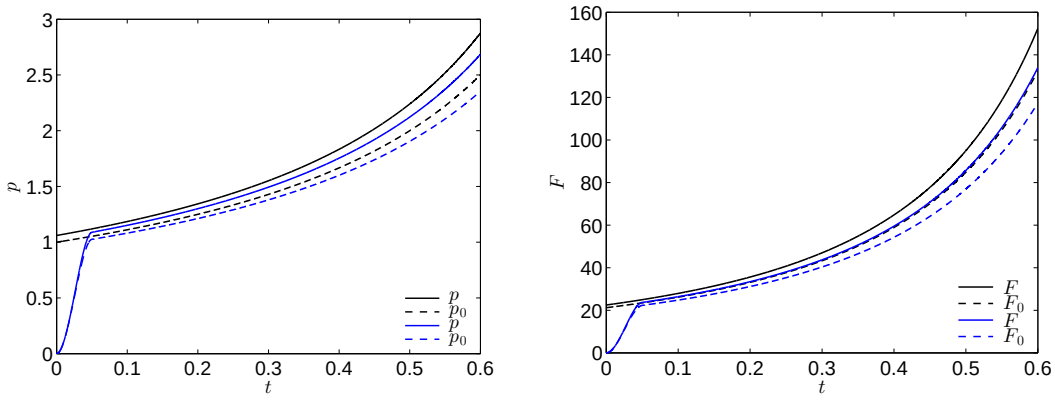

(a) p_0 given by (3.21); p given by (3.25). **(b)** F_0 given by (3.22); F given by (3.26).

Figure 6: Dimensionless pressure and force in perfect-slip squeeze flow, computed for $\hat{\alpha} = 0.06$, $t_0 = 0.05$, $\hat{R}_0 = 1.5$, $t_{\text{end}} = 0.6$. Black lines are solutions for constant closure speed, see (2.38), blue lines correspond to smooth start-up (2.39).

a current shape of the sample cannot be influenced by the pressure-dependent viscosity, which is in accordance with the fact that the pressure, and hence also the viscosity, is homogeneously distributed throughout the sample (as we shall see, this is not true in the case with no-slip anymore). On the other hand, the viscosity increasing with pressure causes that the specimen becomes somehow more stiff, and force exerted by the fluid on the plate has to dominate over the same force computed for the Navier-Stokes fluid. Results are mutually compared in Figure 6.

3.2 No-slip at the sample-plate interface

A common approach used in order to get some analytical solutions of the no-slip squeeze flow is based on the postulate which says that *planes initially normal to the direction of loading remain plane in the deformed state*. Of course, this additional requirement is followed by the fact that instead of the original problem, given by (2.41), (2.42b) and (2.43) – (2.46), we shall solve kind of its approximation, which is justifiable particularly at the very beginning of the experiment (supposing the flow starts from the rest) and/or in the case in which the sample radius is much larger than its initial height.

By virtue of the mentioned postulate, velocity component v_z cannot depend on r and so we shall assume

$$v_z(z,t) = \dot{h}(t)\phi(z,t).$$

Using the incompressibility condition (2.41a) together with the first condition in (2.43), one obtains corresponding radial velocity component as a solution of the boundary value problem

$$\frac{\partial}{\partial r}(rv_r) = -\dot{h}r\phi', \qquad v_r\big|_{r=0} = 0,$$

where the differentiation of ϕ with respect to z is denoted by prime. This yields

$$v_r(r,z,t) = -\frac{1}{2}\dot{h}(t)r\phi'(z,t).$$

In the previous paragraph we have seen that the perturbation method can provide satisfactory results using the expansion up to the first order. Under above considerations we shall suppose the velocity field of the form

$$\boldsymbol{v} = \begin{bmatrix} -\frac{1}{2}\dot{h}r\phi' \\ 0 \\ \dot{h}\phi \end{bmatrix} = \begin{bmatrix} -\frac{1}{2}\dot{h}r\left(\phi_0' + \phi_1'\hat{\alpha}\right) + O(\hat{\alpha}^2) \\ 0 \\ \dot{h}\phi_0 + \dot{h}\phi_1\hat{\alpha} + O(\hat{\alpha}^2) \end{bmatrix}. \tag{3.27}$$

Let us remark that the velocity field (3.7) for the perfect-slip squeeze flow simply corresponds to the choice $\phi(z,t) = \frac{z}{h(t)}$.

3.2.1 Zeroth-order subproblem

At this point we shall forget boundary conditions in (2.45) for a moment and we shall seek a solution of the system (3.5) satisfying

$$\begin{aligned} v_{z,0}\big|_{z=h} &= \dot{h}, & v_{r,0}\big|_{r=0} &= 0, & v_{z,0}\big|_{z=0} &= 0, \\ v_{r,0}\big|_{z=h} &= 0, & \mathrm{T}_{rz,0}\big|_{r=0} &= 0, & \mathrm{T}_{rz,0}\big|_{z=0} &= 0. \end{aligned}$$

According to (3.27) we consider $v_{r,0} = -\frac{1}{2}\dot{h}r\phi_0'$, $v_{z,0} = \dot{h}\phi_0$ with the corresponding symmetric part of the velocity gradient

$$\mathbb{D}_0 = \frac{\dot{h}}{2}\begin{bmatrix} -\phi_0' & 0 & -\frac{1}{2}r\phi_0'' \\ 0 & -\phi_0' & 0 \\ -\frac{1}{2}r\phi_0'' & 0 & 2\phi_0' \end{bmatrix}. \tag{3.28}$$

Governing equations (3.5b) and (3.5c) yield

$$\frac{\partial p_0}{\partial r} = -\frac{1}{2}\dot{h}r\phi_0''', \tag{3.29}$$

$$\frac{\partial p_0}{\partial z} = \dot{h}\phi_0''. \tag{3.30}$$

Let us suppose that $t \in [0, t_{\mathrm{end}}]$ is fixed for a moment. Through the compatibility of mixed (second order) derivatives of p_0 one gets the ordinary differential equation

$$\phi_0^{(4)}(z,t) = 0. \tag{3.31}$$

An appropriate set of boundary conditions for the latter equation is obtained from the velocity boundary conditions at the sample-plate interface and central plane. It reads

$$\phi_0\big|_{z=h} = \dot{h}, \qquad \phi_0'\big|_{z=h} = 0, \tag{3.32}$$

$$\phi_0\big|_{z=0} = 0, \qquad \phi_0''\big|_{z=0} = 0. \tag{3.33}$$

It remains to carry out some basic calculus in order to get the solution

$$\phi_0 = \frac{z}{2h}\left(3 - \frac{z^2}{h^2}\right), \tag{3.34}$$

which is time dependent through $h(t)$. The latter relation results in velocity components

$$v_{r,0} = \frac{3r}{4h}\left(\frac{z^2}{h^2} - 1\right)\dot{h}, \qquad v_{z,0} = \frac{z}{2h}\left(3 - \frac{z^2}{h^2}\right)\dot{h}. \tag{3.35}$$

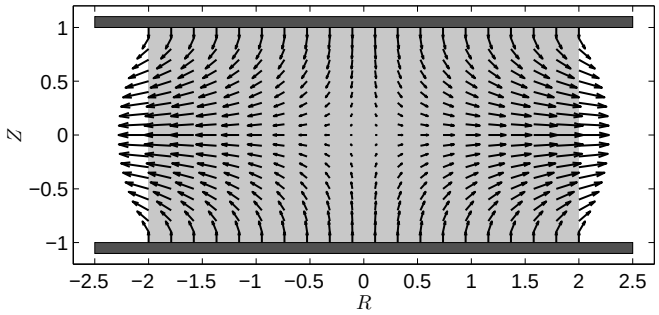

Figure 7: Dimensionless velocity field (3.35) mapped into the reference coordinate system $\{R, Z\}$ for the no-slip squeeze flow at $t = 0.3$. Computed for $h(t) = 1 - t$, $\hat{R}_0 = 2$. Vectors are scaled by a factor of 0.1.

In contrast to the perfect-slip setting, one can see that the shear rate $\mathrm{D}_{rz,0}$ in (3.28) is no longer zero and distribution of the shear stress $\mathrm{T}_{rz,0}$ throughout the sample is depicted in Figure 9c. Further, integration of equations (3.29) and (3.30) yields

$$p_0 = \frac{3\dot{h}}{4h}\left(\frac{r^2}{h^2} - \frac{2z^2}{h^2}\right) + C_0, \tag{3.36}$$

where constant of integration C_0 is generally time-dependent and has to be determined using an appropriate boundary condition on the free surface (see the discussion below). Normal force defined by (3.18) is given through

$$F_0 = \frac{3\dot{h}}{2h}\left(\frac{\hat{R}_0^2}{4h^2} - 1\right)\hat{A}_0 + C_0\hat{A}_0. \tag{3.37}$$

3.2.2 First-order subproblem

Following the established procedure, we shall solve the system of equations (3.6) with boundary conditions

$$\begin{aligned} &v_{z,1}\big|_{z=h} = 0, && v_{r,1}\big|_{r=0} = 0, && v_{z,1}\big|_{z=0} = 0, \\ &v_{r,1}\big|_{z=h} = 0, && \mathrm{T}_{rz,1}\big|_{r=0} = 0, && \mathrm{T}_{rz,1}\big|_{z=0} = 0. \end{aligned}$$

As in the previous case, mixed second order derivatives of p_1 can be obtained from (3.6b) and (3.6c), this time in the form

$$\frac{\partial^2 p_1}{\partial z \partial r} = -\frac{1}{2}\dot{h} r \phi_1^{(4)} - \frac{9rz\,\dot{h}^2}{h^6}, \tag{3.38}$$

$$\frac{\partial^2 p_1}{\partial r \partial z} = 0. \tag{3.39}$$

Through compatibility of these derivatives, we get the ordinary differential equation

$$\phi_1^{(4)}(z,t) = -18\frac{\dot{h}(t) z}{h(t)^6}, \tag{3.40}$$

again with t fixed for a moment. One can integrate the latter equation using boundary conditions

$$\phi_1\big|_{z=h} = 0, \qquad \phi_1\big|_{z=0} = 0, \tag{3.41}$$

$$\phi_1'\big|_{z=h} = 0, \qquad \phi_1''\big|_{z=0} = 0. \tag{3.42}$$

Corresponding solution reads

$$\phi_1 = -\frac{3z}{20h^2}\left(\left(\frac{z}{h}\right)^4 - 2\left(\frac{z}{h}\right)^2 + 1\right)\dot{h}. \tag{3.43}$$

This further yields velocity components

$$v_{r,1} = \frac{3r}{40h^2}\left(5\left(\frac{z}{h}\right)^4 - 6\left(\frac{z}{h}\right)^2 + 1\right)\dot{h}^2, \quad v_{z,1} = -\frac{3z}{20h^2}\left(\left(\frac{z}{h}\right)^4 - 2\left(\frac{z}{h}\right)^2 + 1\right)\dot{h}^2, \tag{3.44}$$

and pressure contribution p_1 is calculated to be

$$p_1 = \frac{3\dot{h}^2}{32h^6}\left(3r^4 + 28z^4\right) - \frac{9\dot{h}^2}{40h^4}\left(7r^2 + 16z^2\right) + \frac{3\dot{h}}{4h^3}\left(r^2 - 2z^2\right)C_0 + C_1, \tag{3.45}$$

with C_0 and C_1 being time-dependent. First-order contribution F_1 to the normal force $F = F_0 + F_1\hat{\alpha} + O(\hat{\alpha}^2)$ is determined using the definition (3.18), which yields

$$F_1 = \frac{3\dot{h}\hat{R}_0^2}{8h^3}\left(\frac{\dot{h}\hat{R}_0^2}{4h^3} - \frac{7\dot{h}}{10h} + C_0\right)\hat{A}_0 - \frac{3\dot{h}}{2h}\left(\frac{13\dot{h}}{20h} + C_0\right)\hat{A}_0 + C_1\hat{A}_0. \tag{3.46}$$

3.2.3 Results and discussion

Velocity components obtained using the perturbation expansion up to the first order are

$$v_r \approx \frac{3r}{4h}\left(\left(\frac{z}{h}\right)^2 - 1\right)\dot{h} + \frac{3r}{40h^2}\left(5\left(\frac{z}{h}\right)^4 - 6\left(\frac{z}{h}\right)^2 + 1\right)\hat{\alpha}\dot{h}^2, \tag{3.47a}$$

$$v_z \approx \frac{z}{2h}\left(3 - \left(\frac{z}{h}\right)^2\right)\dot{h} - \frac{3z}{20h^2}\left(\left(\frac{z}{h}\right)^4 - 2\left(\frac{z}{h}\right)^2 + 1\right)\hat{\alpha}\dot{h}^2. \tag{3.47b}$$

Let us examine first order contributions to the velocity components given in (3.44). There are some polynomial functions in one variable $x = \frac{z}{h}$, which extends from zero to one. These polynomials are shown in Figure 8a and 8b. It is clear that v_r in (3.47a) is faster (compared to $v_{r,0}$) near the central plane, and on the contrary slower in the upper half within the region of our interest. Similarly, v_z in (3.47b) is a little bit faster mainly in the middle of the computational domain (compared to $v_{z,0}$). These subtle differences captured on the free surface are shown in Figure 8c (parameter $\hat{\alpha}$ was chosen quite large to make the differences visible).

Pressure values $p \approx p_0 + p_1\hat{\alpha}$ are determined except for constants of integration C_0 and C_1, see (3.36), (3.45). In our calculation we have omitted boundary conditions in (2.45) which are inappropriate to be used with the assumed form of the solution.

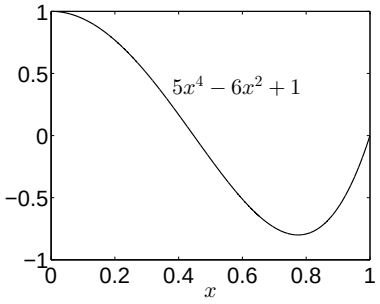

(a) Contribution to v_r.

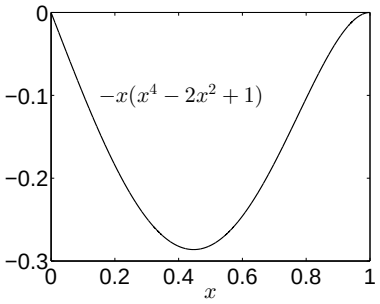

(b) Contribution to v_z.

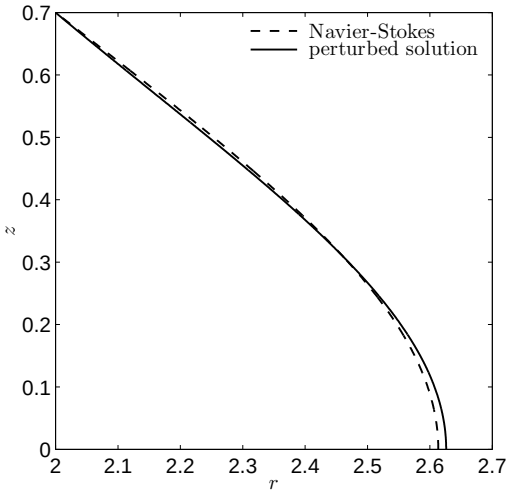

(c) Upper half of the free surface profiles in dimensionless variables; $t = 0.3$, $\hat{R}_0 = 2$, $\hat{\alpha} = 0.15$.

Figure 8: Polynomial functions in one variable $x = \frac{z}{h}$ appearing on right-hand sides of expressions in (3.44), and free surface profiles obtained for the fluid with pressure-dependent viscosity and the classical Navier-Stokes fluid respectively.

We shall need another assumption for the pressure boundary condition in order to determine mentioned constants. Usually, the z-averaged pressure at the free surface,

$$<p> = \frac{1}{h(t)} \int_0^{h(t)} p(\xi(z,t), z, t)\, \mathrm{d}z,$$

is required to be equal to the ambient pressure at every time instant t. Another possibility is to fix the pressure value at some particular point on the free surface. Here we have used[5]

$$p(\xi(0,t), 0, t) = 0. \tag{3.48}$$

It is necessary to bear in mind that we may introduce an additional error to the solution in this case.

[5]More precisely, for the classical Navier-Stokes solution (equivalent to solution for the zeroth-order subproblem), one has to use (3.48) with $p = p_0$ and ξ satisfying $\dot{\xi}(0,t) = v_{r,0}(\xi(0,t),0,t)$. This yields

$$C_0 = -\frac{3\dot{h}}{4h^{\frac{9}{2}}}\hat{R}_0^2.$$

Similarly, for the perturbed solution one has to use the same condition with $p = p_0 + \hat{\alpha}p_1$ and ξ satisfying $\dot{\xi}(0,t) = v_r(\xi(0,t),0,t)$, for v_r given by (3.47a). In this case we have

$$C_0 = -\frac{3\dot{h}\xi^2}{4h^3}, \qquad C_1 = \frac{1}{2}C_0^2 - \frac{21\dot{h}}{10h}C_0.$$

Remark: ξ in the latter relation can be obtained explicitly for the setting with constant closure speed, see (2.38), and it reads

$$\xi = \hat{R}_0 h^{-\frac{3}{4}} e^{\frac{3\hat{\alpha}}{40}(\frac{1}{h}-1)}.$$

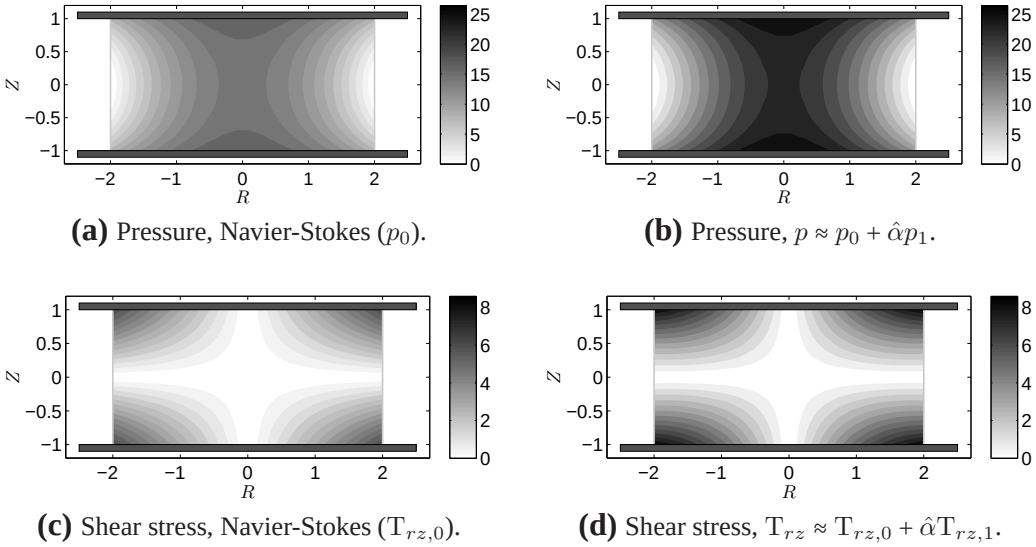

(a) Pressure, Navier-Stokes (p_0).

(b) Pressure, $p \approx p_0 + \hat{\alpha} p_1$.

(c) Shear stress, Navier-Stokes ($\mathrm{T}_{rz,0}$).

(d) Shear stress, $\mathrm{T}_{rz} \approx \mathrm{T}_{rz,0} + \hat{\alpha}\mathrm{T}_{rz,1}$.

Figure 9: Dimensionless pressure field and shear stress distribution in no-slip squeeze flow at $t = 0.3$, computed for $h(t) = 1 - t$, $\hat{R}_0 = 2$, $\hat{\alpha} = 0.05$. Everything is mapped into the reference coordinate system $\{R, Z\}$.

Pressure fields for the classical Navier-Stokes solution and for the perturbed solution are compared in Figure 9, as well as the distribution of the shear stress throughout the sample. As one would expect, the sample becomes "locally" more stiff, which seems to be promising for the numerical simulation. One can notice significant differences between pressure values (located in the center of the plate) and corresponding normal forces in Figure 10.

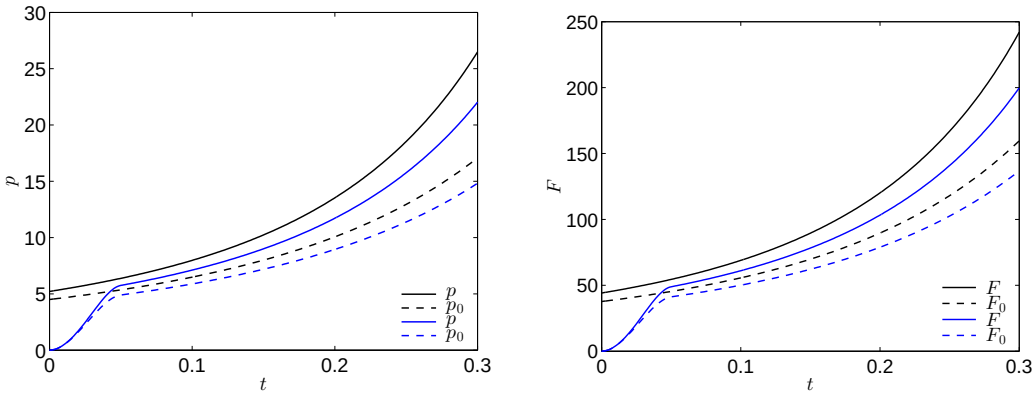

(a) p_0 given by (3.36); $p \approx p_0 + p_1\hat{\alpha}$ with p_1 from (3.45).

(b) F_0 given by (3.37); $F \approx F_0 + F_1\hat{\alpha}$ with F_1 from (3.46).

Figure 10: Dimensionless pressure in the center of the plate and corresponding normal force, both in no-slip squeeze flow, computed for $\hat{\alpha} = 0.05$, $t_0 = 0.05$, $\hat{R}_0 = 2$, $t_{\text{end}} = 0.3$. Black lines are solutions for constant closure speed, see (2.38), blue lines correspond to smooth start-up (2.39).

4. Numerical simulation for the no-slip squeeze flow

In this chapter we would like to solve the no-slip squeeze flow problem in its full version as stated in Section 2.2.5. We forget the postulate about non-deforming horizontal planes and we want to employ no traction (2.45) on the free surface as well as the kinematic condition (2.46).

As we have already seen, in the no-slip squeeze flow a certain part of the boundary of the domain is not known in advance and has to be determined as a part of the solution. There are several techniques for solving free boundary problems, see for example Crank (1987). We shall describe a numerical method based on the application of *body-fitted curvilinear coordinates*, which conceptually belongs to the family of so called "front-fixing methods", and on the application of a *spectral collocation method*.

4.1 Reformulation of the problem

Let Ω_t denotes the dimensionless version of the domain occupied by the sample in the rz-plane using the coordinate system introduced in Section 2.2.1. It means[1]

$$\Omega_t = \{(r,z) : z \in [-h(t), h(t)], r \in [-\xi(z,t), \xi(z,t)]\}. \tag{4.1}$$

Free boundary is simply described as $r = \pm\,\xi(z,t)$. Supposing we know its shape at any fixed t, we can construct a *bivariate blending function*[2] $U : \bar{\Omega} \longrightarrow \Omega_t$ which maps the fixed domain $\bar{\Omega}$, corresponding to image of rectangle $[-1,1] \times [-1,1]$, onto Ω_t in physical space, see Figure 11. We define U and U^{-1} to be

$$U : \begin{bmatrix} \bar{r} \\ \bar{z} \end{bmatrix} \longmapsto \begin{bmatrix} r \\ z \end{bmatrix} = \begin{bmatrix} \bar{r}\bar{\xi}(\bar{z},t) \\ \bar{z}h(t) \end{bmatrix}, \qquad U^{-1} : \begin{bmatrix} r \\ z \end{bmatrix} \longmapsto \begin{bmatrix} \bar{r} \\ \bar{z} \end{bmatrix} = \begin{bmatrix} \frac{r}{\xi(z,t)} \\ \frac{z}{h(t)} \end{bmatrix}, \tag{4.2}$$

with $\bar{\xi}(\bar{z},t) =_{\text{def}} \xi(\bar{z}h(t),t)$. The mapping is constructed in such a way that it maintains both axes of symmetry ($\bar{r} = 0$ and $\bar{z} = 0$ are mapped onto $r = 0$, $z = 0$ respectively).

The attraction of this method consists in the possibility of working in a fixed simple domain which corresponds to the moving region for all the time. In fact, transformation (4.2) provides suitable choice of new space coordinates $(\bar{r},\bar{z})$ which are commonly called *body-fitted* coordinates. Moving free surface $r = \pm\xi(z,t)$ is now fixed at $r = \pm 1$.

Apparent simplification of the problem is presently offset to some extent by the increased complexity of the transformed system of partial differential equations and boundary conditions. For an arbitrary function ω defined on Ω_t we shall use the notation

$$\omega(r,z,t) = \omega(\bar{r}\bar{\xi}(\bar{z},t), \bar{z}h(t), t) =_{\text{def}} \bar{\omega}(\bar{r},\bar{z},t) = \bar{\omega}\left(r\xi(z,t)^{-1}, zh(t)^{-1}, t\right). \tag{4.3}$$

[1] See (2.24) for comparison.

[2] For more information see Gordon and Hall (1973).

The system of governing equations (2.41) is then transformed[3] as follows,

$$0 = \frac{\partial \bar{v}_{\bar{r}}}{\partial \bar{r}} + \frac{\bar{v}_{\bar{r}}}{\bar{r}} + \frac{\bar{\xi}}{h}\frac{\partial \bar{v}_{\bar{z}}}{\partial \bar{z}} - \frac{\bar{r}}{h}\frac{\partial \bar{\xi}}{\partial \bar{z}}\frac{\partial \bar{v}_{\bar{z}}}{\partial \bar{r}}, \tag{4.4a}$$

$$\begin{aligned}\bar{\xi}\frac{\partial \bar{p}}{\partial \bar{r}} = e^{\hat{\alpha}\bar{p}}\Bigg[&\left(1+\left(\frac{\bar{r}}{h}\frac{\partial \bar{\xi}}{\partial \bar{z}}\right)^2\right)\frac{\partial^2 \bar{v}_{\bar{r}}}{\partial \bar{r}^2} - \frac{2\bar{r}\bar{\xi}}{h^2}\frac{\partial \bar{\xi}}{\partial \bar{z}}\frac{\partial^2 \bar{v}_{\bar{r}}}{\partial \bar{r}\partial \bar{z}} + \frac{\bar{\xi}^2}{h^2}\frac{\partial^2 \bar{v}_{\bar{r}}}{\partial \bar{z}^2} + \\ &+\left(\frac{1}{\bar{r}} - \frac{\bar{r}\bar{\xi}}{h^2}\frac{\partial^2 \bar{\xi}}{\partial \bar{z}^2} + \frac{2\bar{r}}{h^2}\left(\frac{\partial \bar{\xi}}{\partial \bar{z}}\right)^2\right)\frac{\partial \bar{v}_{\bar{r}}}{\partial \bar{r}} - \frac{\bar{v}_{\bar{r}}}{\bar{r}^2} + 2\hat{\alpha}\frac{\partial \bar{p}}{\partial \bar{r}}\frac{\partial \bar{v}_{\bar{r}}}{\partial \bar{r}} + \\ &+\hat{\alpha}\left(-\frac{\bar{r}}{h}\frac{\partial \bar{\xi}}{\partial \bar{z}}\frac{\partial \bar{p}}{\partial \bar{r}} + \frac{\bar{\xi}}{h}\frac{\partial \bar{p}}{\partial \bar{z}}\right)\left(-\frac{\bar{r}}{h}\frac{\partial \bar{\xi}}{\partial \bar{z}}\frac{\partial \bar{v}_{\bar{r}}}{\partial \bar{r}} + \frac{\bar{\xi}}{h}\frac{\partial \bar{v}_{\bar{r}}}{\partial \bar{z}} + \frac{\partial \bar{v}_{\bar{z}}}{\partial \bar{r}}\right)\Bigg],\end{aligned} \tag{4.4b}$$

$$\begin{aligned}\frac{\bar{\xi}}{h}\left(\bar{\xi}\frac{\partial \bar{p}}{\partial \bar{z}} - \bar{r}\frac{\partial \bar{\xi}}{\partial \bar{z}}\frac{\partial \bar{p}}{\partial \bar{r}}\right) = e^{\hat{\alpha}\bar{p}}\Bigg[&\left(1+\left(\frac{\bar{r}}{h}\frac{\partial \bar{\xi}}{\partial \bar{z}}\right)^2\right)\frac{\partial^2 \bar{v}_{\bar{z}}}{\partial \bar{r}^2} - \frac{2\bar{r}\bar{\xi}}{h^2}\frac{\partial \bar{\xi}}{\partial \bar{z}}\frac{\partial^2 \bar{v}_{\bar{z}}}{\partial \bar{r}\partial \bar{z}} + \\ &+\frac{\bar{\xi}^2}{h^2}\frac{\partial^2 \bar{v}_{\bar{z}}}{\partial \bar{z}^2} + \left(\frac{1}{\bar{r}} - \frac{\bar{r}\bar{\xi}}{h^2}\frac{\partial^2 \bar{\xi}}{\partial \bar{z}^2} + \frac{2\bar{r}}{h^2}\left(\frac{\partial \bar{\xi}}{\partial \bar{z}}\right)^2\right)\frac{\partial \bar{v}_{\bar{z}}}{\partial \bar{r}} + \\ &+\hat{\alpha}\frac{\partial \bar{p}}{\partial \bar{r}}\left(-\frac{\bar{r}}{h}\frac{\partial \bar{\xi}}{\partial \bar{z}}\frac{\partial \bar{v}_{\bar{r}}}{\partial \bar{r}} + \frac{\bar{\xi}}{h}\frac{\partial \bar{v}_{\bar{r}}}{\partial \bar{z}} + \frac{\partial \bar{v}_{\bar{z}}}{\partial \bar{r}}\right) + \\ &+2\hat{\alpha}\left(-\frac{\bar{r}}{h}\frac{\partial \bar{\xi}}{\partial \bar{z}}\frac{\partial \bar{p}}{\partial \bar{r}} + \frac{\bar{\xi}}{h}\frac{\partial \bar{p}}{\partial \bar{z}}\right)\left(-\frac{\bar{r}}{h}\frac{\partial \bar{\xi}}{\partial \bar{z}}\frac{\partial \bar{v}_{\bar{z}}}{\partial \bar{r}} + \frac{\bar{\xi}}{h}\frac{\partial \bar{v}_{\bar{z}}}{\partial \bar{z}}\right)\Bigg].\end{aligned} \tag{4.4c}$$

For further use let us denote

$$\boldsymbol{v} = \begin{bmatrix} v_r \\ v_z \end{bmatrix} = \begin{bmatrix} u \\ v \end{bmatrix}, \tag{4.5}$$

and

$$\bar{a} = \frac{1}{\bar{r}}, \qquad \bar{b} = \frac{\bar{\xi}}{h}, \qquad \bar{c} = -\frac{\bar{r}}{h}\frac{\partial \bar{\xi}}{\partial \bar{z}}, \qquad \bar{g} = -\frac{\bar{r}}{h}\frac{\partial^2 \bar{\xi}}{\partial \bar{z}^2}, \qquad \bar{q} = \frac{2\bar{r}}{h^2}\left(\frac{\partial \bar{\xi}}{\partial \bar{z}}\right)^2. \tag{4.6}$$

Equations (4.4) then can be rewritten in the compact form

$$0 = \frac{\partial \bar{u}}{\partial \bar{r}} + \bar{a}\bar{u} + \bar{b}\frac{\partial \bar{v}}{\partial \bar{z}} + \bar{c}\frac{\partial \bar{v}}{\partial \bar{r}}, \tag{4.7a}$$

$$\begin{aligned}h\bar{b}\frac{\partial \bar{p}}{\partial \bar{r}} = e^{\hat{\alpha}\bar{p}}\Bigg[&\left(1+\bar{c}^2\right)\frac{\partial^2 \bar{u}}{\partial \bar{r}^2} + 2\bar{b}\bar{c}\frac{\partial^2 \bar{u}}{\partial \bar{r}\partial \bar{z}} + \bar{b}^2\frac{\partial^2 \bar{u}}{\partial \bar{z}^2} + \\ &+\left(\bar{a}+\bar{g}+\bar{q}\right)\frac{\partial \bar{u}}{\partial \bar{r}} - \bar{a}^2\bar{u} + 2\hat{\alpha}\frac{\partial \bar{p}}{\partial \bar{r}}\frac{\partial \bar{u}}{\partial \bar{r}} + \\ &+\hat{\alpha}\left(\bar{c}\frac{\partial \bar{p}}{\partial \bar{r}} + \bar{b}\frac{\partial \bar{p}}{\partial \bar{z}}\right)\left(\bar{c}\frac{\partial \bar{u}}{\partial \bar{r}} + \bar{b}\frac{\partial \bar{u}}{\partial \bar{z}} + \frac{\partial \bar{v}}{\partial \bar{r}}\right)\Bigg],\end{aligned} \tag{4.7b}$$

$$\begin{aligned}h\bar{b}\left(\bar{b}\frac{\partial \bar{p}}{\partial \bar{z}} + \bar{c}\frac{\partial \bar{p}}{\partial \bar{r}}\right) = e^{\hat{\alpha}\bar{p}}\Bigg[&\left(1+\bar{c}^2\right)\frac{\partial^2 \bar{v}}{\partial \bar{r}^2} + 2\bar{b}\bar{c}\frac{\partial^2 \bar{v}}{\partial \bar{r}\partial \bar{z}} + \bar{b}^2\frac{\partial^2 \bar{v}}{\partial \bar{z}^2} + \\ &+\left(\bar{a}+\bar{g}+\bar{q}\right)\frac{\partial \bar{v}}{\partial \bar{r}} + \hat{\alpha}\frac{\partial \bar{p}}{\partial \bar{r}}\left(\bar{c}\frac{\partial \bar{u}}{\partial \bar{r}} + \bar{b}\frac{\partial \bar{u}}{\partial \bar{z}} + \frac{\partial \bar{v}}{\partial \bar{r}}\right) + \\ &+2\hat{\alpha}\left(\bar{c}\frac{\partial \bar{p}}{\partial \bar{r}} + \bar{b}\frac{\partial \bar{p}}{\partial \bar{z}}\right)\left(\bar{c}\frac{\partial \bar{v}}{\partial \bar{r}} + \bar{b}\frac{\partial \bar{v}}{\partial \bar{z}}\right)\Bigg].\end{aligned} \tag{4.7c}$$

[3] See Appendix B for detailed information on transformation rules.

Boundary condition in (2.42b) now has to be prescribed at both sample-plate interfaces. One can write them down in the form

$$\bar{v}\big|_{\bar{z}=\pm 1} = \pm\dot{h}, \qquad \bar{u}\big|_{\bar{z}=\pm 1} = 0. \tag{4.8a}$$

Similarly, dynamic boundary condition (2.45) has to be prescribed not only on the right-hand side of the domain but also on the opposite side. Its transformation yields

$$\left[-\bar{\xi}\bar{p} + e^{\hat{\alpha}\bar{p}}\left(2\frac{\partial\bar{u}}{\partial\bar{r}} - \frac{\bar{\xi}}{h^2}\frac{\partial\bar{\xi}}{\partial\bar{z}}\frac{\partial\bar{u}}{\partial\bar{z}} + \frac{\bar{r}}{h^2}\left(\frac{\partial\bar{\xi}}{\partial\bar{z}}\right)^2\frac{\partial\bar{u}}{\partial\bar{r}} - \frac{1}{h}\frac{\partial\bar{\xi}}{\partial\bar{z}}\frac{\partial\bar{v}}{\partial\bar{r}}\right)\right]_{\bar{r}=1} = 0, \tag{4.8b}$$

$$\left[\frac{\bar{\xi}}{h}\frac{\partial\bar{\xi}}{\partial\bar{z}}\,\bar{p} + e^{\hat{\alpha}\bar{p}}\left(\frac{\bar{\xi}}{h}\frac{\partial\bar{u}}{\partial\bar{z}} - \frac{\bar{r}}{h}\frac{\partial\bar{\xi}}{\partial\bar{z}}\frac{\partial\bar{u}}{\partial\bar{r}} + \frac{\partial\bar{v}}{\partial\bar{r}} - \right.\right.$$
$$\left.\left. - \frac{2\bar{\xi}}{h^2}\frac{\partial\bar{\xi}}{\partial\bar{z}}\frac{\partial\bar{v}}{\partial\bar{z}} + \frac{2\bar{r}}{h^2}\left(\frac{\partial\bar{\xi}}{\partial\bar{z}}\right)^2\frac{\partial\bar{v}}{\partial\bar{r}}\right)\right]_{\bar{r}=1} = 0, \tag{4.8c}$$

$$\left[\bar{\xi}\bar{p} + e^{\hat{\alpha}\bar{p}}\left(-2\frac{\partial\bar{u}}{\partial\bar{r}} - \frac{\bar{\xi}}{h^2}\frac{\partial\bar{\xi}}{\partial\bar{z}}\frac{\partial\bar{u}}{\partial\bar{z}} + \frac{\bar{r}}{h^2}\left(\frac{\partial\bar{\xi}}{\partial\bar{z}}\right)^2\frac{\partial\bar{u}}{\partial\bar{r}} - \frac{1}{h}\frac{\partial\bar{\xi}}{\partial\bar{z}}\frac{\partial\bar{v}}{\partial\bar{r}}\right)\right]_{\bar{r}=-1} = 0, \tag{4.8d}$$

$$\left[\frac{\bar{\xi}}{h}\frac{\partial\bar{\xi}}{\partial\bar{z}}\bar{p} + e^{\hat{\alpha}\bar{p}}\left(-\frac{\bar{\xi}}{h}\frac{\partial\bar{u}}{\partial\bar{z}} + \frac{\bar{r}}{h}\frac{\partial\bar{\xi}}{\partial\bar{z}}\frac{\partial\bar{u}}{\partial\bar{r}} - \frac{\partial\bar{v}}{\partial\bar{r}} - \right.\right.$$
$$\left.\left. - \frac{2\bar{\xi}}{h^2}\frac{\partial\bar{\xi}}{\partial\bar{z}}\frac{\partial\bar{v}}{\partial\bar{z}} + \frac{2\bar{r}}{h^2}\left(\frac{\partial\bar{\xi}}{\partial\bar{z}}\right)^2\frac{\partial\bar{v}}{\partial\bar{r}}\right)\right]_{\bar{r}=-1} = 0. \tag{4.8e}$$

Finally, kinematic condition (2.46) transformed in the same manner reads

$$\left(-\frac{\partial\bar{\xi}}{\partial t} + \bar{u} + \frac{1}{h}\left(\bar{z}\dot{h} - \bar{v}\right)\frac{\partial\bar{\xi}}{\partial\bar{z}}\right)\Big|_{\bar{r}=1} = 0. \tag{4.8f}$$

Let us remark that once the latter condition is satisfied, its analogy is automatically fulfilled on the opposite side of the domain boundary due to assumed symmetry of the solution.

4.2 Discretization of governing equations

We will seek a solution $(\bar{u},\ \bar{v},\ \bar{p},\ \bar{\xi})$ satisfying (4.7), (4.8) at discrete time levels and properly chosen discrete points in the domain $\bar{\Omega}$. The space discretization itself leads to the system of *differential algebraic equations* obtained from (4.7a) – (4.7c) and (4.8f). The time discretization is added in an effort to decouple the system in the sense that one gets the time update on $\bar{\xi}$ at first, using the discrete version of (4.8f), and after that it is possible to solve the discrete versions of equations in (4.7) to obtain relevant updates on $\bar{\boldsymbol{v}}$ and $\bar{p}$ respectively. This procedure gives rise to plenty of numerical schemes. One possibility is described below.

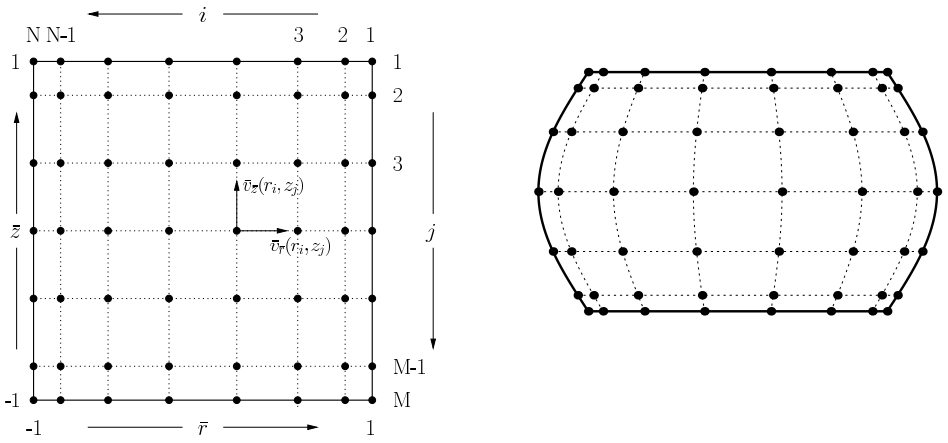

(a) Computational grid. **(b)** Grid in the physical space.

Figure 11: Computational grid and its mapping into the physical space.

4.2.1 Space discretization

General remarks

Let us suppose that $\bar{\xi}$ is known for a moment. The system of equations (4.7) subjected to boundary conditions (4.8a) – (4.8e) will be solved in the computational domain using a spectral collocation method. Computational grid in Figure 11a consists of Chebyshev collocation points

$$r_i = \cos\left(\frac{(i-1)\pi}{N-1}\right), \quad i = 1, \ldots, N, \tag{4.9a}$$

$$z_j = \cos\left(\frac{(j-1)\pi}{M-1}\right), \quad j = 1, \ldots, M. \tag{4.9b}$$

To these points we shall refer as to the *velocity collocation points* and sometimes we shall talk about the *velocity grid*. In fact, the points in (4.9) are extreme points of the Chebyshev polynomials $\mathrm{T}_{N-1}(\bar{r})$, of degree $N-1$, and $\mathrm{T}_{M-1}(\bar{z})$, of degree $M-1$. For detailed information about spectral methods see for example Trefethen (2000), Canuto et al. (2006).

To follow the notation used by Canuto et al. (2007), a staggered $\mathbb{Q}_N$–$\mathbb{Q}_{N-2}$ method is adopted here. It means that pressure values are considered on a coarser grid with KL collocation points ($K = N-2,\ L = M-2$)

$$r_i^* = \cos\left(\frac{(i-1)\pi}{K-1}\right), \quad i = 1, \ldots, K, \tag{4.10a}$$

$$z_j^* = \cos\left(\frac{(j-1)\pi}{L-1}\right), \quad j = 1, \ldots, L. \tag{4.10b}$$

In other words, the pressure will be approximated by polynomials of degree two orders lower (in each direction) than in the case of polynomials used to approximate the velocity. This time we talk about the *pressure collocation points* and the *pressure grid*.

In what follows we will use a shorthand notation $\omega_{i,j} = \bar{\omega}(r_i, z_j)$, $i = 1, \ldots, N,\ j = 1, \ldots M$, and $\omega^*_{i,j} = \bar{\omega}(r^*_i, z^*_j)$, $i = 1, \ldots, K,\ j = 1, \ldots L$, for values of function ω at the given grid point. Using the $\mathbb{Q}_N - \mathbb{Q}_{N-2}$ method ensures that it is enough to enforce the

divergence equation and the balance of linear momentum at all inner velocity collocation points. From this reason we will need to interpolate pressure values, as well as values of the pressure gradient, from the coarser grid to the finer grid. For differentiation we will use spectral differentiation matrices in the form given by Weideman and Reddy (2000).

Let $\mathbb{D}^{\bar{r},\,k;N\times N}$ denotes the Chebyshev spectral differentiation matrix corresponding to differentiation of order $k \in \mathbb{N}$ with respect to $\bar{r}$, and let $D_{i,j}^{\bar{r},\,k;N\times N}$ denotes its elements for $i = 1,\ldots,N,\ j = 1,\ldots M$. Using the matrices one can easy find derivatives, indeed,

$$\frac{\partial\bar{\omega}}{\partial\bar{r}}(r_i,z_j) = \sum_{k=1}^{N} D_{i,k}^{\bar{r},1;N\times N}\omega_{k,j}, \tag{4.11a}$$

$$\frac{\partial^2\bar{\omega}}{\partial\bar{r}^2}(r_i,z_j) = \sum_{k=1}^{N} D_{i,k}^{\bar{r},2;N\times N}\omega_{k,j}. \tag{4.11b}$$

Similarly, for differentiation with respect to $\bar{z}$ we use $\mathbb{D}^{\bar{z},1;M\times M}$, $\mathbb{D}^{\bar{z},2;M\times M}$ and we have

$$\frac{\partial\bar{\omega}}{\partial\bar{z}}(r_i,z_j) = \sum_{k=1}^{M} D_{j,k}^{\bar{z},1;M\times M}\omega_{i,k}, \tag{4.12a}$$

$$\frac{\partial^2\bar{\omega}}{\partial\bar{z}^2}(r_i,z_j) = \sum_{k=1}^{M} D_{j,k}^{\bar{z},2;M\times M}\omega_{i,k}. \tag{4.12b}$$

Now we can introduce the interpolation matrix $\mathbb{J}^{NM\times KL}$ (components $J_{i,j}^{NM\times KL}$, with $i = 1,\ldots,NM,\ j = 1,\ldots,KL$), which interpolates function values from the pressure grid to the velocity grid. In what follows we will appreciate the notation

$$\mathbf{P}_{\text{all}} = \left[\begin{array}{c} p_{1,1} \\ p_{2,1} \\ \vdots \\ \hline p_{N,1} \\ p_{1,2} \\ p_{2,2} \\ \vdots \\ \hline p_{N,2} \\ \vdots \\ \hline p_{1,M} \\ p_{2,M} \\ \vdots \\ p_{N,M} \end{array}\right], \qquad \mathbf{P} = \left[\begin{array}{c} p_{2,2} \\ p_{3,2} \\ \vdots \\ \hline p_{N-1,2} \\ p_{2,3} \\ p_{3,3} \\ \vdots \\ \hline p_{N-1,3} \\ \vdots \\ \hline p_{2,M-1} \\ p_{3,M-1} \\ \vdots \\ p_{N-1,M-1} \end{array}\right], \qquad \mathbf{P}^* = \left[\begin{array}{c} p^*_{1,1} \\ p^*_{2,1} \\ \vdots \\ \hline p^*_{K,1} \\ p^*_{1,2} \\ p^*_{2,2} \\ \vdots \\ \hline p^*_{K,2} \\ \vdots \\ \hline p^*_{1,L} \\ p^*_{2,L} \\ \vdots \\ p^*_{K,L} \end{array}\right] = \left[\begin{array}{c} p^*_{1} \\ p^*_{2} \\ \vdots \\ \hline p^*_{K} \\ p^*_{K+1} \\ p^*_{K+2} \\ \vdots \\ \hline p^*_{2K} \\ \vdots \\ \hline p^*_{K(L-1)+1} \\ p^*_{K(L-1)+2} \\ \vdots \\ p^*_{KL} \end{array}\right]. \tag{4.13}$$

Clearly, $\mathbb{J}^{NM\times KL}$ transforms $\mathbf{P}^*$ to $\mathbf{P}_{\text{all}}$, thus

$$\mathbf{P}_{\text{all}} = \mathbb{J}^{NM\times KL}\mathbf{P}^*, \tag{4.14a}$$

or in the component form

$$p_{i,j} = \sum_{k=1}^{KL} J_{i+(j-1)N,k}^{NM\times KL}\, p^*_k, \quad i = 1,\ldots,N,\ j = 1,\ldots,M. \tag{4.14b}$$

In order to determine particular values of the pressure gradient at velocity collocation points one has the following two possibilities:

A) First differentiate the pressure on the coarse grid and subsequently interpolate the derivatives to the velocity grid.

B) First interpolate the pressure values from the coarse grid and subsequently differentiate the "new" values on the velocity grid.

Let $\mathbb{G}_A^{\bar{r},1;NM\times KL}$ denotes the reinterpolated differentiation matrix corresponding to differentiation with respect to $\bar{r}$, which was obtained using the former approach. Similarly, $\mathbb{G}_B^{\bar{r},1;NM\times KL}$ denotes the same matrix obtained using the second option. In our code we combine the two approaches in effort to compensate an influence of the computer arithmetics. Therefore we use the reinterpolated differentiation matrix in the form (symmetrization trick)

$$\mathbb{G}^{\bar{r},1;NM\times KL} = \frac{1}{2}\left(\mathbb{G}_A^{\bar{r},1;NM\times KL} + \mathbb{G}_B^{\bar{r},1;NM\times KL}\right). \tag{4.15}$$

The notation $G_{i,j}^{\bar{r},1;NM\times KL}$, where $i = 1,\ldots,NM,\ j = 1,\ldots,KL$, is used for the components of the matrix, and relation

$$\left(\frac{\partial p}{\partial \bar{r}}\right)_{i,j} = \frac{\partial \bar{p}}{\partial \bar{r}}(r_i, z_j) = \sum_{k=1}^{KL} G_{i+(j-1)N,k}^{\bar{r},1;NM\times KL}\, p_k^* \tag{4.16a}$$

holds for every $i = 1,\ldots,N,\ j = 1,\ldots,M$. Of course, in the same manner we introduce $\mathbb{G}^{\bar{z},1;NM\times KL}$ corresponding to differentiation with respect to $\bar{z}$ and we have

$$\left(\frac{\partial p}{\partial \bar{z}}\right)_{i,j} = \frac{\partial \bar{p}}{\partial \bar{z}}(r_i, z_j) = \sum_{k=1}^{KL} G_{i+(j-1)N,k}^{\bar{z},1;NM\times KL}\, p_k^*. \tag{4.16b}$$

Getting the system of algebraic equations

Before we proceed with deriving the discrete version of the differential operator representing the problem, let us remind the values of the coefficients from (4.6) at particular collocation points (4.9). The assumption from the beginning of this paragraph, saying that $\bar{\xi}$ as a function of $\bar{z}$ is known, should be specified in the sense that we know its values ξ_j at z_j for $j = 1,\ldots,M$. This notation leads us to the expressions[4]

$$a_{i,j} = \frac{1}{r_i}, \tag{4.17a}$$

$$b_{i,j} = \frac{\xi_j}{h}, \tag{4.17b}$$

$$c_{i,j} = -\frac{r_i}{h}\sum_{k=1}^{M} D_{j,k}^{\bar{z},1;M\times M}\xi_k, \tag{4.17c}$$

$$g_{i,j} = -\frac{r_i}{h}\sum_{k=1}^{M} D_{j,k}^{\bar{z},2;M\times M}\xi_k, \tag{4.17d}$$

$$q_{i,j} = \frac{2r_i}{h^2}\left(\sum_{k=1}^{M} D_{j,k}^{\bar{z},1;M\times M}\xi_k\right)^2. \tag{4.17e}$$

Enforcing the divergence equation (4.7a) at all inner velocity collocation points (thus at points (r_i, z_j), where $i = 2,\ldots,N-1$ and $j = 2,\ldots,M-1$) gives

$$0 = \sum_{k=1}^{N} D_{i,k}^{\bar{r},1;N\times N} u_{k,j} + a_{i,j}u_{i,j} + b_{i,j}\sum_{k=1}^{M} D_{j,k}^{\bar{z},1;M\times M} v_{i,k} + c_{i,j}\sum_{k=1}^{N} D_{i,k}^{\bar{r},1;N\times N} v_{k,j}. \tag{4.18a}$$

[4]From (4.17a) it follows that N in (4.9a) must be even to avoid division by zero.

Using $p_{i,j}$ given by (4.14b) and $\left(\frac{\partial p}{\partial \bar{r}}\right)_{i,j}$, $\left(\frac{\partial p}{\partial \bar{z}}\right)_{i,j}$ from (4.16), the balance of linear momentum (4.7b), (4.7c) enforced at all inner velocity collocation points gives

$$
\begin{aligned}
hb_{i,j}\left(\frac{\partial p}{\partial \bar{r}}\right)_{i,j} = e^{\hat{\alpha}p_{i,j}}\Bigg[&\left(1+c_{i,j}^2\right)\sum_{k=1}^{N} D_{i,k}^{\bar{r},2;N\times N}u_{k,j} + \\
&+ 2b_{i,j}c_{i,j}\sum_{k=1}^{N} D_{i,k}^{\bar{r},1;N\times N}\left(\sum_{l=1}^{M} D_{j,l}^{\bar{z},1;M\times M}u_{k,l}\right) + b_{i,j}^2\sum_{k=1}^{M} D_{j,k}^{\bar{z},2;M\times M}u_{i,k} - a_{i,j}^2 u_{i,j} + \\
&+ \left(a_{i,j}+g_{i,j}+q_{i,j}\right)\sum_{k=1}^{N} D_{i,k}^{\bar{r},1;N\times N}u_{k,j} + 2\hat{\alpha}\left(\frac{\partial p}{\partial \bar{r}}\right)_{i,j}\sum_{k=1}^{N} D_{i,k}^{\bar{r},1;N\times N}u_{k,j} + \hat{\alpha}\Bigg(c_{i,j}\left(\frac{\partial p}{\partial \bar{r}}\right)_{i,j} + \\
&+ b_{i,j}\left(\frac{\partial p}{\partial \bar{z}}\right)_{i,j}\Bigg)\left(c_{i,j}\sum_{k=1}^{N} D_{i,k}^{\bar{r},1;N\times N}u_{k,j} + b_{i,j}\sum_{k=1}^{M} D_{j,k}^{\bar{z},1;M\times M}u_{i,k} + \sum_{k=1}^{N} D_{i,k}^{\bar{r},1;N\times N}v_{k,j}\right)\Bigg],
\end{aligned}
\tag{4.18b}
$$

for $\bar{r}$ component of the balance of linear momentum,

$$
\begin{aligned}
&hb_{i,j}\left(b_{i,j}\left(\frac{\partial p}{\partial \bar{z}}\right)_{i,j} + c_{i,j}\left(\frac{\partial p}{\partial \bar{r}}\right)_{i,j}\right) = \\
&= e^{\hat{\alpha}p_{i,j}}\Bigg[\left(1+c_{i,j}^2\right)\sum_{k=1}^{N} D_{i,k}^{\bar{r},2;N\times N}v_{k,j} + 2b_{i,j}c_{i,j}\sum_{k=1}^{N} D_{i,k}^{\bar{r},1;N\times N}\left(\sum_{l=1}^{M} D_{j,l}^{\bar{z},1;M\times M}v_{k,l}\right) + \\
&\qquad + b_{i,j}^2\sum_{k=1}^{M} D_{j,k}^{\bar{z},2;M\times M}v_{i,k} + \left(a_{i,j}+g_{i,j}+q_{i,j}\right)\sum_{k=1}^{N} D_{i,k}^{\bar{r},1;N\times N}v_{k,j} + \\
&+ \hat{\alpha}\left(\frac{\partial p}{\partial \bar{r}}\right)_{i,j}\left(c_{i,j}\sum_{k=1}^{N} D_{i,k}^{\bar{r},1;N\times N}u_{k,j} + b_{i,j}\sum_{k=1}^{M} D_{j,k}^{\bar{z},1;M\times M}u_{i,k} + \sum_{k=1}^{N} D_{i,k}^{\bar{r},1;N\times N}v_{k,j}\right) + \\
&+ 2\hat{\alpha}\left(c_{i,j}\left(\frac{\partial p}{\partial \bar{r}}\right)_{i,j} + b_{i,j}\left(\frac{\partial p}{\partial \bar{z}}\right)_{i,j}\right)\left(c_{i,j}\sum_{k=1}^{N} D_{i,k}^{\bar{r},1;N\times N}v_{k,j} + b_{i,j}\sum_{k=1}^{M} D_{j,k}^{\bar{z},1;M\times M}v_{i,k}\right)\Bigg],
\end{aligned}
\tag{4.18c}
$$

for $\bar{z}$ component of the balance of linear momentum.

The no-slip condition (4.8a) gives us the values of $\bar{\boldsymbol{v}}$ at the velocity collocation points at the sample-plate interfaces. Indeed, for $i = 1, \ldots, N$ we have

$$
v_{i,1} = v_{\text{top}} = \dot{h},\ v_{i,M} = v_{\text{bottom}} = -\dot{h},\ u_{i,1} = u_{i,M} = 0. \tag{4.19}
$$

Substituting (4.19) to (4.18) we get a final version of the discretized equations. At this point we have $(3N-2)(M-2)$ unknowns[5]. Unfortunately, so far we have found only $3(N-2)(M-2)$ equations presented in (4.18). In order to close the system of algebraic equations, it remains to introduce a discrete version of boundary conditions (4.8b) – (4.8e). For $j = 1, \ldots, M$ let us denote

$$
\xi'_j = \sum_{k=1}^{M} D_{j,k}^{\bar{z},1;M\times M}\xi_k. \tag{4.20}
$$

[5] $KL = (N-2)(M-2)$ unknown values for p at all pressure collocation points, and $2 * N(M-2)$ unknown values for u and v at all velocity collocation points except those situated on the boundaries corresponding to the sample-plate interfaces.

Enforcing the boundary conditions at appropriate collocation points (it means (r_1, z_j), (r_N, z_j), for $j = 2, \ldots, M-1$) we get another $4(M-2)$ equations in the form

$$-\xi_j p_{1,j} + e^{\hat{\alpha} p_{1,j}} \left(\left(2 + \left(\frac{\xi'_j}{h} \right)^2 \right) \sum_{k=1}^{N} D^{\bar{r},1;N\times N}_{1,k} u_{k,j} - \right.$$
$$\left. - \frac{\xi_j \xi'_j}{h^2} \sum_{k=1}^{M} D^{\bar{z},1;M\times M}_{j,k} u_{1,k} - \frac{\xi'_j}{h} \sum_{k=1}^{N} D^{\bar{r},1;N\times N}_{1,k} v_{k,j} \right) = 0, \quad (4.21a)$$

$$\frac{\xi_j \xi'_j}{h} p_{1,j} + e^{\hat{\alpha} p_{1,j}} \left(\frac{\xi_j}{h} \sum_{k=1}^{M} D^{\bar{z},1;M\times M}_{j,k} u_{1,k} - \frac{\xi'_j}{h} \sum_{k=1}^{N} D^{\bar{r},1;N\times N}_{1,k} u_{k,j} + \right.$$
$$\left. + \left(1 + 2 \left(\frac{\xi'_j}{h} \right)^2 \right) \sum_{k=1}^{N} D^{\bar{r},1;N\times N}_{1,k} v_{k,j} - \frac{2\xi_j \xi'_j}{h^2} \sum_{k=1}^{M} D^{\bar{z},1;M\times M}_{j,k} v_{1,k} \right) = 0, \quad (4.21b)$$

$$\xi_j p_{N,j} + e^{\hat{\alpha} p_{N,j}} \left(- \left(2 + \left(\frac{\xi'_j}{h} \right)^2 \right) \sum_{k=1}^{N} D^{\bar{r},1;N\times N}_{N,k} u_{k,j} - \right.$$
$$\left. - \frac{\xi_j \xi'_j}{h^2} \sum_{k=1}^{M} D^{\bar{z},1;M\times M}_{j,k} u_{N,k} - \frac{\xi'_j}{h} \sum_{k=1}^{N} D^{\bar{r},1;N\times N}_{N,k} v_{k,j} \right) = 0, \quad (4.21c)$$

$$\frac{\xi_j \xi'_j}{h} p_{N,j} + e^{\hat{\alpha} p_{N,j}} \left(-\frac{\xi_j}{h} \sum_{k=1}^{M} D^{\bar{z},1;M\times M}_{j,k} u_{N,k} - \frac{\xi'_j}{h} \sum_{k=1}^{N} D^{\bar{r},1;N\times N}_{N,k} u_{k,j} - \right.$$
$$\left. - \left(1 + 2 \left(\frac{\xi'_j}{h} \right)^2 \right) \sum_{k=1}^{N} D^{\bar{r},1;N\times N}_{N,k} v_{k,j} - \frac{2\xi_j \xi'_j}{h^2} \sum_{k=1}^{M} D^{\bar{z},1;M\times M}_{j,k} v_{N,k} \right) = 0. \quad (4.21d)$$

Notation

At first let us introduce some extra notation for various "subselections" from the differentiation matrix $\mathbb{D}^{\bar{r},1;N\times N}$ (of course, at the same time we introduce a parallel notation also for other matrices $\mathbb{D}^{\bar{r},2;N\times N}$, $\mathbb{D}^{\bar{z},1;M\times M}$ and $\mathbb{D}^{\bar{z},2;M\times M}$). Using the following schematic drawings,

$$\mathbb{D}^{\bar{r},1;N\times N} = \left[\begin{array}{c|c|c} D^{\bar{r},1;N\times N}_{1,1} & \cdots & D^{\bar{r},1;N\times N}_{1,N} \\ \hline \vdots & \tilde{\mathbb{D}}^{\bar{r},1;(N-2)\times(N-2)} & \vdots \\ \hline D^{\bar{r},1;N\times N}_{N,1} & \cdots & D^{\bar{r},1;N\times N}_{N,N} \end{array} \right], \quad (4.22a)$$

$$\mathbb{D}^{\bar{r},1;N\times N} = \left[\begin{array}{ccc} D^{\bar{r},1;N\times N}_{1,1} & \cdots & D^{\bar{r},1;N\times N}_{1,N} \\ \hline & \hat{\mathbb{D}}^{\bar{r},1;(N-2)\times N} & \\ \hline D^{\bar{r},1;N\times N}_{N,1} & \cdots & D^{\bar{r},1;N\times N}_{N,N} \end{array} \right]. \quad (4.22b)$$

it should be clear that $\tilde{\mathbb{D}}^{\bar{r},1;(N-2)\times(N-2)}$ is nothing but $\mathbb{D}^{\bar{r},1;N\times N}$ with removed first and last row and column, whereas $\hat{\mathbb{D}}^{\bar{r},1;(N-2)\times N}$ is $\mathbb{D}^{\bar{r},1;N\times N}$ with removed first and last row only. Symbols $\mathbf{D}^{\bar{z},1;1}$, $\mathbf{D}^{\bar{z},1;M}$ and $\mathbf{D}^{\bar{z},2;1}$, $\mathbf{D}^{\bar{z},2;M}$ are used for vectors consisting of the

first or last column of matrix $\hat{\mathbb{D}}^{\bar{z},1;(N-2)\times N}$ and $\hat{\mathbb{D}}^{\bar{z},2;(N-2)\times N}$ respectively. It means

$$\mathbf{D}^{\bar{z},1;1} = \begin{bmatrix} D_{2,1}^{\bar{z},1;M\times M} \\ D_{3,1}^{\bar{z},1;M\times M} \\ \vdots \\ D_{M-1,1}^{\bar{z},1;M\times M} \end{bmatrix}, \qquad \mathbf{D}^{\bar{z},1;M} = \begin{bmatrix} D_{2,M}^{\bar{z},1;M\times M} \\ D_{3,M}^{\bar{z},1;M\times M} \\ \vdots \\ D_{M-1,M}^{\bar{z},1;M\times M} \end{bmatrix}, \tag{4.23}$$

and similarly for the other matrix. On the other side, symbols $\mathbf{D}_1^{\bar{r},1}$, $\mathbf{D}_N^{\bar{r},1}$ are reserved for the first and last rows of matrix $\mathbb{D}^{\bar{r},1;N\times N}$,

$$\mathbf{D}_1^{\bar{r},1} = \left[D_{1,1}^{\bar{r},1;N\times N}, D_{1,2}^{\bar{r},1;N\times N}, \ldots, D_{1,N}^{\bar{r},1;N\times N}\right], \tag{4.24a}$$

$$\mathbf{D}_N^{\bar{r},1} = \left[D_{N,1}^{\bar{r},1;N\times N}, D_{N,2}^{\bar{r},1;N\times N}, \ldots, D_{N,N}^{\bar{r},1;N\times N}\right]. \tag{4.24b}$$

Further, for any fixed $n \in \mathbb{N}$ let us define the following operators: $\mathcal{M}_1 : \mathbb{R}^{NM\times n} \longrightarrow \mathbb{R}^{NL\times n}$ which removes first and last N rows in an arbitrary matrix from $\mathbb{R}^{NM\times n}$, and $\mathcal{M}_2 : \mathbb{R}^{KM\times n} \longrightarrow \mathbb{R}^{KL\times n}$ which takes a matrix from $\mathbb{R}^{NL\times n}$ and removes its rows with indices $1 + (k-1)N,\ kN$ for $k = 1, \ldots, L$. Using $\mathcal{M} = \mathcal{M}_2 \circ \mathcal{M}_1$ we introduce modified interpolation matrix

$$\tilde{\mathbb{J}}^{KL\times KL} = \mathcal{M}\left(\mathbb{J}^{NM\times KL}\right), \tag{4.25}$$

which gives the transformation rule (see (4.14a) for comparison)

$$\mathbf{P} = \tilde{\mathbb{J}}^{KL\times KL}\mathbf{P}^*. \tag{4.26}$$

Similarly, we introduce modified reinterpolated differentiation matrices (see (4.16))

$$\tilde{\mathbb{G}}^{\bar{r},1;KL\times KL} = \mathcal{M}\left(\mathbb{G}^{\bar{r},1;NM\times KL}\right), \qquad \tilde{\mathbb{G}}^{\bar{z},1;KL\times KL} = \mathcal{M}\left(\mathbb{G}^{\bar{z},1;NM\times KL}\right), \tag{4.27}$$

which are used to get values of the pressure gradient at inner velocity collocation points. Another two operators $\mathcal{J}_R,\ \mathcal{J}_L : \mathbb{R}^{NM\times KL} \longrightarrow \mathbb{R}^{(M-2)\times KL}$ are defined in such a way that matrices

$$\mathbb{J}_{\text{right}}^{(M-2)\times KL} = \mathcal{J}_R\left(\mathbb{J}^{NM\times KL}\right), \qquad \mathbb{J}_{\text{left}}^{(M-2)\times KL} = \mathcal{J}_L\left(\mathbb{J}^{NM\times KL}\right) \tag{4.28}$$

consist of rows of matrix $\mathbb{J}^{NM\times KL}$ with indices $1+kN$ and $(k+1)N$ respectively (both for $k = 1, \ldots, M-2$)[6].

In (4.13) we introduced $\mathbf{P}^*$ to be a vector of unknown pressure values. At this point we add vectors of unknowns of size $N(M-2)$ for velocity values

$$\mathbf{U} = \begin{bmatrix} u_{1,2} \\ u_{2,2} \\ \vdots \\ u_{N,2} \\ \hline u_{1,3} \\ u_{2,3} \\ \vdots \\ u_{N,3} \\ \hline \vdots \\ \hline u_{1,M-1} \\ u_{2,M-1} \\ \vdots \\ u_{N,M-1} \end{bmatrix}, \qquad \mathbf{V} = \begin{bmatrix} v_{1,2} \\ v_{2,2} \\ \vdots \\ v_{N,2} \\ \hline v_{1,3} \\ v_{2,3} \\ \vdots \\ v_{N,3} \\ \hline \vdots \\ \hline v_{1,M-1} \\ v_{2,M-1} \\ \vdots \\ v_{N,M-1} \end{bmatrix}. \tag{4.29}$$

[6]Application of the matrices on $\mathbf{P}^*$ returns pressure values at corresponding collocation points on the right and left boundary of the velocity grid.

For vectors of values of coefficients $\bar{a}$, $\bar{b}$ – see (4.17) – we write

$$\hat{\mathbf{A}} = \left[\begin{array}{c} a_{1,2} \\ a_{2,2} \\ \vdots \\ a_{N,2} \\ \hline a_{1,3} \\ a_{2,3} \\ \vdots \\ a_{N,3} \\ \hline \vdots \\ \hline a_{1,M-1} \\ a_{2,M-1} \\ \vdots \\ a_{N,M-1} \end{array}\right], \quad \mathbf{A} = \left[\begin{array}{c} a_{2,2} \\ a_{3,2} \\ \vdots \\ a_{N-1,2} \\ \hline a_{2,3} \\ a_{3,3} \\ \vdots \\ a_{N-1,3} \\ \hline \vdots \\ \hline a_{2,M-1} \\ a_{3,M-1} \\ \vdots \\ a_{N-1,M-1} \end{array}\right], \quad \hat{\mathbf{B}} = \left[\begin{array}{c} b_{1,2} \\ b_{2,2} \\ \vdots \\ b_{N,2} \\ \hline b_{1,3} \\ b_{2,3} \\ \vdots \\ b_{N,3} \\ \hline \vdots \\ \hline b_{1,M-1} \\ b_{2,M-1} \\ \vdots \\ b_{N,M-1} \end{array}\right], \quad \mathbf{B} = \left[\begin{array}{c} b_{2,2} \\ b_{3,2} \\ \vdots \\ b_{N-1,2} \\ \hline b_{2,3} \\ b_{3,3} \\ \vdots \\ b_{N-1,3} \\ \hline \vdots \\ \hline b_{2,M-1} \\ b_{3,M-1} \\ \vdots \\ b_{N-1,M-1} \end{array}\right], \tag{4.30}$$

In the same manner we use $\hat{\mathbf{C}}$, $\mathbf{C}$, $\hat{\mathbf{G}}$, $\mathbf{G}$, $\hat{\mathbf{Q}}$, $\mathbf{Q}$ for values of $\bar{c}$, $\bar{g}$, $\bar{q}$ respectively. Further, let $\bar{\xi}' =_{\text{def}} \frac{\partial \bar{\xi}}{\partial \bar{z}}$ in compliance with (4.20). Then for values of $\bar{\xi}$ and $\bar{\xi}'$ at relevant grid points we have

$$\boldsymbol{\Xi}_{\text{all}} = \begin{bmatrix} \xi_1 \\ \xi_2 \\ \xi_3 \\ \vdots \\ \xi_{M-2} \\ \xi_{M-1} \\ \xi_M \end{bmatrix}, \quad \boldsymbol{\Xi} = \begin{bmatrix} \xi_2 \\ \xi_3 \\ \vdots \\ \xi_{M-2} \\ \xi_{M-1} \end{bmatrix}, \quad \boldsymbol{\Xi}'_{\text{all}} = \begin{bmatrix} \xi'_1 \\ \xi'_2 \\ \xi'_3 \\ \vdots \\ \xi'_{M-2} \\ \xi'_{M-1} \\ \xi'_M \end{bmatrix}, \quad \boldsymbol{\Xi}' = \begin{bmatrix} \xi'_2 \\ \xi'_3 \\ \vdots \\ \xi'_{M-2} \\ \xi'_{M-1} \end{bmatrix}. \tag{4.31a}$$

Clearly, according to (4.20) one can write

$$\boldsymbol{\Xi}'_{\text{all}} = \mathbb{D}^{\bar{z},1;M\times M}\, \boldsymbol{\Xi}_{\text{all}}, \qquad \boldsymbol{\Xi}' = \hat{\mathbb{D}}^{\bar{z},1;(M-2)\times M}\, \boldsymbol{\Xi}_{\text{all}}. \tag{4.31b}$$

Last but not least, we will need to use identity matrices and some of their modifications. By $\mathbb{I}^{n\times n}$ we denote the identity matrix of size $n\times n$. One convenient modification of $\mathbb{I}^{(N-2)\times(N-2)}$ is defined by the following schematic drawing

$$\overline{\mathbb{I}}^{(N-2)\times N} = \left[\begin{array}{c|c|c} 0 & & 0 \\ \vdots & \mathbb{I}^{(N-2)\times(N-2)} & \vdots \\ 0 & & 0 \end{array}\right]. \tag{4.32}$$

Symbols $\mathbf{I}_1$, $\mathbf{I}_N$ are used to denote row vectors of size N in the form

$$\mathbf{I}_1 = \left[1, 0, \ldots, 0, 0\right], \qquad \mathbf{I}_N = \left[0, 0, \ldots, 0, 1\right]. \tag{4.33}$$

Finally, symbol $\mathbb{1}^{n\times 1}$ denotes a column vector of size n whose every component is equal to 1.

$$\mathbb{1}^{n\times 1} = \left.\begin{bmatrix} 1 \\ 1 \\ \vdots \\ 1 \\ 1 \end{bmatrix}\right\} n \in \mathbb{N}. \tag{4.34}$$

System matrix for the classical Stokes problem

As we have already discussed in Section (2.1), our problem is reduced to the classical Stokes problem when we put $\hat{\alpha} = 0$. Hence, putting $\hat{\alpha} = 0$ in (4.18) and (4.21) we get the discrete version of the classical Stokes problem. Using the notation introduced above, it can be rewritten in the following compact form

$$\begin{bmatrix} \mathbb{A}_{1,U} & \mathbb{A}_{1,V} & \mathbb{A}_{1,P} \\ \mathbb{A}_{2,U} & \mathbb{A}_{2,V} & \mathbb{A}_{2,P} \\ \mathbb{A}_{3,U} & \mathbb{A}_{3,V} & \mathbb{A}_{3,P} \\ \mathbb{A}_{4,U} & \mathbb{A}_{4,V} & \mathbb{A}_{4,P} \\ \mathbb{A}_{5,U} & \mathbb{A}_{5,V} & \mathbb{A}_{5,P} \\ \mathbb{A}_{6,U} & \mathbb{A}_{6,V} & \mathbb{A}_{6,P} \\ \mathbb{A}_{7,U} & \mathbb{A}_{7,V} & \mathbb{A}_{7,P} \end{bmatrix} \begin{bmatrix} \mathbf{U} \\ \mathbf{V} \\ \mathbf{P}^* \end{bmatrix} = \begin{bmatrix} \mathbf{F}_1 \\ \mathbf{F}_2 \\ \mathbf{F}_3 \\ \mathbf{F}_4 \\ \mathbf{F}_5 \\ \mathbf{F}_6 \\ \mathbf{F}_7 \end{bmatrix}, \tag{4.35}$$

where (bold symbol $\mathbf{0}$ is commonly used for zero matrices of different sizes)

$$\mathbb{A}_{1,U} = \mathbb{I}^{(M-2)\times(M-2)} \otimes \hat{\mathbb{D}}^{\bar{r},1;(N-2)\times N} + \mathcal{M}_2\left(\operatorname{diag}\hat{\mathbf{A}}\right), \tag{4.36a}$$

$$\mathbb{A}_{1,V} = \left(\operatorname{diag}\mathbf{B}\right)\left(\tilde{\mathbb{D}}^{\bar{z},1;(M-2)\times(M-2)} \otimes \bar{\mathbb{I}}^{(N-2)\times N}\right) + \\ + \left(\operatorname{diag}\mathbf{C}\right)\left(\mathbb{I}^{(M-2)\times(M-2)} \otimes \hat{\mathbb{D}}^{\bar{r},1;(N-2)\times N}\right), \tag{4.36b}$$

$$\mathbb{A}_{1,P} = \mathbf{0}, \tag{4.36c}$$

$$\mathbb{A}_{2,U} = \left(\mathbb{I}^{KL\times KL} + \operatorname{diag}\left(\mathbf{C} * \mathbf{C}\right)\right)\left(\mathbb{I}^{(M-2)\times(M-2)} \otimes \hat{\mathbb{D}}^{\bar{r},2;(N-2)\times N}\right) + \\ + 2\left(\operatorname{diag}\left(\mathbf{B} * \mathbf{C}\right)\right)\left(\mathbb{I}^{(M-2)\times(M-2)} \otimes \hat{\mathbb{D}}^{\bar{r},1;(N-2)\times N}\right)\left(\tilde{\mathbb{D}}^{\bar{z},1;(M-2)\times(M-2)} \otimes \mathbb{I}^{N\times N}\right) + \\ + \left(\operatorname{diag}\left(\mathbf{B} * \mathbf{B}\right)\right)\left(\tilde{\mathbb{D}}^{\bar{z},2;(M-2)\times(M-2)} \otimes \bar{\mathbb{I}}^{(N-2)\times N}\right) - \mathcal{M}_2\left(\operatorname{diag}\left(\hat{\mathbf{A}} * \hat{\mathbf{A}}\right)\right) + \\ + \left(\operatorname{diag}\left(\mathbf{A} + \mathbf{G} + \mathbf{Q}\right)\right)\left(\mathbb{I}^{(M-2)\times(M-2)} \otimes \hat{\mathbb{D}}^{\bar{r},1;(N-2)\times N}\right), \tag{4.36d}$$

$$\mathbb{A}_{2,V} = \mathbf{0}, \tag{4.36e}$$

$$\mathbb{A}_{2,P} = -h\left(\operatorname{diag}\mathbf{B}\right)\tilde{\mathbb{G}}^{\bar{r},1;KL\times KL}, \tag{4.36f}$$

$$\mathbb{A}_{3,U} = \mathbf{0}, \tag{4.36g}$$

$$\mathbb{A}_{3,V} = A_{2,U} + \mathcal{M}_2\left(\operatorname{diag}\left(\hat{\mathbf{A}} * \hat{\mathbf{A}}\right)\right), \tag{4.36h}$$

$$\mathbb{A}_{3,P} = -h\left(\operatorname{diag}\mathbf{B}\right)\left(\left(\operatorname{diag}\mathbf{B}\right)\tilde{\mathbb{G}}^{\bar{z},1;KL\times KL} + \left(\operatorname{diag}\mathbf{C}\right)\tilde{\mathbb{G}}^{\bar{r},1;KL\times KL}\right), \tag{4.36i}$$

$$\mathbb{A}_{4,U} = \left(2\mathbb{I}^{(M-2)\times(M-2)} + \frac{1}{h^2}\left(\operatorname{diag}\left(\boldsymbol{\Xi}' * \boldsymbol{\Xi}'\right)\right)\right)\left(\mathbb{I}^{(M-2)\times(M-2)} \otimes \mathbf{D}_1^{\bar{r},1}\right) - \\ - \frac{1}{h^2}\left(\operatorname{diag}\left(\boldsymbol{\Xi} * \boldsymbol{\Xi}'\right)\right)\left(\tilde{\mathbb{D}}^{\bar{z},1;(M-2)\times(M-2)} \otimes \mathbf{I}_1\right), \tag{4.36j}$$

$$\mathbb{A}_{4,V} = -\frac{1}{h}\left(\operatorname{diag}\boldsymbol{\Xi}'\right)\left(\mathbb{I}^{(M-2)\times(M-2)} \otimes \mathbf{D}_1^{\bar{r},1}\right), \tag{4.36k}$$

$$\mathbb{A}_{4,P} = -\left(\operatorname{diag}\boldsymbol{\Xi}\right)\mathbb{J}_{\text{right}}^{(M-2)\times KL}, \tag{4.36l}$$

$$\mathbb{A}_{5,U} = \frac{1}{h}\left(\operatorname{diag}\boldsymbol{\Xi}\right)\left(\tilde{\mathbb{D}}^{\bar{z},1;(M-2)\times(M-2)} \otimes \mathbf{I}_1\right) - \\ - \frac{1}{h}\left(\operatorname{diag}\boldsymbol{\Xi}'\right)\left(\mathbb{I}^{(M-2)\times(M-2)} \otimes \mathbf{D}_1^{\bar{r},1}\right), \tag{4.36m}$$

$$\mathbb{A}_{5,V} = \left(\mathbb{I}^{(M-2)\times(M-2)} + \frac{2}{h^2}\left(\operatorname{diag}\left(\boldsymbol{\Xi}' * \boldsymbol{\Xi}'\right)\right)\right)\left(\mathbb{I}^{(M-2)\times(M-2)} \otimes \mathbf{D}_1^{\bar{r},1}\right) - \\ - \frac{2}{h^2}\left(\operatorname{diag}\left(\boldsymbol{\Xi} * \boldsymbol{\Xi}'\right)\right)\left(\tilde{\mathbb{D}}^{\bar{z},1;(M-2)\times(M-2)} \otimes \mathbf{I}_1\right), \tag{4.36n}$$

$$\mathbb{A}_{5,P} = \frac{1}{h}\left(\operatorname{diag}\left(\boldsymbol{\Xi} * \boldsymbol{\Xi}'\right)\right)\mathbb{J}_{\text{right}}^{(M-2)\times KL}, \tag{4.36o}$$

$$\mathbb{A}_{6,U} = -\left(2\mathbb{I}^{(M-2)\times(M-2)} + \frac{1}{h^2}\left(\operatorname{diag}\left(\boldsymbol{\Xi}' * \boldsymbol{\Xi}'\right)\right)\right)\left(\mathbb{I}^{(M-2)\times(M-2)} \otimes \mathbf{D}_N^{\bar{r},1}\right) -$$
$$- \frac{1}{h^2}\left(\operatorname{diag}\left(\boldsymbol{\Xi} * \boldsymbol{\Xi}'\right)\right)\left(\tilde{\mathbb{D}}^{\bar{z},1;(M-2)\times(M-2)} \otimes \mathbf{I}_N\right), \tag{4.36p}$$

$$\mathbb{A}_{6,V} = -\frac{1}{h}\left(\operatorname{diag}\boldsymbol{\Xi}'\right)\left(\mathbb{I}^{(M-2)\times(M-2)} \otimes \mathbf{D}_N^{\bar{r},1}\right), \tag{4.36q}$$

$$\mathbb{A}_{6,P} = \left(\operatorname{diag}\boldsymbol{\Xi}\right)\mathbb{J}_{\text{left}}^{(M-2)\times KL}, \tag{4.36r}$$

$$\mathbb{A}_{7,U} = -\frac{1}{h}\left(\operatorname{diag}\boldsymbol{\Xi}\right)\left(\tilde{\mathbb{D}}^{\bar{z},1;(M-2)\times(M-2)} \otimes \mathbf{I}_N\right) -$$
$$- \frac{1}{h}\left(\operatorname{diag}\boldsymbol{\Xi}'\right)\left(\mathbb{I}^{(M-2)\times(M-2)} \otimes \mathbf{D}_N^{\bar{r},1}\right), \tag{4.36s}$$

$$\mathbb{A}_{7,V} = -\left(\mathbb{I}^{(M-2)\times(M-2)} + \frac{2}{h^2}\left(\operatorname{diag}\left(\boldsymbol{\Xi}' * \boldsymbol{\Xi}'\right)\right)\right)\left(\mathbb{I}^{(M-2)\times(M-2)} \otimes \mathbf{D}_N^{\bar{r},1}\right) -$$
$$- \frac{2}{h^2}\left(\operatorname{diag}\left(\boldsymbol{\Xi} * \boldsymbol{\Xi}'\right)\right)\left(\tilde{\mathbb{D}}^{\bar{z},1;(M-2)\times(M-2)} \otimes \mathbf{I}_N\right), \tag{4.36t}$$

$$\mathbb{A}_{7,P} = \frac{1}{h}\left(\operatorname{diag}\left(\boldsymbol{\Xi} * \boldsymbol{\Xi}'\right)\right)\mathbb{J}_{\text{left}}^{(M-2)\times KL}, \tag{4.36u}$$

and vectors on the right hand side are given by formulae[7]

$$\mathbf{F}_1 = -\mathbf{B} * \left(\left(v_{\text{top}}\mathbf{D}^{\bar{z},1;1} + v_{\text{bottom}}\mathbf{D}^{\bar{z},1;M}\right) \otimes \mathbb{1}^{(N-2)\times 1}\right), \tag{4.37a}$$

$$\mathbf{F}_2 = \mathbf{0}, \tag{4.37b}$$

$$\mathbf{F}_3 = -\mathbf{B} * \mathbf{B} * \left(\left(v_{\text{top}}\mathbf{D}^{\bar{z},2;1} + v_{\text{bottom}}\mathbf{D}^{\bar{z},2;M}\right) \otimes \mathbb{1}^{(N-2)\times 1}\right), \tag{4.37c}$$

$$\mathbf{F}_4 = \mathbf{0}, \tag{4.37d}$$

$$\mathbf{F}_5 = \frac{2}{h^2}\left(\boldsymbol{\Xi} * \boldsymbol{\Xi}' * \left(v_{\text{top}}\mathbf{D}^{\bar{z},1;1} + v_{\text{bottom}}\mathbf{D}^{\bar{z},1;M}\right)\right), \tag{4.37e}$$

$$\mathbf{F}_6 = \mathbf{0}, \tag{4.37f}$$

$$\mathbf{F}_7 = \mathbf{F}_5. \tag{4.37g}$$

In (4.36) and (4.37) we denote $\mathbb{A} \otimes \mathbb{B} \in \mathbb{R}^{rp\times qs}$ the Kronecker product of matrices $\mathbb{A} \in \mathbb{R}^{p\times q}$ and $\mathbb{B} \in \mathbb{R}^{r\times s}$, and diag denotes the operator that creates, from a given vector $\mathbf{A} \in \mathbb{R}^n$, a diagonal matrix of size $n \times n$ whose diagonal elements are given by the vector $\mathbf{A}$,

$$\mathbb{A} \otimes \mathbb{B} = \left[\begin{array}{c|c|c|c} a_{1,1}\mathbb{B} & a_{1,2}\mathbb{B} & \cdots & a_{1,q}\mathbb{B} \\ \hline a_{2,1}\mathbb{B} & a_{2,2}\mathbb{B} & \cdots & a_{2,q}\mathbb{B} \\ \hline \vdots & \vdots & \ddots & \vdots \\ \hline a_{p,1}\mathbb{B} & a_{p,2}\mathbb{B} & \cdots & a_{p,q}\mathbb{B} \end{array}\right], \quad \operatorname{diag}\mathbf{A} = \operatorname{diag}\begin{bmatrix} a_1 \\ a_2 \\ \vdots \\ a_n \end{bmatrix} = \begin{bmatrix} a_1 & 0 & \cdots & 0 \\ 0 & a_2 & \cdots & 0 \\ \vdots & \vdots & \ddots & \vdots \\ 0 & 0 & \cdots & a_n \end{bmatrix}. \tag{4.38}$$

Further we denote $\mathbf{A} * \mathbf{B} \in \mathbb{R}^k$ the element-by-element multiplication of vectors $\mathbf{A} \in \mathbb{R}^k$ and $\mathbf{B} \in \mathbb{R}^k$,

$$\mathbf{A} * \mathbf{B} = \begin{bmatrix} a_1 \\ a_2 \\ \vdots \\ a_k \end{bmatrix} * \begin{bmatrix} b_1 \\ b_2 \\ \vdots \\ b_k \end{bmatrix} = \begin{bmatrix} a_1 b_1 \\ a_2 b_2 \\ \vdots \\ a_k b_k \end{bmatrix}. \tag{4.39}$$

[7] When deriving (4.37c), we mutely use the fact that the term $\sum_{k=1}^{N} D_{i,k}^{\bar{r},1;N\times N}$ vanishes for any $i = 1, \ldots, N$ since derivative of a constant is zero even at the discrete level.

System matrix for the full problem

Equations (4.18) and (4.21) with $\hat{\alpha} > 0$ are clearly non-linear. To get rid of the non-linearities we will use the pressure values from the previous time level (for these values we use the notation $\mathbf{P}^*_{\text{old}}$). Let us introduce the notation

$$\mathbf{E}_{\hat{\alpha}} = \exp\left(\hat{\alpha}\bar{\mathbf{P}}_{\text{old}}\right), \tag{4.40}$$

where $\bar{\mathbf{P}}_{\text{old}}$ denotes the following column vector of size $(3N-2)(M-2)$,

$$\bar{\mathbf{P}}_{\text{old}} = \begin{bmatrix} \mathbf{0} \\ \tilde{\mathbb{J}}^{KL\times KL} \\ \tilde{\mathbb{J}}^{KL\times KL} \\ \mathbb{J}^{(M-2)\times KL}_{\text{right}} \\ \mathbb{J}^{(M-2)\times KL}_{\text{right}} \\ \mathbb{J}^{(M-2)\times KL}_{\text{left}} \\ \mathbb{J}^{(M-2)\times KL}_{\text{left}} \end{bmatrix} \mathbf{P}^*_{\text{old}}, \tag{4.41}$$

and $\exp$ is the matrix function that provides, for a given matrix $\mathbb{A} \in \mathbb{R}^{n\times m}$, a matrix of the same size whose elements are $e^{a_{i,j}}$ (for $i = 1,\ldots,n$, $j = 1,\ldots,m$). Now it is possible to rewrite the problem in the compact form[8]

$$\begin{bmatrix} \mathbf{0}\ \mathbf{0} & \mathbf{0} \\ \mathbf{0}\ \mathbf{0} & \mathbb{A}_{2,P} \\ \mathbf{0}\ \mathbf{0} & \mathbb{A}_{3,P} \\ \mathbf{0}\ \mathbf{0} & \mathbb{A}_{4,P} \\ \mathbf{0}\ \mathbf{0} & \mathbb{A}_{5,P} \\ \mathbf{0}\ \mathbf{0} & \mathbb{A}_{6,P} \\ \mathbf{0}\ \mathbf{0} & \mathbb{A}_{7,P} \end{bmatrix} \begin{bmatrix} \mathbf{U} \\ \mathbf{V} \\ \mathbf{P}^* \end{bmatrix} + \left(\operatorname{diag}\mathbf{E}_{\hat{\alpha}}\right) \begin{bmatrix} \mathbb{A}_{1,U} & \mathbb{A}_{1,V} & \mathbb{A}_{1,P} \\ \mathbb{A}_{2,U} & \mathbb{A}_{2,V} & \mathbf{0} \\ \mathbb{A}_{3,U} & \mathbb{A}_{3,V} & \mathbf{0} \\ \mathbb{A}_{4,U} & \mathbb{A}_{4,V} & \mathbf{0} \\ \mathbb{A}_{5,U} & \mathbb{A}_{5,V} & \mathbf{0} \\ \mathbb{A}_{6,U} & \mathbb{A}_{6,V} & \mathbf{0} \\ \mathbb{A}_{7,U} & \mathbb{A}_{7,V} & \mathbf{0} \end{bmatrix} \begin{bmatrix} \mathbf{U} \\ \mathbf{V} \\ \mathbf{P}^* \end{bmatrix} +$$

$$+ \hat{\alpha}\left(\operatorname{diag}\mathbf{E}_{\hat{\alpha}}\right) \begin{bmatrix} \mathbf{0} & \mathbf{0} & \mathbf{0} \\ \mathbb{B}_{2,U} & \mathbb{B}_{2,V} & \mathbf{0} \\ \mathbb{B}_{3,U} & \mathbb{B}_{3,V} & \mathbf{0} \\ \mathbf{0} & \mathbf{0} & \mathbf{0} \\ \mathbf{0} & \mathbf{0} & \mathbf{0} \\ \mathbf{0} & \mathbf{0} & \mathbf{0} \\ \mathbf{0} & \mathbf{0} & \mathbf{0} \end{bmatrix} \begin{bmatrix} \mathbf{U} \\ \mathbf{V} \\ \mathbf{P}^* \end{bmatrix} = \mathbf{E}_{\hat{\alpha}} * \begin{bmatrix} \mathbf{F}_1 \\ \mathbf{F}_2 + \hat{\alpha}\mathbf{F}_2^B \\ \mathbf{F}_3 + \hat{\alpha}\mathbf{F}_3^B \\ \mathbf{F}_4 \\ \mathbf{F}_5 \\ \mathbf{F}_6 \\ \mathbf{F}_7 \end{bmatrix}. \tag{4.42}$$

At this point it is necessary to realize that the mentioned non-linearity is present also in newly introduced terms $\mathbb{B}_{2,U}$, $\mathbb{B}_{2,V}$, $\mathbb{B}_{3,U}$, $\mathbb{B}_{3,V}$ and $\mathbf{F}_2^B$, $\mathbf{F}_3^B$. Let us denote

$$\mathbf{\Gamma}_1 = \tilde{\mathbb{G}}^{\bar{r},1;KL\times KL}\mathbf{P}^*_{\text{old}}, \tag{4.43a}$$

$$\mathbf{\Gamma}_2 = \left(\operatorname{diag}\mathbf{C}\right)\tilde{\mathbb{G}}^{\bar{r},1;KL\times KL}\mathbf{P}^*_{\text{old}} + \left(\operatorname{diag}\mathbf{B}\right)\tilde{\mathbb{G}}^{\bar{z},1;KL\times KL}\mathbf{P}^*_{\text{old}}, \tag{4.43b}$$

then we write

$$\mathbb{B}_{2,U} = 2\left(\operatorname{diag}\mathbf{\Gamma}_1\right)\left(\mathbb{I}^{(M-2)\times(M-2)} \otimes \hat{\mathbb{D}}^{\bar{r},1;(N-2)\times N}\right) +$$

[8] It is worth noting that for $\hat{\alpha} = 0$ we have $\operatorname{diag}\mathbf{E}_{\hat{\alpha}} = \mathbb{I}^{(3N-2)(M-2)\times(3N-2)(M-2)}$ and (4.42) is simply reduced to (4.35).

$$
\begin{aligned}
&+ (\operatorname{diag}\boldsymbol{\Gamma}_2)\left[(\operatorname{diag}\mathbf{C})\left(\mathbb{I}^{(M-2)\times(M-2)} \otimes \hat{\mathbb{D}}^{\bar{r},1;(N-2)\times N}\right) + \right.\\
&\left. + (\operatorname{diag}\mathbf{B})\left(\tilde{\mathbb{D}}^{\bar{z},1;(M-2)\times(M-2)} \otimes \bar{\mathbb{I}}^{(N-2)\times N}\right)\right], \qquad (4.44a)\\
\mathbb{B}_{2,V} &= (\operatorname{diag}\boldsymbol{\Gamma}_2)\left(\mathbb{I}^{(M-2)\times(M-2)} \otimes \hat{\mathbb{D}}^{\bar{r},1;(N-2)\times N}\right), \qquad (4.44b)\\
\mathbb{B}_{3,U} &= (\operatorname{diag}\boldsymbol{\Gamma}_1)\left[(\operatorname{diag}\mathbf{C})\left(\mathbb{I}^{(M-2)\times(M-2)} \otimes \hat{\mathbb{D}}^{\bar{r},1;(N-2)\times N}\right) + \right.\\
&\left. + (\operatorname{diag}\mathbf{B})\left(\tilde{\mathbb{D}}^{\bar{z},1;(M-2)\times(M-2)} \otimes \bar{\mathbb{I}}^{(N-2)\times N}\right)\right], \qquad (4.44c)\\
\mathbb{B}_{3,V} &= (\operatorname{diag}\boldsymbol{\Gamma}_1)\left(\mathbb{I}^{(M-2)\times(M-2)} \otimes \hat{\mathbb{D}}^{\bar{r},1;(N-2)\times N}\right) + \\
&+ 2(\operatorname{diag}\boldsymbol{\Gamma}_2)\left[(\operatorname{diag}\mathbf{C})\left(\mathbb{I}^{(M-2)\times(M-2)} \otimes \hat{\mathbb{D}}^{\bar{r},1;(N-2)\times N}\right) + \right.\\
&\left. + (\operatorname{diag}\mathbf{B})\left(\tilde{\mathbb{D}}^{\bar{z},1;(M-2)\times(M-2)} \otimes \bar{\mathbb{I}}^{(N-2)\times N}\right)\right], \qquad (4.44d)
\end{aligned}
$$

and new vectors on the right hand side read

$$
\begin{aligned}
\mathbf{F}_2^B &= \mathbf{0}, \qquad (4.45a)\\
\mathbf{F}_3^B &= -2\mathbf{B} * \boldsymbol{\Gamma}_2 * \left(\left(v_{\text{top}}\mathbf{D}^{\bar{z},2;1} + v_{\text{bottom}}\mathbf{D}^{\bar{z},2;M}\right) \otimes \mathbb{1}^{(N-2)\times 1}\right). \qquad (4.45b)
\end{aligned}
$$

This simple approach using the pressure values from the previous time level can be later improved using some sophisticated method for solving the system of non-linear equations, for example Newton-Raphson method.

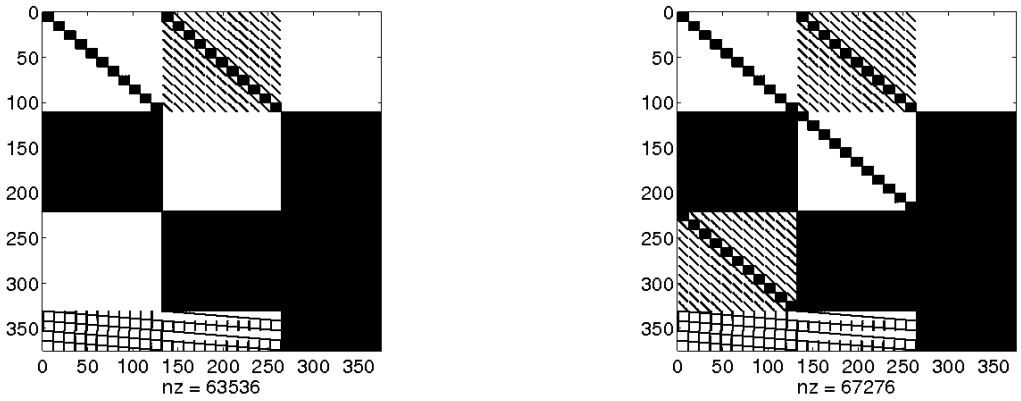

(a) $\hat{\alpha} = 0$ **(b)** $\hat{\alpha} > 0$

Figure 12: Matrices assembled for systems of linear equations (4.35), (4.42). Values $N = 12,\ M = 13$ were chosen for better resolution.

4.2.2 Time discretization

The time interval $[0, t_{\text{end}}]$ is divided using a small time step $\Delta t = \frac{1}{n} t_{\text{end}}$ for any fixed $n \in \mathbb{N}$. We shall write

$$
t^{(k)} = k\,\Delta t, \qquad k = 0, 1, \ldots, n, \qquad (4.46)
$$

and solutions at particular time levels will be denoted by $\bar{\boldsymbol{v}}^{(k)}$, $\bar{p}^{(k)}$, $\bar{\xi}^{(k)}$.

4.2.3 Numerical scheme

Following the discussion stated at the beginning of this section, we shall seek a solution of the given problem on consecutive time levels using the predictor-corrector scheme stated below. For better understanding the scheme is described using the equations

in their original form (2.22), (2.46) in physical space. Of course, subsequent computations has to be carried out with the equations being transformed in the previous sense.

In every cycle of the following scheme we seek the values $\xi^{(k+1)}$, $\boldsymbol{v}^{(k+1)}$ and $p^{(k+1)}$ on a new time level using their values $\xi^{(k)}$, $\boldsymbol{v}^{(k)}$, $p^{(k)}$ on the current level. The initial conditions used to start the scheme read

$$\boldsymbol{v}^{(0)} = 0, \qquad p^{(0)} = 0, \qquad \xi^{(0)} = \hat{R}_0. \tag{4.47}$$

PREDICTOR-CORRECTOR SCHEME:

1. An update on ξ is obtained from

$$-\frac{\xi^{(k+1)} - \xi^{(k)}}{\Delta t} + {v_r}^{(k)}\Big|_{r=\xi^{(k)}} - \frac{\partial \xi^{(k)}}{\partial z}{v_z}^{(k)}\Big|_{r=\xi^{(k)}} = 0. \tag{4.48}$$

2. Using the new geometry with $\xi^{(k+1)}$ we solve

$$\operatorname{div} \boldsymbol{v}^{(k+1)} = 0, \tag{4.49a}$$

$$-\operatorname{grad} p^{(k+1)} + e^{\hat{\alpha} p^{(k)}} \left(\Delta \boldsymbol{v}^{(k+1)} + 2\hat{\alpha}\, \mathbb{D}^{(k+1)} \operatorname{grad} p^{(k)} \right) = 0, \tag{4.49b}$$

for $\boldsymbol{v}^{(k+1)}$, $p^{(k+1)}$ subjected to corresponding boundary conditions.

3. Finally, it is possible to improve $\xi^{(k+1)}$ obtained from (4.48) using

$$-\frac{\xi_{\text{new}}^{(k+1)} - \xi^{(k)}}{\Delta t} + {v_r}^{(k+1)}\Big|_{r=\xi^{(k+1)}} - \frac{\partial \xi_{\text{new}}^{(k+1)}}{\partial z}{v_z}^{(k+1)}\Big|_{r=\xi^{(k+1)}} = 0. \tag{4.50}$$

After that, we can go back to the first step with $\xi^{(k)} := \xi_{\text{new}}^{(k+1)}$, $\boldsymbol{v}^{(k)} := \boldsymbol{v}^{(k+1)}$, and $p^{(k)} := p^{(k+1)}$.

At this point let us make an important observation in advance. Using the scheme directly in the form just presented, one obtains quite unsatisfactory results due to the presence of spurious oscillations apparent on the free surface – see Figure 17a and related discussion in Section 5.2.1. In order to smooth these oscillations we add the regularization term

$$\varepsilon \Delta \xi = \varepsilon \frac{\partial^2 \xi}{\partial z^2}, \tag{4.51}$$

to our numerical scheme (ε is typically a small number). It means that instead of (4.48) and (4.50) we shall consider

$$-\frac{\xi^{(k+1)} - \xi^{(k)}}{\Delta t} + {v_r}^{(k)}\Big|_{r=\xi^{(k)}} - \frac{\partial \xi^{(k)}}{\partial z}{v_z}^{(k)}\Big|_{r=\xi^{(k)}} = -\varepsilon \frac{\partial^2 \xi^{(k)}}{\partial z^2}, \tag{4.52}$$

$$-\frac{\xi_{\text{new}}^{(k+1)} - \xi^{(k)}}{\Delta t} + {v_r}^{(k+1)}\Big|_{r=\xi^{(k+1)}} - \frac{\partial \xi_{\text{new}}^{(k+1)}}{\partial z}{v_z}^{(k+1)}\Big|_{r=\xi^{(k+1)}} = -\varepsilon \frac{\partial^2 \xi_{\text{new}}^{(k+1)}}{\partial z^2}. \tag{4.53}$$

4.3 Benchmark problem

Once we have designed the numerical method, we need to provide some error estimates or any other relevant information concerning the convergence of the method. For this purpose we shall construct a benchmark problem using the method of manufactured solutions (MMS), see for example Roache (2002). Our manufactured solution will be based on the analytical results obtained in Section 3.2. In fact, we will modify the classical Stokes problem in the sense we add some additional terms to the equations. In the following chapter we shall compare numerical results (obtained with corresponding modifications in the discrete problem) to the exact analytical solution.

Velocity components (3.35) rewritten into the computational domain using (4.2) read[9]

$$\bar{v}_{\bar{r}} = \frac{3\bar{r}\bar{\xi}}{4h}\left(\bar{z}^2 - 1\right)\dot{h}, \qquad \bar{v}_{\bar{z}} = \frac{\bar{z}}{2}\left(3 - \bar{z}^2\right)\dot{h}. \tag{4.54}$$

Similarly, for the pressure (3.36) we write

$$\bar{p} = \frac{3\dot{h}}{4h}\left(\frac{\bar{r}^2\bar{\xi}^2}{h^2} - 2\bar{z}^2\right) + C_0, \tag{4.55a}$$

where (see the discussion in Section 3.2.3)

$$C_0 = -\frac{3\dot{h}}{4h^{\frac{9}{2}}}\hat{R}_0^2. \tag{4.55b}$$

Clearly, since (3.35) and (3.36) were found to satisfy (3.5), their counterparts (4.54), (4.55) must satisfy – independently on $\bar{\xi}$ – transformed equations (see (4.4) for comparison)

$$0 = \frac{\partial\bar{v}_{\bar{r}}}{\partial\bar{r}} + \frac{\bar{v}_{\bar{r}}}{\bar{r}} + \frac{\bar{\xi}}{h}\frac{\partial\bar{v}_{\bar{z}}}{\partial\bar{z}} - \frac{\bar{r}}{h}\frac{\partial\bar{\xi}}{\partial\bar{z}}\frac{\partial\bar{v}_{\bar{z}}}{\partial\bar{r}}, \tag{4.56a}$$

$$\begin{aligned}\bar{\xi}\frac{\partial\bar{p}}{\partial\bar{r}} = &\left(1 + \left(\frac{\bar{r}}{h}\frac{\partial\bar{\xi}}{\partial\bar{z}}\right)^2\right)\frac{\partial^2\bar{v}_{\bar{r}}}{\partial\bar{r}^2} - \frac{2\bar{r}\bar{\xi}}{h^2}\frac{\partial\bar{\xi}}{\partial\bar{z}}\frac{\partial^2\bar{v}_{\bar{r}}}{\partial\bar{r}\partial\bar{z}} + \frac{\bar{\xi}^2}{h^2}\frac{\partial^2\bar{v}_{\bar{r}}}{\partial\bar{z}^2} + \\ &+ \left(\frac{1}{\bar{r}} - \frac{\bar{r}\bar{\xi}}{h^2}\frac{\partial^2\bar{\xi}}{\partial\bar{z}^2} + \frac{2\bar{r}}{h^2}\left(\frac{\partial\bar{\xi}}{\partial\bar{z}}\right)^2\right)\frac{\partial\bar{v}_{\bar{r}}}{\partial\bar{r}} - \frac{\bar{v}_{\bar{r}}}{\bar{r}^2},\end{aligned} \tag{4.56b}$$

$$\begin{aligned}\frac{\bar{\xi}}{h}\left(\bar{\xi}\frac{\partial\bar{p}}{\partial\bar{z}} - \bar{r}\frac{\partial\bar{\xi}}{\partial\bar{z}}\frac{\partial\bar{p}}{\partial\bar{r}}\right) = &\left(1 + \left(\frac{\bar{r}}{h}\frac{\partial\bar{\xi}}{\partial\bar{z}}\right)^2\right)\frac{\partial^2\bar{v}_{\bar{z}}}{\partial\bar{r}^2} - \frac{2\bar{r}\bar{\xi}}{h^2}\frac{\partial\bar{\xi}}{\partial\bar{z}}\frac{\partial^2\bar{v}_{\bar{z}}}{\partial\bar{r}\partial\bar{z}} + \\ &+ \frac{\bar{\xi}^2}{h^2}\frac{\partial^2\bar{v}_{\bar{z}}}{\partial\bar{z}^2} + \left(\frac{1}{\bar{r}} - \frac{\bar{r}\bar{\xi}}{h^2}\frac{\partial^2\bar{\xi}}{\partial\bar{z}^2} + \frac{2\bar{r}}{h^2}\left(\frac{\partial\bar{\xi}}{\partial\bar{z}}\right)^2\right)\frac{\partial\bar{v}_{\bar{z}}}{\partial\bar{r}}.\end{aligned} \tag{4.56c}$$

Since we would like to include an analogy of the no traction condition to our problem, we need to know an exact form of the function $\bar{\xi}$, which determines profile of the free surface. Sample radius at the central plane $\xi(0,t)$ is computed using the ordinary differential equation $\dot{\xi}(0,t) = v_r(\xi(0,t),0,t)$, together with the initial condition $\xi(0,0) = \hat{R}_0$. This yields

$$\xi(0,t) = \bar{\xi}(0,t) = \hat{R}_0 h(t)^{-\frac{3}{4}}. \tag{4.57}$$

[9] We intentionally omit the lower index 0 which was used to denote the zeroth-order subproblem equivalent to the classical Stokes problem.

Let us suppose a parabolic description of the free surface $\bar{\xi} = a\bar{z}^2 + b\bar{z} + c$, where a, b, c are time-dependent constants. Using the known values of $\bar{\xi}$ at the sample-plate interface and central plane,

$$\bar{\xi}\big|_{\bar{z}=\pm 1} = \hat{R}_0, \qquad \bar{\xi}\big|_{\bar{z}=0} = \hat{R}_0 h^{-\frac{3}{4}} \tag{4.58}$$

we get profile of the form

$$\bar{\xi} = \left(\left(1 - h^{-\frac{3}{4}}\right)\bar{z}^2 + h^{-\frac{3}{4}}\right)\hat{R}_0. \tag{4.59}$$

The no-slip boundary condition at the sample-plate interfaces remains untouched, it means

$$\bar{v}_{\bar{z}}\big|_{\bar{z}=\pm 1} = \pm\dot{h}, \qquad \bar{v}_{\bar{r}}\big|_{\bar{z}=\pm 1} = 0. \tag{4.60a}$$

Modified dynamic boundary condition (originally no traction), obtained using the templates (4.54), (4.55) and (4.59) in the equations (4.8b) – (4.8e) with $\hat{\alpha} = 0$, reads

$$\left[-\bar{\xi}\bar{p} + 2\frac{\partial \bar{v}_{\bar{r}}}{\partial \bar{r}} - \frac{\bar{\xi}}{h^2}\frac{\partial \bar{\xi}}{\partial \bar{z}}\frac{\partial \bar{v}_{\bar{r}}}{\partial \bar{z}} + \frac{\bar{r}}{h^2}\left(\frac{\partial \bar{\xi}}{\partial \bar{z}}\right)^2\frac{\partial \bar{v}_{\bar{r}}}{\partial \bar{r}} - \frac{1}{h}\frac{\partial \bar{\xi}}{\partial \bar{z}}\frac{\partial \bar{v}_{\bar{z}}}{\partial \bar{r}}\right]_{\bar{r}=1} = \bar{g}_1, \tag{4.60b}$$

$$\left[\frac{\bar{\xi}}{h}\frac{\partial \bar{\xi}}{\partial \bar{z}}\bar{p} + \frac{\bar{\xi}}{h}\frac{\partial \bar{v}_{\bar{r}}}{\partial \bar{z}} - \frac{\bar{r}}{h}\frac{\partial \bar{\xi}}{\partial \bar{z}}\frac{\partial \bar{v}_{\bar{r}}}{\partial \bar{r}} + \frac{\partial \bar{v}_{\bar{z}}}{\partial \bar{r}} - \frac{2\bar{\xi}}{h^2}\frac{\partial \bar{\xi}}{\partial \bar{z}}\frac{\partial \bar{v}_{\bar{z}}}{\partial \bar{z}} + \frac{2\bar{r}}{h^2}\left(\frac{\partial \bar{\xi}}{\partial \bar{z}}\right)^2\frac{\partial \bar{v}_{\bar{z}}}{\partial \bar{r}}\right]_{\bar{r}=1} = \bar{g}_2, \tag{4.60c}$$

$$\left[\bar{\xi}\bar{p} - 2\frac{\partial \bar{v}_{\bar{r}}}{\partial \bar{r}} - \frac{\bar{\xi}}{h^2}\frac{\partial \bar{\xi}}{\partial \bar{z}}\frac{\partial \bar{v}_{\bar{r}}}{\partial \bar{z}} + \frac{\bar{r}}{h^2}\left(\frac{\partial \bar{\xi}}{\partial \bar{z}}\right)^2\frac{\partial \bar{v}_{\bar{r}}}{\partial \bar{r}} - \frac{1}{h}\frac{\partial \bar{\xi}}{\partial \bar{z}}\frac{\partial \bar{v}_{\bar{z}}}{\partial \bar{r}}\right]_{\bar{r}=-1} = -\bar{g}_1, \tag{4.60d}$$

$$\left[\frac{\bar{\xi}}{h}\frac{\partial \bar{\xi}}{\partial \bar{z}}\bar{p} - \frac{\bar{\xi}}{h}\frac{\partial \bar{v}_{\bar{r}}}{\partial \bar{z}} + \frac{\bar{r}}{h}\frac{\partial \bar{\xi}}{\partial \bar{z}}\frac{\partial \bar{v}_{\bar{r}}}{\partial \bar{r}} - \frac{\partial \bar{v}_{\bar{z}}}{\partial \bar{r}} - \frac{2\bar{\xi}}{h^2}\frac{\partial \bar{\xi}}{\partial \bar{z}}\frac{\partial \bar{v}_{\bar{z}}}{\partial \bar{z}} + \frac{2\bar{r}}{h^2}\left(\frac{\partial \bar{\xi}}{\partial \bar{z}}\right)^2\frac{\partial \bar{v}_{\bar{z}}}{\partial \bar{r}}\right]_{\bar{r}=-1} = \bar{g}_2, \tag{4.60e}$$

where the terms on right hand sides are given by

$$\bar{g}_1 = -\frac{3\hat{R}_0\left(\bar{z}^2 h^{\frac{3}{4}} - \bar{z}^2 + 1\right)\dot{h}}{4h^{\frac{21}{4}}}\Big(5\hat{R}_0^2\bar{z}^4 h^{\frac{3}{2}} + 2\hat{R}_0^2\left(3 - 5\bar{z}^2\right)\bar{z}^2 h^{\frac{3}{4}} + \\ + \left(2 - 4\bar{z}^2\right)h^{\frac{7}{2}} + \hat{R}_0^2\left(5\bar{z}^2 - 6\right)\bar{z}^2\Big), \tag{4.60f}$$

and

$$\bar{g}_2 = \frac{3\hat{R}_0^2\bar{z}\left(\bar{z}^2 h^{\frac{3}{4}} - \bar{z}^2 + 1\right)\dot{h}}{2h^7}\Big(\hat{R}_0^2\bar{z}^4 h^{\frac{9}{4}} + \hat{R}_0^2\bar{z}^2\left(2 - 3\bar{z}^2\right)h^{\frac{3}{2}} + \\ + \hat{R}_0^2\bar{z}^2\left(3\bar{z}^2 - 4\right)h^{\frac{3}{4}} + \left(3\bar{z}^2 - 4\right)h^{\frac{17}{4}} + \left(5 - 3\bar{z}^2\right)h^{\frac{7}{2}} - \hat{R}_0^2\bar{z}^2\left(\bar{z}^2 - 2\right)\Big). \tag{4.60g}$$

Finally, substituting (4.59) into the kinematic condition (4.8f) we obtain modified transport equation

$$-\frac{\partial \bar{\xi}}{\partial t} + \bar{v}_{\bar{r}}\big|_{\bar{r}=1} + \frac{1}{h}\left(\bar{z}\dot{h} - \bar{v}_{\bar{z}}\right)\frac{\partial \bar{\xi}}{\partial \bar{z}} = \bar{g}_3, \tag{4.60h}$$

where

$$\bar{g}_3 = \frac{7\hat{R}_0\bar{z}^2}{4h^{\frac{7}{4}}}\left(\bar{z}^2 - 1\right)\left(h^{\frac{3}{4}} - 1\right)\dot{h}. \tag{4.60i}$$

The quartet $(\bar{v}_{\bar{r}},\ \bar{v}_{\bar{z}},\ \bar{p},\ \bar{\xi})$ satisfying (4.54), (4.55) and (4.59) is called the exact solution of the benchmark problem (4.56) – (4.60).

5. Results

The numerical method was implemented in MATLAB and numerical results were obtained for several combinations of parameter values. In what follows, we mainly report results for a particular setting specified by the parameters summarized in Table 2. Note that we consider h given by (2.39). The choice of the time data corresponds to the situation where the sample is compressed approximately up to four fifths of its initial height, which seems to be more than enough in order to get some basic knowledge about the behaviour of the material in the squeeze flow geometry.

At first we shall briefly investigate questions concerning the convergence of the numerical method using the benchmark problem described in the previous chapter. Numerical solutions obtained for the classical Navier-Stokes fluid will help us to reveal some fundamental drawbacks related to the physical model and we shall point out the role of the parabolic regularization introduced at the end of Section 4.2.3. Finally, the pressure-viscosity coefficient $\hat{\alpha}$ will be varied in order to determine the influence of the pressure-dependent viscosity on the solution[1].

Parameter	$\hat{R}_0$	t_{end}	t_0	ε
Value	2	0.2	0.05	0 to 0.01

Table 2: Parameter values used in computations.

5.1 Convergence of the numerical method

In order to verify whether the numerical method provides plausible results, we carry out some simple tests comparing the numerical solution of the benchmark problem (4.56), (4.60) to the quartet $(\bar{u}_{\text{ex}},\ \bar{v}_{\text{ex}},\ \bar{p}_{\text{ex}},\ \bar{\xi}_{\text{ex}})$ that represents the exact solution of the same problem[2]. We need to measure the difference between the two solutions appropriately. For this purpose we introduce the notation

$$|\,\bar{\omega}\,|_{t;N,M} = \max_{i=1,\dots,N,j=1,\dots,M} |\,\bar{\omega}(r_i,z_j,t)\,|, \tag{5.1a}$$

$$|\,\bar{\omega}\,|^*_{t;K,L} = \max_{i=1,\dots,K,j=1,\dots,L} \left|\,\bar{\omega}(r_i^*,z_j^*,t)\,\right|, \tag{5.1b}$$

where $\bar{\omega}$ is an arbitrary function on the computational domain $\bar{\Omega}$ and collocation points (r_i,z_j), (r_i^*,z_j^*) are defined in (4.9), (4.10) respectively. Since $\bar{\xi}$ does not depend on $\bar{r}$, we modify the previous notation and further we will also use

$$\left|\,\bar{\xi}\,\right|_{t;M} = \max_{j=1,\dots,M} \left|\,\bar{\xi}(z_j,t)\,\right|, \tag{5.1c}$$

[1] Let us remind that when reporting results for the pressure p, we in fact report results concerning the difference of p from a reference level p_0.

[2] Numerical solution of the problem is obtained by adding the discrete version of $\bar{g}_1$, $\bar{g}_2$ into (4.37d), (4.37g), according to (4.60b) – (4.60e), and it is also necessary to adjust the discrete version of the transport equation in the first and last step of our predictor-corrector scheme, this time according to (4.60h).

Now it is possible to define functions

$$\delta_u(t;N,M) = |\,\bar{u}_{\text{ex}}\,|^{-1}_{t;N,M}\,|\,\bar{u}-\bar{u}_{\text{ex}}\,|_{t;N,M}\,, \tag{5.2a}$$

$$\delta_v(t;N,M) = |\,\bar{v}_{\text{ex}}\,|^{-1}_{t;N,M}\,|\,\bar{v}-\bar{v}_{\text{ex}}\,|_{t;N,M}\,, \tag{5.2b}$$

$$\delta_p(t;K,L) = \left(|\,\bar{p}_{\text{ex}}\,|^{*}_{t;K,L}\right)^{-1}|\,\bar{p}-\bar{p}_{\text{ex}}\,|^{*}_{t;K,L}\,, \tag{5.2c}$$

$$\delta_\xi(t;M) = \left|\,\bar{\xi}_{\text{ex}}\,\right|^{-1}_{t;M}\left|\,\bar{\xi}-\bar{\xi}_{\text{ex}}\,\right|_{t;M}\,, \tag{5.2d}$$

which provide an information about relative errors for the solution $(\bar{u},\ \bar{v},\ \bar{p},\ \bar{\xi})$.

In Figure 13 we have plotted the relative errors (5.2) for $t = 0.1$ and $N = M$. One can see that for $\Delta t = 10^{-3}$, and N sufficiently large, solutions $\bar{u}$, $\bar{v}$ approximate $\bar{u}_{\text{ex}}$ and $\bar{v}_{\text{ex}}$ with the relative error of order 10^{-3}, $\bar{p}$ approximates $\bar{p}_{\text{ex}}$ with the relative error of order 10^{-2}, and $\bar{\xi}$ approximates $\bar{\xi}_{\text{ex}}$ with the relative error of order 10^{-4}. It is worth noting that an improvement of the order of approximation is reached easily using smaller time steps. This seems to be more efficient than incessant increase of the number of collocation points with Δt being fixed.

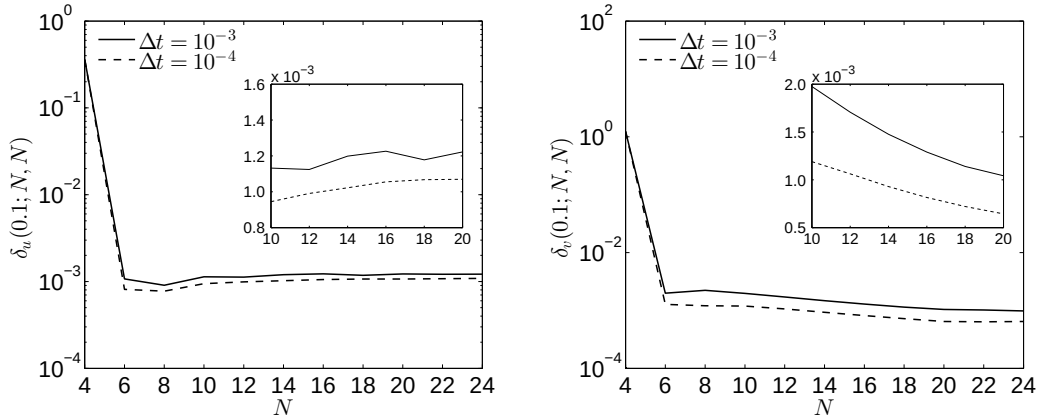

(a) velocity component $\bar{u}$ **(b)** velocity component $\bar{v}$

(c) pressure $\bar{p}$ **(d)** free surface $\bar{\xi}$

Figure 13: Relative errors at $t = 0.1$. Individual curves express the dependence of relative errors (5.2) on the number of velocity collocation points $N = M$.

For further computations we use the time step $\Delta t = 10^{-3}$ and velocity grid of the size $N \times M = 20 \times 25$ (we use more collocation points in the vertical direction since we want to capture the curvature of the free surface as well as possible). In Figure 14a one

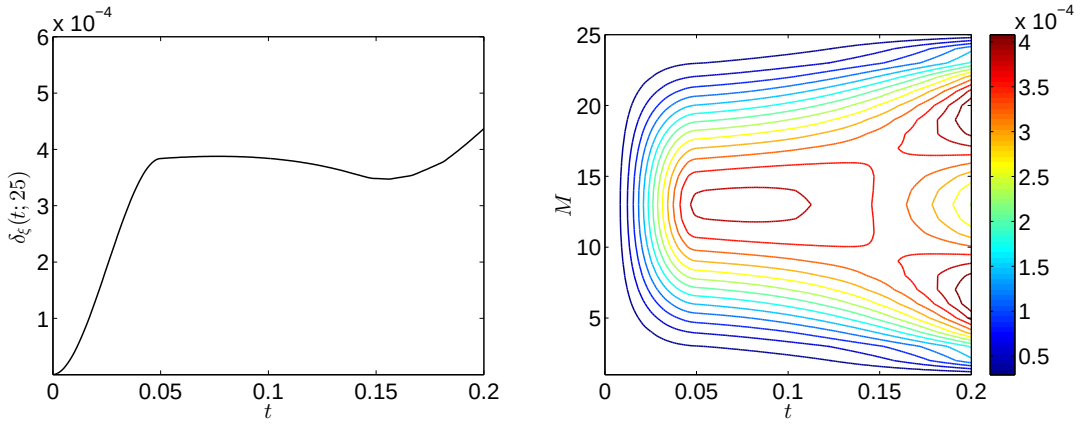

(a) time dependence **(b)** spatial distribution

Figure 14: Values of the relative error $\delta_\xi(t; M)$ given by (5.2d). The error was computed on the velocity grid $N \times M = 20 \times 25$, using $\Delta t = 10^{-3}$.

can see the time dependent relative error $\delta_\xi(t; M)$ computed on the mentioned grid, while Figure 14b illustrates also the spatial distribution of the error.

The results obtained in this section show that the numerical scheme for solution of the Stokes-type problem with moving boundary has been implemented without coding errors.

The analysis of the relative error between the exact solution of the benchmark problem and the numerical solution provides us with a heuristic guideline how to choose computational parameters $(N, M, \Delta t)$ in order to obtain reasonably accurate numerical results in the benchmark problem and, more importantly, in the full problem. Using the results concerning the relative error we can also make a qualified guess on the error in the numerical calculations for the full problem.

5.2 Numerical solution for the classical Stokes problem

First, we consider the classical Navier-Stokes fluid model and its behaviour in the simulation. The system of linear algebraic equations given by (4.35) is solved in the second step of every cycle in our predictor-corrector scheme.

5.2.1 Behaviour in corners

For the Navier-Stokes fluid solution we expect presence of the pressure singularities located in the corners of the computational domain. Distribution of the pressure throughout the sample at different time instants is captured in Figure 15. One can observe that the pressure is increasing in the corners at first but after some time it starts to descend very rapidly. Consequently, there are pressure singularities in the negative direction which is quite strange, and it possibly indicates breakdown of the numerical solution in this time interval.

As it is shown in Figure 16a, it seems that pressure values start to descend when the velocity of the plates becomes constant. On the other side, Figure 16b illustrates that pressure values localized in the center of the plate behave in an expected way (see Figures 10a and 25b for comparison).

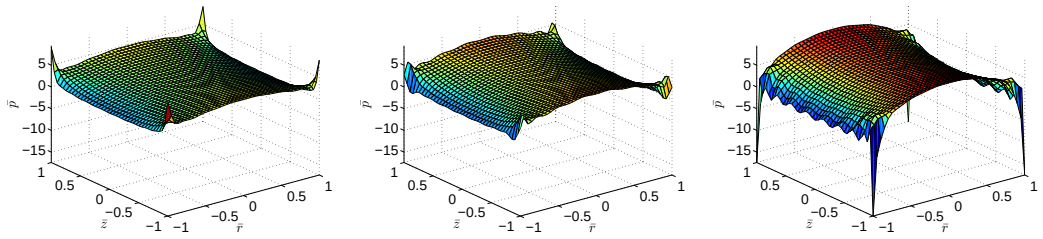

(a) $t = 0.04$ **(b)** $t = 0.1$ **(c)** $t = 0.2$

Figure 15: Pressure distribution for the Navier-Stokes fluid at different time instants. Computed with $\varepsilon = 0$. Results were reinterpolated from the pressure grid at a finer grid using the Chebyshev interpolation implemented in Weideman and Reddy (2000).

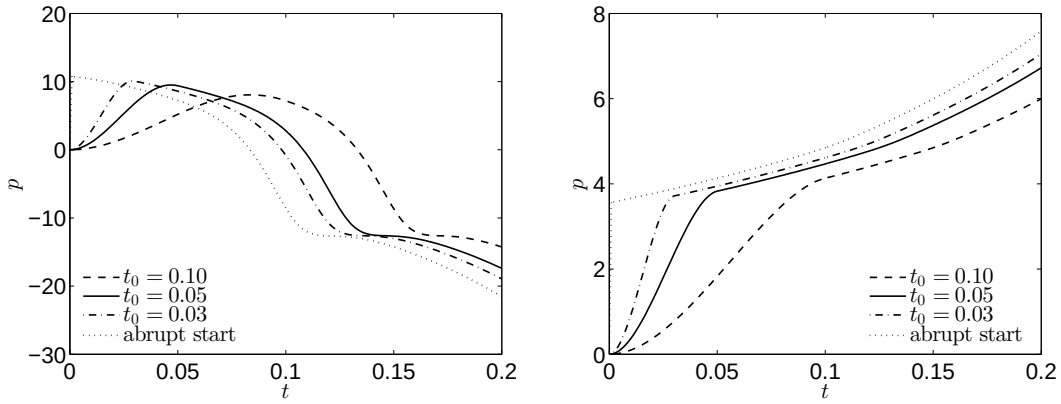

(a) Pressure values in the corner. **(b)** Pressure values in the center of the plate.

Figure 16: Pressure localized in particular places of the computationaldomain. Computed for the Navier-Stokes fluid with $\varepsilon = 0$ and various settings of the plate motion.

Another interesting feature that possibly indicates the collapse of the numerical solution for large times arises on the free surface. The oscillations apparent near the sample-plate interface in Figure 17a confirm that the solution in the corners is ill-behaved.

Using the velocity field computed in corresponding collocation points, it is possible to reconstruct the motion of individual particles. In Figure 17b we have plotted the trajectories of particles that in the reference configuration occupy the position of collocation points on the free surface (black squares). Looking at their current position at $t = 0.15$ (white squares), it seems that the free surface should be smooth non-oscillating curve. At this point we would guess that the velocity field does not suffer from the serious drawbacks.

Of course, this is not the case as it is clear from the nature of the problem. Experimental tests have shown that by increasing the number of collocation points in vertical direction, thus increasing their density in the corners, the oscillations of the free surface become stronger. As a consequence, the velocity field suffers from some abrupt changes as it is captured in Figure 18. Further increase in the number of collocation points even damages symmetry of the solution.

We believe that the inconsistencies described above are closely connected to the *physically* incorrect choice of the boundary condition at the sample plate interface near the corners of the domain. When the no-slip condition is applied, one should consider an apparent motion of the contact line over the plate surface, see for example

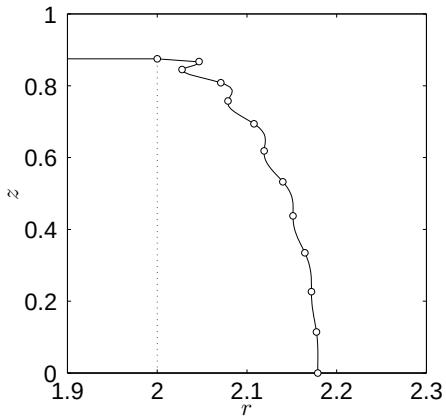

(a) Free surface at $t = 0.15$. Values were reinterpolated at a finer grid (white circles show the current position of the velocity collocation points).

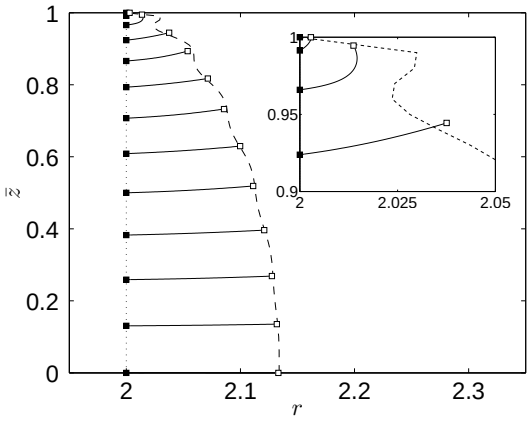

(b) Trajectories of individual particles on the free surface (black squares show the position at $t = 0$, white squares at $t = 0.15$).

Figure 17: Motion of the free surface for the Navier-Stokes fluid. Computed with $\varepsilon = 0$. Note that in figure (b) we have used $\bar{z}$ coordinate on the vertical axis, see (4.2), in order to see the motion of the particles relatively to the sample height.

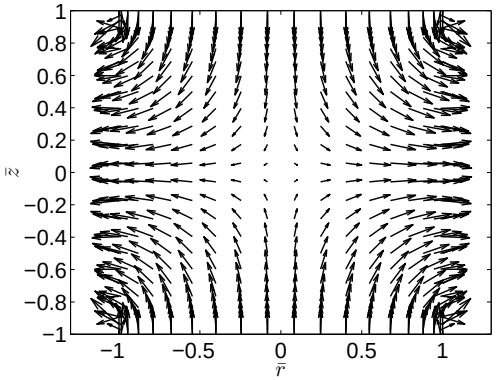

(a) $t = 0.78$

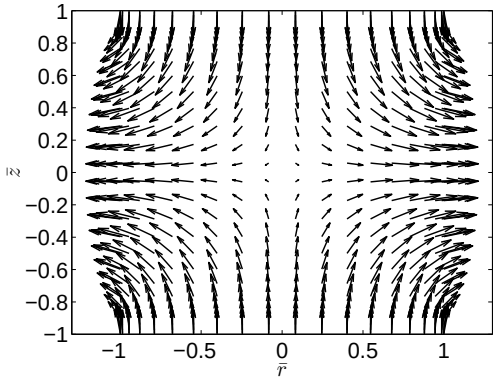

(b) $t = 0.79$

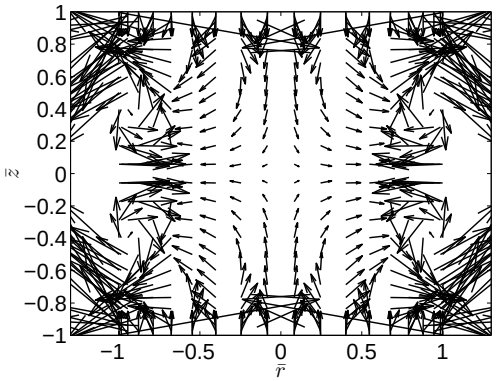

(c) $t = 1.73$

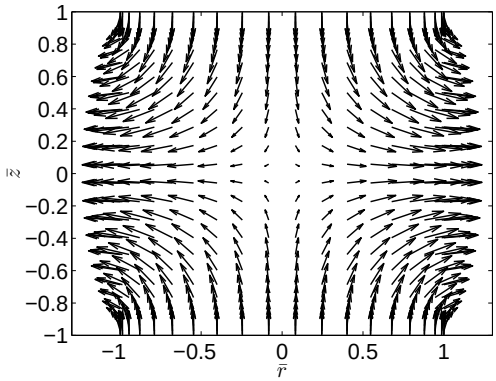

(d) $t = 1.74$

Figure 18: Velocity field in the computational domain with $N \times M = 20 \times 28$ collocation points. Computed for the Navier-Stokes fluid with $\varepsilon = 0$. Figures (a), (c) show abrupt unexpected changes of the velocity field. Vectors are scaled by the factor 0.1.

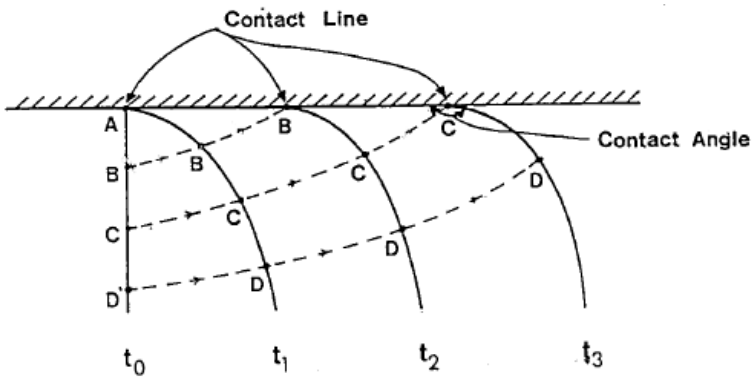

Figure 19: Contact line motion over a solid surface. Reprinted from Mavridis (1988).

Mavridis (1988), when the free surface of the material gradually sticks to the plate, see Figure 19. Presence of this phenomenon in our case seems to be confirmed following trajectories of the particles in the close proximity of the sample-plate interface in Figure 17b.

In order to fix the solution behaviour in the corners, the numerical simulation should be improved according to the scheme depicted in Figure 19. Unfortunately, this requires some extensive changes in our code which are out of scope of the thesis (especially because of the time reasons).

5.2.2 Results obtained using parabolic regularization

As we have already mentioned at the end of Section 4.2.3, another way how to improve the numerical scheme is to use the regularization term (4.51). Really, in Figure 20a one can see the smooth boundary computed with $\varepsilon = 0.01$.

Concerning the velocity field, there are no abrupt changes in its values anymore and trajectories of the individual particles are depicted in Figure 20b. Note that the

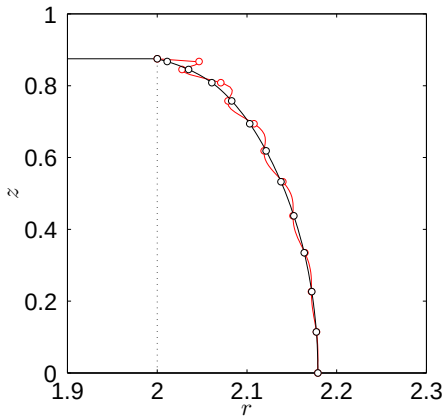

(a) Free surface at $t = 0.15$. Values were reinterpolated at a finer grid (white circles show the current position of the velocity collocation points).

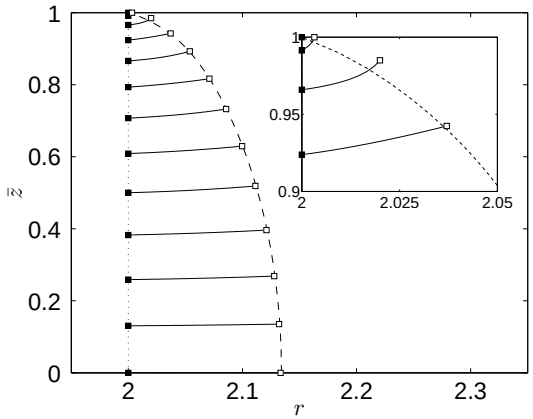

(b) Trajectories of individual particles on the free surface (black squares show the position at $t = 0$, white squares at $t = 0.15$).

Figure 20: Motion of the free surface for the Navier-Stokes fluid. Computed with $\varepsilon = 0.01$. Red line in figure (a) is used to denote the profile from Figure 17a.

current position of the particles located near the sample-plate interface does not exactly coincide with the position of the free surface. Clearly, this is caused by the artificial regularization term in the governing equations. However, the situation on the rest of the free boundary is more than promising.

An influence of the regularization term on the pressure is captured in Figures 21, 22. Unfortunately, one can observe that the decreasing tendency of the pressure values in the corners is not influenced by this technique, see Figure 22a.

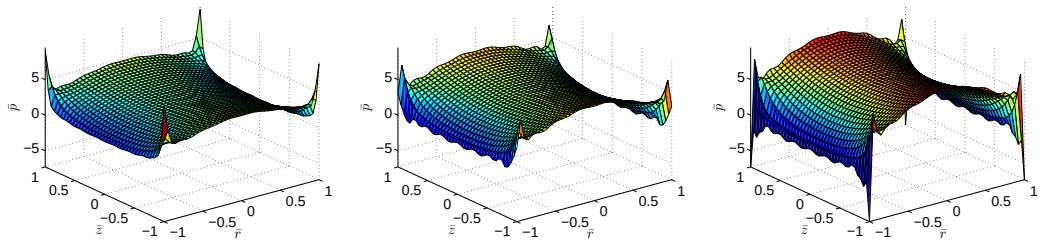

(a) $t = 0.04$ **(b)** $t = 0.1$ **(c)** $t = 0.2$

Figure 21: Pressure distribution for the Navier-Stokes fluid at different time instants. Computed with $\varepsilon = 0.01$. See Figure 15 for comparison.

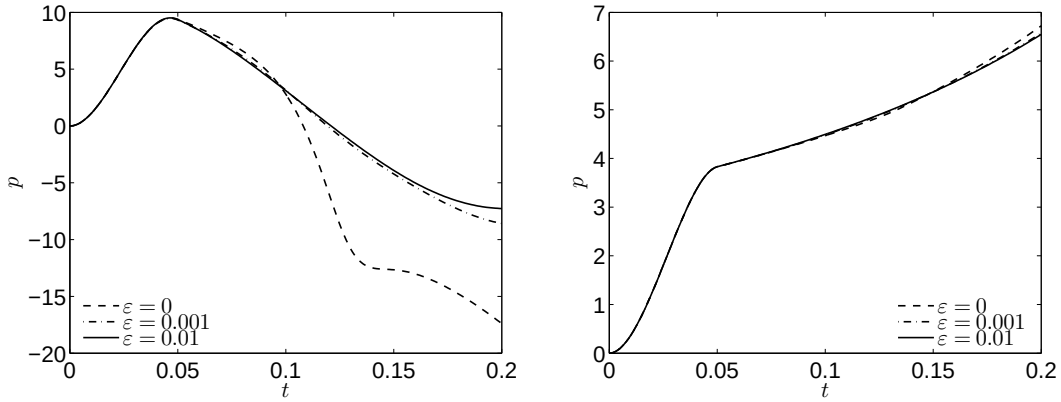

(a) Pressure values in the corner. **(b)** Pressure values in the center of the plate.

Figure 22: Pressure localized in particular places of the computational domain. Computed for the Navier-Stokes fluid with various strength of the regularization term.

5.2.3 Direct comparison to the analytical solution

In Section 3.2 we have introduced an *approximation* of the no-slip squeeze flow problem based on the assumption that planes initially normal to the direction of loading remain plane in the deformed state. We have argued that such an assumption is justifiable only at the very beginning of the experiment.

At this point we can verify the latter hypothesis by comparing the analytical solution of the approximate problem corresponding to Navier-Stokes fluid, see (3.35) – (3.36), with the numerical solution obtained in the previous paragraph for the full regularized problem. This comparison also provides us with a qualified guess whether the numerical solution can be regarded as plausible.

In Figure 23 we compare free surfaces at different time instants. Note that the centre part of the free surface computed using the numerical simulation moves slower

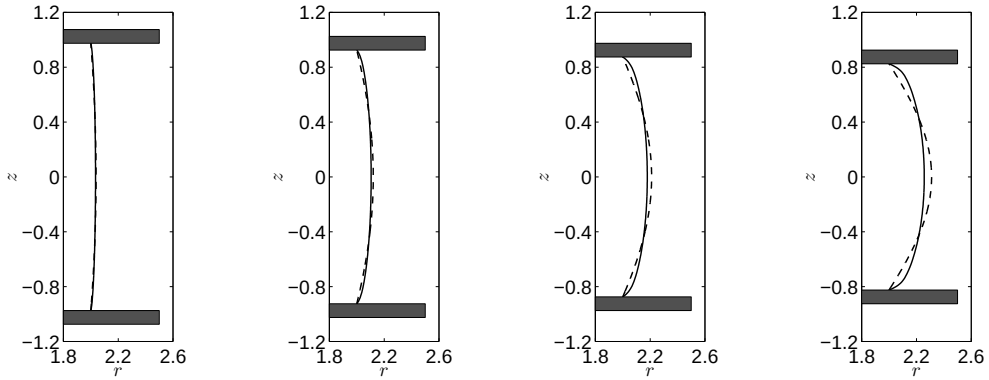

(a) $t = 0.05$ **(b)** $t = 0.1$ **(c)** $t = 0.15$ **(d)** $t = 0.2$

Figure 23: Motion of the free surface corresponding to numerical solution (——) and analytical solution (– – –). Both profiles were computed for the Navier-Stokes fluid.

than in the case of analytical solution. This is caused by the fact that particles near the free surface move towards the plates as it was shown in Figure 20b. Deformation patterns studied by Mavridis et al. (1992) reveal that in a real situation the planes initially normal to the direction of loading are indeed deformed during the compression, see Figure 24, which contradicts the assumption made for the approximate problem. In order to see this explicitly, the numerical tracking of individual particles inside the sample should be additionally involved in our code.

Previous statement comparing the velocities of individual profiles is confirmed in Figure 25a. Radial velocity components were compared at the tips of the corresponding free surfaces and one can notice that both solutions coincide only at the beginning of the time interval.

Finally, in Figure 25b one can see the pressure located in the center of the upper plate. As we have already mentioned in Section 3.2.3, it is necessary to bear in mind that the analytical solution is influenced by the choice of boundary condition (3.48). However, at this point it is possible to improve the result doing some "post-processing". We add the pressure value at the tip of the free surface, obtained from the numerical solution, to the analytical solution which was originally fixed to zero at the same point.

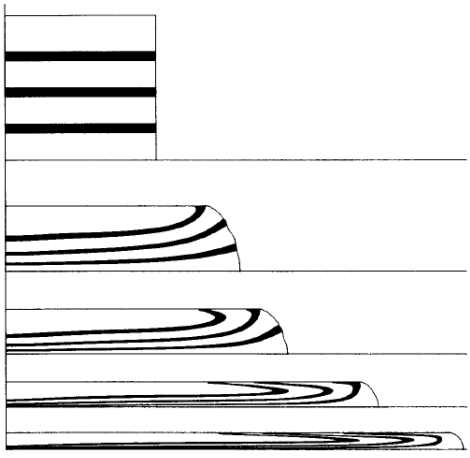

Figure 24: Deformation of planes initially normal to the direction of loading. Reprinted from Mavridis et al. (1992).

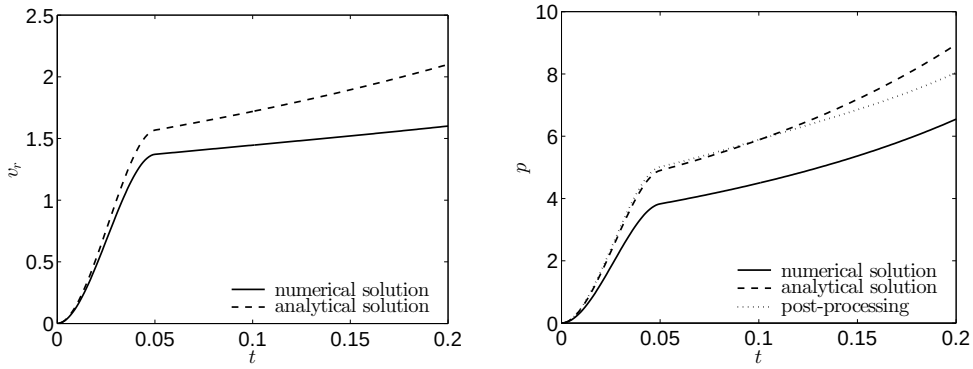

(a) Radial velocity component as a function of time at the tip of the free surface.

(b) Pressure located at the center of the upper plate.

Figure 25: Comparison of the numerical and analytical solutions for the velocities and pressure values at specific points in the computational domain.

5.3 Role of pressure-dependent viscosity

At this point we finally come to the main topic of the thesis. We want to solve the full problem for an incompressible fluid with pressure-dependent viscosity. Hence, in the second step of every cycle in our numerical scheme we solve the system of equations (4.42) with $\hat{\alpha} > 0$.

Originally, we have expected that the effect of the pressure-dependent viscosity will be important especially in the corners of the domain. We were wondering if it is somehow capable to resolve drawbacks discussed above, thus if it yields solutions markedly different from those obtained in the previous paragraph. Unfortunately, due to the presence of the moving boundary, singular-like behaviour of the pressure in the corners persists also in this case. As a consequence, we can guess that the effect of the pressure-dependent viscosity will be reduced to the same level as in the case of analytical solution.

Numerical experiments confirm that solutions obtained without the regularization term (4.51) suffer from the drawbacks already discussed in Section 5.2.1. Hence, we shall present only results obtained using the regularization term with $\varepsilon = 0.01$.

Let $\bar{\xi}$ denotes the sample radius computed for $\hat{\alpha} = 0$, which corresponds to the Navier-Stokes fluid, and similarly let $\bar{\xi}_{\hat{\alpha}}$ is computed for $\hat{\alpha} = 0.01$. In Figure 26 we

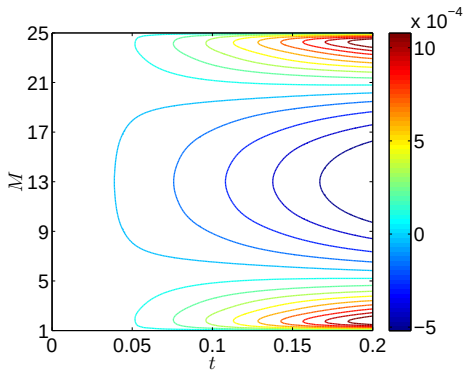

Figure 26: Space and time distribution of the difference defined by (5.3).

have plotted the difference

$$\bar{\xi}\left(\bar{z}_j, t\right) - \bar{\xi}_{\hat{\alpha}}\left(\bar{z}_j, t\right), \quad j = 1, \ldots, M, \tag{5.3}$$

at velocity collocation points on the free surface. Although the difference is really small, it is worth emphasizing that its distribution on the free surface corresponds to the behaviour captured in Figure 8c. It means that the solution for Navier-Stokes fluid lags behind the other solution in the middle of the free surface, while it is faster in the upper and lower quarter of the free surface.

As in the case of analytical solution, most significant changes are observable concerning the pressure. Distribution of the pressure throughout the computational domain is captured in Figure 27, including the comparison of pressure values at selected points.

The results obtained here lead us to the conclusion that the pressure-dependent viscosity is probably not a tool to resolve the issue with physically incorrect choice of boundary condition in the corner. On the other hand, we should realize that the chosen geometry is too complex in order to make some premature conclusions about the real influence of the pressure-dependent viscosity on the solution. In fact, there are at least two possibilities how to proceed with our studies. We can do the side step and repeat the computations in an appropriate geometry without moving boundary[3], the other possibility is to improve the code in the sense discussed at the end of Section 5.2.1.

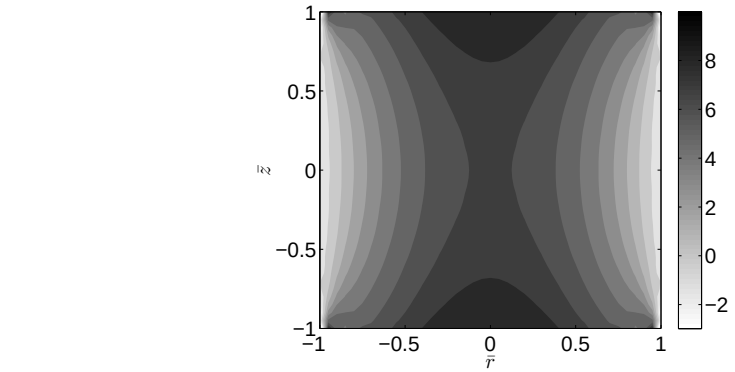

(a) Pressure distribution in the computational domain at $t = 0.2$. Computed for $\hat{\alpha} = 0.01$.

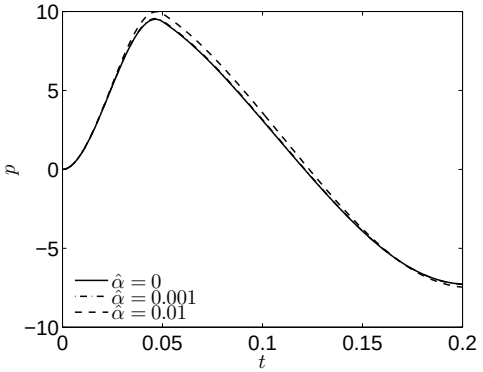

(b) Pressure values in the corner.

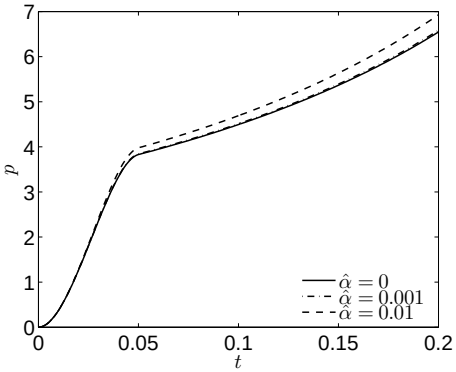

(c) Pressure values in the center of the plate.

Figure 27: Pressure computed for the Navier-Stokes fluid ($\hat{\alpha} = 0$) and for the incompressible fluid with pressure-dependent viscosity.

[3]One can think about "lid-driven cavity" problem for example.

6. Conclusion

6.1 Summary

The axisymmetric squeeze flow problem was solved for an incompressible material that can be described using the constitutive equation

$$\mathbb{T} = -p\mathbb{I} + 2\mu(p)\mathbb{D}, \tag{6.1}$$

where the pressure-dependent viscosity obeys the Barus law

$$\mu(p) = \mu_0 e^{\alpha p}. \tag{6.2}$$

Solutions were sought in two different settings depending on the choice of boundary condition at the sample-plate interfaces.

Perfect-slip

In the perfect-slip squeeze flow the velocity field corresponds to the homogeneous biaxial extension. It was found that pressure remains homogeneously distributed throughout the sample and its values are given implicitly by the relation (3.14). An approximate solution for the pressure was obtained using the perturbation method. It was shown that the material in question becomes more stiff in comparison to the classical Navier-Stokes fluid.

No-slip

The no-slip squeeze flow problem was solved using two different approaches.

Analytical solution was found using the perturbation method, supposing that planes initially normal to the direction of loading are not deformed during the compression. In this case, the pressure distribution is no longer homogeneous throughout the sample and material characteristics are changed locally in comparison to the Navier-Stokes fluid. The analytical solution was further used to derive the benchmark problem important from the point of view of numerical computations. It was used for code verification later in the thesis.

The numerical simulation poses second approach used to solve the no-slip squeeze flow which has to be treated as a free boundary problem. The method of body-fitted curvilinear coordinates was used to transform the governing equations into the fixed computational domain, whose spatial discretization was achieved using the spectral collocation method. The no traction condition derived in Section 2.2.2 was involved in the numerical simulation as well as the kinematic condition (2.33) which determines the motion of the free surface. Solutions at different time levels were obtained using the predictor-corrector scheme. Non-linear terms, appearing in the equations through (6.2), were linearized using the pressure values known from the previous time level.

Results and drawbacks

The numerical simulation was used to solve the problem for the classical Navier-Stokes fluid at first. Obtained results revealed some fundamental drawbacks in the form of oscillations of the free surface and singular-like behaviour of the pressure in the corners.

These inconsistencies are attributed to the choice of the no-slip boundary condition in the corners which is not a good one and leads to an ill-posed physical problem.

Apparently spurious oscillations were eliminated using the parabolic regularization (4.51) in the equation of transport (kinematic condition). This technique helped to suppress the oscillations of the free surface. The numerical solution was subsequently compared to the analytical one in order to see that the simplifying assumption about non-deforming horizontal planes is justifiable only at the very beginning of squeezing.

Numerical experiments, which were carried out for the full problem, revealed that the pressure-dependent viscosity is probably not a tool to resolve the issue with incorrect choice of the boundary condition (the problems observed in the case with Navier-Stokes fluid persisted also in the case with pressure-dependent viscosity). Some acceptable results were obtained, as in the previous case, using the regularization term. It was shown that departures from the solution for Navier-Stokes fluid are approximately on the same level as in the case of analytical solution.

6.2 Outlook

One of the main outputs of the present thesis is the numerical simulation which is ready to be modified in different ways. The simulation was implemented in MATLAB and its code is contained within the file *squeeze-flow-simulation.zip* which can be found attached to the electronic version of the thesis.

As it is clear from Summary, we need a better boundary condition near the corners of the computational domain. In this situation several possibilities are available. For example partial-slip at the sample-plate interface can be easily included into the code, as well as the dynamic condition in its original form (2.29) instead of the no traction condition. Finally, moving contact line poses indisputably the biggest challenge of how to improve our numerical simulation. All of these improvements should be successively implemented in order to make the effect of the pressure-dependent viscosity on the solution more transparent.

Bibliography

Bonn, D., J. Eggers, J. Indekeu, J. Meunier, and E. Rolley (2009). Wetting and spreading. *Rev. Mod. Phys. 81*, 739–805.

Brdička, M., L. Samek, and B. Sopko (2000). *Mechanika kontinua*. Praha: Academia.

Bridgman, P. W. (1926). The effect of pressure on the viscosity of forty-three pure liquids. *Proc. Am. Acad. Art. Sci. 61*(3), 57–99.

Bush, A. W. (1992). *Perturbation methods for engineers and scientists*. Boca Raton: CRC Press.

Canuto, C., M. Y. Hussaini, A. Quarteroni, and T. A. Zang (2006). *Spectral methods: Fundamentals in single domains*. Scientific Computation. Berlin: Springer-Verlag.

Canuto, C., M. Y. Hussaini, A. Quarteroni, and T. A. Zang (2007). *Spectral methods: Evolution to complex geometries and applications to fluid dynamics*. Scientific Computation. Berlin: Springer.

Cardinaels, R., P. Van Puyvelde, and P. Moldenaers (2007). Evaluation and comparison of routes to obtain pressure coefficients from high-pressure capillary rheometry data. *Rheol. Acta 46*, 495–505.

Chatraei, S., C. W. Macosko, and H. H. Winter (1981). Lubricated squeezing flow: a new biaxial extensional rheometer. *J. Rheol. 25*(4), 433–443.

Crank, J. (1987). *Free and Moving Boundary Problems*. Oxford Science Publications. Clarendon Press.

Engmann, J., C. Servais, and A. S. Burbidge (2005). Squeeze flow theory and applications to rheometry: A review. *J. Non-Newton. Fluid Mech. 132*(1-3), 1–27.

Ferry, J. D. (1980). *Viscoelastic properties of polymers* (3rd ed.). New York: John Wiley & Sons.

Gordon, W. J. and C. A. Hall (1973). Construction of curvilinear co-ordinate systems and applications to mesh generation. *Int. J. Numer. Methods Eng. 7*(4), 461–477.

Gurtin, M. E. (1981). *An introduction to continuum mechanics*. New York: Academic Press.

Gwynllyw, D. R., A. R. Davies, and T. N. Phillips (1996, NOV-DEC). On the effects of a piezoviscous lubricant on the dynamics of a journal bearing. *J. Rheol. 40*(6), 1239–1266.

Harris, K. R. and S. Bair (2007). Temperature and pressure dependence of the viscosity of diisodecyl phthalate at temperatures between (0 and 100) °C and at pressures to 1 GPa. *J. Chem. Eng. Data 52*(1), 272–278.

Hron, J., J. Málek, and K. R. Rajagopal (2001). Simple flows of fluids with pressure-dependent viscosities. *Proc. R. Soc. Lond., Ser. A, Math. Phys. Eng. Sci. 457*(2011), 1603–1622.

Huh, C. and L. Scriven (1971). Hydrodynamic model of steady movement of a solid/liquid/fluid contact line. *Journal of Colloid and Interface Science 35*(1), 85 – 101.

King, H. E., E. Herbolzheimer, and R. L. Cook (1992). The diamond-anvil cell as a high-pressure viscometer. *J. Appl. Phys. 71*(5), 2071–2081.

Lanzendörfer, M. (2011). *Flows of incompressible fluids with pressure-dependent viscosity (and their application to modelling the flow in journal bearing)*. Ph. D. thesis, Mathematical Institute of Charles University, Czech Republic.

Liang, J. Z. (2001). Pressure effect of viscosity for polymer fluids in die flow. *Polymer 42*(8), 3709–3712.

Maršík, F. (1999). *Termodynamika kontinua*. Praha: Academia.

Mavridis, H. (1988). *Finite element studies in injection mold filling*. Ph. D. thesis, Department of Chemical Engineering, McMaster University, Canada.

Mavridis, H., G. D. Bruce, G. J. Vancso, G. C. Weatherly, and J. Vlachopoulos (1992). Deformation patterns in the compression of polypropylene disks: Experiments and simulation. *J. Rheol. 36*(1), 27–43.

Neale, M. J. (Ed.) (1973). *Tribology handbook*. New York: John Wiley & Sons, Inc.

Ogden, R. W. (1984). *Nonlinear elastic deformations*. Chichester: Ellis Horwood Ltd.

Paton, J. M. and C. J. Schaschke (2009). Viscosity measurement of biodiesel at high pressure with a falling sinker viscometer. *Chem. Eng. Res. Des. 87*(11), 1520–1526.

Průša, V., S. Srinivasan, and K. Rajagopal (2012). Role of pressure dependent viscosity in measurements with falling cylinder viscometer. *International Journal of Non-Linear Mechanics 47*(7), 743 – 750.

Rajagopal, K. and A. Szeri (2003). On an inconsistency in the derivation of the equations of elastohydrodynamic lubrication. *Proc. R. Soc. Lond., Ser. A, Math. Phys. Eng. Sci. 459*(2039), 2771–2786.

Rajagopal, K. R. and A. R. Srinivasa (2008). On the thermodynamics of fluids defined by implicit constitutive relations. *Z. angew. Math. Phys. 59*(4), 715–729.

Roache, P. J. (2002). Code Verification by the Method of Manufactured Solutions. *Journal of Fluids Engineering 124*(1), 4–10.

Rudin, W. (1976). *Principles of Mathematical Analysis*. International Series in Pure and Applied Mathematics. New York: McGraw-Hill, Inc.

Schaschke, C., S. Allio, and E. Holmberg (2006). Viscosity measurement of vegetable oil at high pressure. *Food Bioprod. Process. 84*(3), 173–178.

Sedláček, T., M. Zatloukal, P. Filip, A. Boldizar, and P. Sáha (2004). On the effect of pressure on the shear and elongational viscosities of polymer melts. *Polym. Eng. Sci. 44*(7), 1328–1337.

Trefethen, L. (2000). *Spectral Methods in Matlab*. Software, Environments, Tools. Society for Industrial and Applied Mathematics.

Weideman, J. A. and S. C. Reddy (2000). A MATLAB differentiation matrix suite. *ACM Trans. Math. Softw. 26*(4), 465–519.

Appendix A
Cylindrical coordinates

Let us consider a three-dimensional Euclidean space together with a *Cartesian coordinate system* consisting of an orthonormal basis $\{\boldsymbol{e}_i\} = \{\boldsymbol{e}_1, \boldsymbol{e}_2, \boldsymbol{e}_3\}$ and a point O called an *origin*. Any point in this space can be identified with its *Cartesian coordinates* x_i $(i = 1, 2, 3)$ with respect to the established basis.

Due to the geometry of the problem considered in the main scope of this paper we introduce *cylindrical coordinates* in the classical way. We use the notation

$$\xi^1 \equiv r\,, \quad \xi^2 \equiv \theta\,, \quad \xi^3 \equiv z\,,$$

whereas relations

$$\begin{aligned} x_1 &= r\cos\theta\,, \\ x_2 &= r\sin\theta\,, \\ x_3 &= z \end{aligned}$$

hold for $r \in [0, \infty),\ \theta \in [0, 2\pi),\ z \in \mathbb{R}$.

Covariant basis

At each point (r, θ, z) we introduce a *covariant basis* in the form

$$\boldsymbol{g}_i = \frac{\partial x_j}{\partial \xi^i}\,\boldsymbol{e}_j, \tag{A.1}$$

it means

$$\boldsymbol{g}_1 \equiv \boldsymbol{g}_r = \begin{bmatrix} \cos\theta \\ \sin\theta \\ 0 \end{bmatrix}, \qquad \boldsymbol{g}_2 \equiv \boldsymbol{g}_\theta = \begin{bmatrix} -r\sin\theta \\ r\cos\theta \\ 0 \end{bmatrix}, \qquad \boldsymbol{g}_3 \equiv \boldsymbol{g}_z = \begin{bmatrix} 0 \\ 0 \\ 1 \end{bmatrix}.$$

In an analogous way we can refer to a *contravariant basis* given by

$$\boldsymbol{g}^i = \frac{\partial \xi^i}{\partial x_j}\,\boldsymbol{e}_j, \tag{A.2}$$

It is not necessary to emphasize this regarding the fact that further we use so called *physical coordinates* introduced with respect to normed bases (see below).

Metric tensor

$$\mathbb{g} = [g_{ij}] = \begin{bmatrix} 1 & 0 & 0 \\ 0 & r^2 & 0 \\ 0 & 0 & 1 \end{bmatrix}, \qquad \boldsymbol{J} = \det \mathbb{g} = r^2\,.$$

Since cylindrical coordinates are orthogonal, the relation $g^{ij} = 1/g_{ij}$ holds.

Physical coordinates

Normed basis is obtained as

$$\hat{\boldsymbol{g}}_i = \frac{\boldsymbol{g}_i}{|\boldsymbol{g}_i|} = \frac{\boldsymbol{g}_i}{(\boldsymbol{g}_i \cdot \boldsymbol{g}_i)^{1/2}} = \frac{\boldsymbol{g}_i}{\sqrt{g_{ii}}}\,, \tag{A.3}$$

$$\hat{\boldsymbol{g}}_1 \equiv \hat{\boldsymbol{g}}_r = \begin{bmatrix} \cos\theta \\ \sin\theta \\ 0 \end{bmatrix}, \quad \hat{\boldsymbol{g}}_2 \equiv \hat{\boldsymbol{g}}_\theta = \begin{bmatrix} -\sin\theta \\ \cos\theta \\ 0 \end{bmatrix}, \quad \hat{\boldsymbol{g}}_3 \equiv \hat{\boldsymbol{g}}_z = \begin{bmatrix} 0 \\ 0 \\ 1 \end{bmatrix}.$$

Now, for a vector $\boldsymbol{v}$ one can write

$$\boldsymbol{v} = v^i\,\boldsymbol{g}_i = v^i\,\sqrt{g_{ii}}\,\frac{\boldsymbol{g}_i}{\sqrt{g_{ii}}} = v^i\,\sqrt{g_{ii}}\,\hat{\boldsymbol{g}}_i\,, \tag{A.4}$$

$$\boldsymbol{v} = v_i\,\boldsymbol{g}^i = v_i\,\sqrt{g^{ii}}\,\frac{\boldsymbol{g}^i}{\sqrt{g^{ii}}} = \frac{v_i}{\sqrt{g_{ii}}}\,\hat{\boldsymbol{g}}_i\,. \tag{A.5}$$

Due to orthogonality of cylindrical coordinates (used in the 3^{rd} equation in the following relation), the physical coordinates of a vector $\boldsymbol{v}$ are given as

$$\hat{v}_i = v^i\,\sqrt{g_{ii}} = g^{ij}v_j\,\sqrt{g_{ii}} = g^{ii}v_i\,\sqrt{g_{ii}} = \frac{v_i}{g^{ii}}\,\sqrt{g_{ii}} = \frac{v_i}{\sqrt{g_{ii}}}\,. \tag{A.6}$$

(no sum over i)

Covariant derivative

Derivative of a vector field $\boldsymbol{v}$ with respect to x_i in a Cartesian coordinate system is

$$\frac{\partial \boldsymbol{v}}{\partial x_i} = \frac{\partial (v_j \boldsymbol{e}_j)}{\partial x_i} = \frac{\partial v_j}{\partial x_i}\,\boldsymbol{e}_j\,.$$

On the other hand, derivative of the same vector field with respect to ξ^i in a curvilinear coordinate system is

$$\frac{\partial \boldsymbol{v}}{\partial \xi^i} = \frac{\partial \left(v^j \boldsymbol{g}_j\right)}{\partial \xi^i} = \frac{\partial v^j}{\partial \xi^i}\,\boldsymbol{g}_j + v^j\,\frac{\partial}{\partial \xi^i}\left(\frac{\partial x_m}{\partial \xi^j}\,\boldsymbol{e}_m\right) = \frac{\partial v^k}{\partial \xi^i}\,\boldsymbol{g}_k + v^j\,\frac{\partial^2 x_m}{\partial \xi^i \partial \xi^j}\,\boldsymbol{e}_m.$$

At the same time the relation (A.1) yields

$$\boldsymbol{e}_m = \frac{\partial \xi^k}{\partial x_m}\,\boldsymbol{g}_k\,,$$

thus

$$\frac{\partial \boldsymbol{v}}{\partial \xi^i} = \left(\frac{\partial v^k}{\partial \xi^i} + v^j\,\Gamma^k_{ij}\right)\boldsymbol{g}_k\,, \text{ where } \Gamma^k_{ij} = \frac{\partial^2 x_m}{\partial \xi^i \partial \xi^j}\,\frac{\partial \xi^k}{\partial x_m}\,.$$

Moreover, Christoffel symbols of the second kind Γ^k_{ij} can be calculated[1] as

$$\Gamma^k_{ij} = \frac{1}{2}\,g^{kl}\left(\frac{\partial g_{il}}{\partial \xi^j} + \frac{\partial g_{lj}}{\partial \xi^i} - \frac{\partial g_{ij}}{\partial \xi^l}\right)\,.$$

[1] For further information see e. g. Brdička et al. (2000).

Considering cylindrical coordinates as above, we can write these symbols in a symbolic notation

$$\Gamma^r = \begin{bmatrix} 0 & 0 & 0 \\ 0 & -r & 0 \\ 0 & 0 & 0 \end{bmatrix}, \qquad \Gamma^\theta = \begin{bmatrix} 0 & \frac{1}{r} & 0 \\ \frac{1}{r} & 0 & 0 \\ 0 & 0 & 0 \end{bmatrix}, \qquad \Gamma^z = \begin{bmatrix} 0 & 0 & 0 \\ 0 & 0 & 0 \\ 0 & 0 & 0 \end{bmatrix}.$$

The term

$$v^k|_i = \frac{\partial v^k}{\partial \xi^i} + \Gamma^k_{ij}\, v^j$$

is called covariant derivative of v^k with rescpect to ξ^i . Then we write

$$\frac{\partial \boldsymbol{v}}{\partial \xi^i} = v^k|_i\, \boldsymbol{g}_k\,.$$

Similarly it is possible to deduce that

$$v_k|_i = \frac{\partial v_k}{\partial \xi^i} - \Gamma^j_{ki}\, v_j,$$

and for second order tensors

$$\frac{\partial \mathbb{S}}{\partial \xi^i} = \mathrm{S}^{jk}|_i\, \boldsymbol{g}_j \otimes \boldsymbol{g}_k = \mathrm{S}_{jk}|_i\, \boldsymbol{g}^j \otimes \boldsymbol{g}^k,$$

where

$$\begin{aligned} \mathrm{S}^{jk}|_i &= \frac{\partial \mathrm{S}^{jk}}{\partial \xi^i} + \Gamma^j_{im}\, \mathrm{S}^{mk} + \Gamma^k_{in}\, \mathrm{S}^{jn}\,, \\ \mathrm{S}_{jk}|_i &= \frac{\partial \mathrm{S}_{jk}}{\partial \xi^i} - \Gamma^m_{ij}\, \mathrm{S}_{mk} - \Gamma^n_{ik}\, \mathrm{S}_{jn}\,. \end{aligned}$$

We can clearly introduce physical components of covariant derivative with recpect to the normed basis (A.3) through

$$\begin{aligned} \hat{v}_j|_i &= \frac{v^j|_i}{\sqrt{g_{ii}}}\sqrt{g_{jj}} = \frac{v_j|_i}{\sqrt{g_{jj}\, g_{ii}}}\,, \qquad \text{(no sum)} \\ \hat{\mathrm{S}}_{jk}|_i &= \frac{\mathrm{S}^{jk}|_i}{\sqrt{g_{ii}}}\sqrt{g_{jj}\, g_{kk}} = \frac{\mathrm{S}_{jk}|_i}{\sqrt{g_{jj}\, g_{kk}\, g_{ii}}}\,. \qquad \text{(no sum)} \end{aligned}$$

It should be obvious after reading the section about gradient below. According to (A.6) we have

$$\hat{v}_r = v_r, \qquad \hat{v}_\theta = \frac{v_\theta}{r}, \qquad \hat{v}_z = v_z,$$

and using previous results one gets

$$\begin{aligned} v_r|_r &= \frac{\partial v_r}{\partial r}, & \hat{v}_r|_r &= \frac{\partial \hat{v}_r}{\partial r}, \\ v_r|_\theta &= \frac{\partial v_r}{\partial \theta} - \frac{v_\theta}{r}, & \hat{v}_r|_\theta &= \frac{1}{r}\frac{\partial \hat{v}_r}{\partial \theta} - \frac{\hat{v}_\theta}{r}, \\ v_r|_z &= \frac{\partial v_r}{\partial z}, & \hat{v}_r|_z &= \frac{\partial \hat{v}_r}{\partial z}, \\ v_\theta|_r &= \frac{\partial v_\theta}{\partial r} - \frac{v_\theta}{r}, & \hat{v}_\theta|_r &= \frac{\partial \hat{v}_\theta}{\partial r}, \end{aligned}$$

$$
\begin{aligned}
v_\theta|_\theta &= \frac{\partial v_\theta}{\partial \theta} + r v_r, & \hat{v}_\theta|_\theta &= \frac{1}{r}\frac{\partial \hat{v}_\theta}{\partial \theta} + \frac{\hat{v}_r}{r},\\
v_\theta|_z &= \frac{\partial v_\theta}{\partial z}, & \hat{v}_\theta|_z &= \frac{\partial \hat{v}_\theta}{\partial z},\\
v_z|_r &= \frac{\partial v_z}{\partial r}, & \hat{v}_z|_r &= \frac{\partial \hat{v}_z}{\partial r},\\
v_z|_\theta &= \frac{\partial v_z}{\partial \theta}, & \hat{v}_z|_\theta &= \frac{1}{r}\frac{\partial \hat{v}_z}{\partial \theta},\\
v_z|_z &= \frac{\partial v_z}{\partial z}, & \hat{v}_z|_z &= \frac{\partial \hat{v}_z}{\partial z}.
\end{aligned}
$$

Gradient

In the Cartesian coordinate system we define an operator nabla

$$\nabla = \frac{\partial}{\partial x_i}\,\boldsymbol{e}_i,$$

while in the curvilinear coordinate system we have

$$\nabla = \frac{\partial}{\partial \xi^i}\,\boldsymbol{g}^i.$$

Throughout the following we use the notation ϕ for a scalar field, $\boldsymbol{v}$ for a vector field and $\mathbb{S}$ for a second order tensor field. Gradient of these particular quantities is given by

$$
\begin{aligned}
\operatorname{grad}\phi &\equiv \nabla\phi = \frac{\partial \phi}{\partial \xi^i}\,\boldsymbol{g}^i = \frac{1}{\sqrt{g_{ii}}}\,\frac{\partial \phi}{\partial \xi^i}\,\hat{\boldsymbol{g}}_i,\\
\operatorname{grad}\boldsymbol{v} &\equiv \nabla\boldsymbol{v} = \frac{\partial \boldsymbol{v}}{\partial \xi^i}\otimes\boldsymbol{g}^i = v_j|_i\,\boldsymbol{g}^j\otimes\boldsymbol{g}^i = \hat{v}_j|_i\,\hat{\boldsymbol{g}}_j\otimes\hat{\boldsymbol{g}}_i,\\
\operatorname{grad}\mathbb{S} &\equiv \nabla\mathbb{S} = \frac{\partial \mathbb{S}}{\partial \xi^i}\otimes\boldsymbol{g}^i = \mathrm{S}_{jk}|_i\,\boldsymbol{g}^j\otimes\boldsymbol{g}^k\otimes\boldsymbol{g}^i = \hat{\mathrm{S}}_{jk}|_i\,\hat{\boldsymbol{g}}_j\otimes\hat{\boldsymbol{g}}_k\otimes\hat{\boldsymbol{g}}_i.
\end{aligned}
$$

First two relations may be rewritten in a matrix form with convenience. We shall omit the hat above particular components, however we must keep in mind that they are still related to the basis (A.3). In this sense the gradient in the cylindrical coordinate system reads

$$
\operatorname{grad}\phi = \begin{bmatrix} \frac{\partial \phi}{\partial r} \\ \frac{1}{r}\frac{\partial \phi}{\partial \theta} \\ \frac{\partial \phi}{\partial z} \end{bmatrix}, \qquad \operatorname{grad}\boldsymbol{v} = \begin{bmatrix} \frac{\partial v_r}{\partial r} & \frac{1}{r}\left(\frac{\partial v_r}{\partial \theta} - v_\theta\right) & \frac{\partial v_r}{\partial z} \\ \frac{\partial v_\theta}{\partial r} & \frac{1}{r}\left(\frac{\partial v_\theta}{\partial \theta} + v_r\right) & \frac{\partial v_\theta}{\partial z} \\ \frac{\partial v_z}{\partial r} & \frac{1}{r}\frac{\partial v_z}{\partial \theta} & \frac{\partial v_z}{\partial z} \end{bmatrix}. \tag{A.7}
$$

Divergence

Differential operator divergence can be applied either to a vector field, so that

$$\operatorname{div}\boldsymbol{v} = \frac{1}{r}\,\frac{\partial (r\,v_r)}{\partial r} + \frac{1}{r}\,\frac{\partial v_\theta}{\partial \theta} + \frac{\partial v_z}{\partial z}\,, \tag{A.8}$$

or to a tensor field and then

$$\operatorname{div}\mathbb{S} = \begin{bmatrix} \frac{\partial \mathrm{S}_{rr}}{\partial r} + \frac{1}{r}\left(\frac{\partial \mathrm{S}_{r\theta}}{\partial \theta} + \mathrm{S}_{rr} - \mathrm{S}_{\theta\theta}\right) + \frac{\partial \mathrm{S}_{rz}}{\partial z} \\ \frac{\partial \mathrm{S}_{\theta r}}{\partial r} + \frac{1}{r}\left(\frac{\partial \mathrm{S}_{\theta\theta}}{\partial \theta} + \mathrm{S}_{r\theta} + \mathrm{S}_{\theta r}\right) + \frac{\partial \mathrm{S}_{\theta z}}{\partial z} \\ \frac{\partial \mathrm{S}_{zr}}{\partial r} + \frac{1}{r}\left(\frac{\partial \mathrm{S}_{z\theta}}{\partial \theta} + \mathrm{S}_{zr}\right) + \frac{\partial \mathrm{S}_{zz}}{\partial z} \end{bmatrix}. \tag{A.9}$$

Laplace

Laplace operator of a scalar field reads

$$\Delta\phi = \frac{\partial^2\phi}{\partial r^2} + \frac{1}{r}\frac{\partial\phi}{\partial r} + \frac{1}{r^2}\frac{\partial^2\phi}{\partial\theta^2} + \frac{\partial^2\phi}{\partial z^2}. \tag{A.10}$$

In the case of a vector field we have

$$\Delta\boldsymbol{v} = \begin{bmatrix} \Delta v_r - \frac{2}{r^2}\frac{\partial v_\theta}{\partial\theta} - \frac{v_r}{r^2} \\ \Delta v_\theta + \frac{2}{r^2}\frac{\partial v_r}{\partial\theta} - \frac{v_\theta}{r^2} \\ \Delta v_z \end{bmatrix}. \tag{A.11}$$

This short appendix should be understood to provide a brief satisfactory overview of the topic. Some profound information can be found for example in Ogden (1984), Brdička et al. (2000), but also in many other books dedicated to the tensorial calculus.

Appendix B
Transformation rules

Here we shall provide some detailed information concerning the reformulation of the problem as it was done in Section 4.1. Let $\bar{\Omega} = [-1,1] \times [-1,1]$ is the fixed computational domain and Ω_t, U, U^{-1} are given by (4.1), (4.2) respectively.

The objective is to rewrite (2.41) – (2.46) in terms of $\bar{v}_{\bar{r}}, \bar{v}_{\bar{z}}, \bar{p}$ and $\bar{\xi}$, which are functions defined on $\bar{\Omega}$. Let us remind that for an arbitrary function ω on Ω_t we have defined its counterpart $\bar{\omega}$ in (4.3),

$$\omega(r,z,t) = \omega(\bar{r}\bar{\xi}(\bar{z},t), \bar{z}h(t), t) =_{\text{def}} \bar{\omega}(\bar{r},\bar{z},t) = \bar{\omega}\left(r\xi(z,t)^{-1}, zh(t)^{-1}, t\right).$$

Jacobian matrix of the inverse mapping U^{-1} reads

$$J(r,z,t) = \begin{bmatrix} \frac{\partial \bar{r}}{\partial r} & \frac{\partial \bar{r}}{\partial z} \\ \frac{\partial \bar{z}}{\partial r} & \frac{\partial \bar{z}}{\partial z} \end{bmatrix} = \begin{bmatrix} \frac{1}{\xi} & -\frac{r}{\xi^2}\frac{\partial \xi}{\partial z} \\ 0 & \frac{1}{h} \end{bmatrix} = \begin{bmatrix} \frac{1}{\bar{\xi}} & -\frac{\bar{r}}{h\bar{\xi}}\frac{\partial \bar{\xi}}{\partial \bar{z}} \\ 0 & \frac{1}{h} \end{bmatrix} = \bar{J}(\bar{r},\bar{z},t). \tag{B.1}$$

Clearly, using the above notation one can write

$$\operatorname{grad}_{r,z}\omega(r,z,t) = \bar{J}(\bar{r},\bar{z},t)^{\mathsf{T}} \operatorname{grad}_{\bar{r},\bar{z}}\bar{\omega}(\bar{r},\bar{z},t), \tag{B.2}$$

or equivalently

$$\frac{\partial \omega}{\partial r} = \frac{1}{\bar{\xi}}\frac{\partial \bar{\omega}}{\partial \bar{r}}, \tag{B.3}$$

$$\frac{\partial \omega}{\partial z} = \frac{1}{h}\frac{\partial \bar{\omega}}{\partial \bar{z}} - \frac{\bar{r}}{h\bar{\xi}}\frac{\partial \bar{\xi}}{\partial \bar{z}}\frac{\partial \bar{\omega}}{\partial \bar{r}}. \tag{B.4}$$

Second derivatives of ω can be obtained using the chain rule. We have

$$\frac{\partial^2 \omega}{\partial r^2} = \frac{1}{\bar{\xi}^2}\frac{\partial^2 \bar{\omega}}{\partial \bar{r}^2}, \tag{B.5}$$

$$\frac{\partial^2 \omega}{\partial z^2} = \left(\frac{\bar{r}}{h\bar{\xi}}\frac{\partial \bar{\xi}}{\partial \bar{z}}\right)^2 \frac{\partial^2 \bar{\omega}}{\partial \bar{r}^2} - \frac{2\bar{r}}{h^2\bar{\xi}}\frac{\partial \bar{\xi}}{\partial \bar{z}}\frac{\partial^2 \bar{\omega}}{\partial \bar{r}\partial \bar{z}} + \frac{1}{h^2}\frac{\partial^2 \bar{\omega}}{\partial \bar{z}^2} + \frac{\bar{r}}{h^2\bar{\xi}^2}\left(2\left(\frac{\partial \bar{\xi}}{\partial \bar{z}}\right)^2 - \bar{\xi}\frac{\partial^2 \bar{\xi}}{\partial \bar{z}^2}\right)\frac{\partial \bar{\omega}}{\partial \bar{r}}, \tag{B.6}$$

Finally, for the time derivative we write

$$\frac{\partial \omega}{\partial t} = \frac{\partial \bar{\omega}}{\partial t} + \frac{\partial \bar{\omega}}{\partial \bar{r}}\frac{\partial \bar{r}}{\partial t} + \frac{\partial \bar{\omega}}{\partial \bar{z}}\frac{\partial \bar{z}}{\partial t} = \frac{\partial \bar{\omega}}{\partial t} + \frac{\bar{z}}{h}\left(\frac{\bar{r}}{\bar{\xi}}\frac{\partial \bar{\xi}}{\partial \bar{z}}\frac{\partial \bar{\omega}}{\partial \bar{r}} - \frac{\partial \bar{\omega}}{\partial \bar{z}}\right)\frac{\mathrm{d}h}{\mathrm{d}t} - \frac{\bar{r}}{\bar{\xi}}\frac{\partial \bar{\xi}}{\partial t}\frac{\partial \bar{\omega}}{\partial \bar{r}}. \tag{B.7}$$

Transformed equations (4.4), (4.8) now can be simply obtained using the above rules.